



Numerical Analysis of Immersed Steel & Composite Cylindrical Shell Structures Submitted to UNDEX.

Md Mahabub Hasan Mousum

Master Thesis

Presented in partial fulfillment
of the requirements for the double degree:
“Advanced Master in Naval Architecture” conferred by University of Liege
“Master of Sciences in Applied Mechanics, specialization in Hydrodynamics,
Energetics and Propulsion” conferred by Ecole Centrale de Nantes

Developed at Institut Catholique d'Arts et Métiers (ICAM), Nantes France
in the framework of the

**“EMSHIP”
Erasmus Mundus Master Course
in “Integrated Advanced Ship Design”**

EMJMD 159652 – Grant Agreement 2015-1687

Supervisor: Prof. Hervé Le Sourne, Institut Catholique d'Arts et Métiers
(ICAM), Nantes France

Reviewer: Prof. Maciej Taczala, West Pomeranian University Szczecin, Poland

Nantes, February 2018



Traditio et Innovatio



Zachodniopomorski
Uniwersytet
Technologiczny
w Szczecinie



This page is intentionally left blank

Declaration of Authorship

I, Md Mahabub Hasan Mousum declare that this thesis and the work presented in it are my own and has been generated by me as the result of my own original research.

“Numerical Analysis of Immersed Steel & Composite Cylindrical Shell Structures Submitted to UNDEX.”

I confirm that:

1. This work was done wholly or mainly while in candidature for a research degree at the Institut Catholique d'Arts et Métiers (ICAM), Nantes, France
2. Where any part of this thesis has previously been submitted for a degree or any other qualification at this University or any other institution, this has been clearly stated;
3. Where I have consulted the published work of others, this is always clearly attributed;
4. Where I have quoted from the work of others, the source is always given. With the exception of such quotations, this thesis is entirely my own work;
5. I have acknowledged all main sources of help;
6. Where the thesis is based on work done by myself jointly with others, I have made clear exactly what was done by others and what I have contributed myself;
7. Either none of this work has been published before submission, or parts of this work have been published as: [please list references below]:
8. I cede copyright of the thesis in favour of the Institut Catholique d'Arts et Métiers (ICAM), Nantes, France

Date:

Signature:



This page is intentionally left blank

CONTENTS

List of Tables	xii
ABSTRACT	xiv
1 INTRODUCTION	1
1.1 Back Ground.....	1
1.2 Scope of Research.....	3
1.3 Objectives.....	4
1.4 Work Flow.....	6
2 UNDERWATER EXPLOSION THEORY AND MODELING	7
2.1 Sequence of events.....	7
2.1.1 Shock Wave.....	8
2.1.2 Gas Bubble	15
2.2 Shock Factor.....	16
3 REVIEW OF THEORETICAL AND COMPUTATIONAL STUDIES	17
3.1 Analysis of Marine Panels.....	17
3.1.1 Panel Response to Free Field Blast Loading.....	17
3.1.2 Fluid–Structure Interaction in Sandwich Composites	23
3.2 Full-Scale Marine Structures Analysis	24
3.3 The UNDEX Loading for Numerical Analysis	28
3.4 Simulation strategies and validation tools.....	35
4 NON-LINEAR FINITE ELEMENT ANALYSIS OF MONOLITHIC MATERIAL STRUCTURE	37
4.1 LS-DYNA	37
4.2 Numerical Analysis with LS-DYNA.....	37
4.2.1 Analysis procedure	38
4.2.2 Model and loads.....	38
4.2.3 Response Analysis of a Monolithic Material Structure	46
4.3 Discussion & Comparison.....	91
5 NON-LINEAR FINITE ELEMENT ANALYSIS OF LAMINATED COMPOSITE STRUCTURE	101
5.1 Simulation Model in LS-DYNA.....	102
5.2 Available material models in LS-DYNA	103
5.3 Material Model MAT54/55	105
5.3.1 Theory of failure model	106
5.4 Materials and Specimen Manufacturing	107
5.5 Response Analysis of Composite Material Structure	108
5.6 Discussions.....	115
6 FURTHER WORK	116

7	ACKNOWLEDGEMENT	117
8	REFERENCE	119

LIST OF FIGURES

Figure 1.4-a LS-DYNA modelling and simulation process.	6
Figure 2.1-a Schematic representation of shockwave and Gas bubble pulsation with respect to time evolution and exponential decay of pressure field of UNDEX. (Keil, 1961).....	8
Figure 2.1-b Snell’s law (Shin 2004)	11
Figure 2.1-c.The ‘image’ charge and Snell’s law for both reflected waves from the bottom and air-water interface (Shin 2004).	12
Figure 2.1-d Bulk Cavitation as a result of UNDEX	13
Figure 2.1-e Bulk Cavitation Region	13
Figure 2.1-f Formation of local cavitation near the surface of a steel cylinder subjected to the shock wave from the underwater explosion (OD 273 mm and wall thickness 2 mm). The images at times (A) 25 μ s, (B) 45 μ s, (C) 55 μ s, and (D) 75 μ s viewed down the axis of cylinder. In the images the dark area at the surface of the cylinder is local cavitation zone. (Cimpoeru, 2017).	14
Figure 2.2-a Geometry layout of the problem for angle of incidence for shock wave on the surface of the structure and the explosion standoff distance. (Liang & Tai, 2006).....	16
Figure 3.1-a Diagram of a ship structure subjected to underwater explosion (Mouritz, 1995)	18
Figure 3.2-a Diagram of a ship structure subjected to underwater explosion (Mouritz, 1995)	25
Figure 3.2-b The response of a full-scale petro boat model subjected to underwater explosion (Liang, 2006)	26
Figure 3.2-c Coupled Ship-fluid model for underwater explosion response analysis (Liang, 2006)	27
Figure 3.3-a Configuration of an Immersed Cylinder Subjected to an UNDEX.....	28
Figure 3.3-b Pressure profile for SF 1.68 with Single Exponential Decay	33
Figure 3.3-c Pressure profile for SF 2.5 with Single Exponential Decay	33
Figure 3.3-d Pressure profile for SF 1.68 with Double Exponential Decay & Time Delay ...	34
Figure 3.3-e Pressure profile for SF 2.5 with Double Exponential Decay & Time Delay	35
Figure 4.2-a Finite Element model of the structure	39
Figure 4.2-b Shell Element mesh size.....	40
Figure 4.2-c Finite Element model of the structure and fluid around it.....	41
Figure 4.2-d Solid Element mesh size.....	41
Figure 4.2-e Non-Reflective Boundary Condition for fluid.....	43

Figure 4.2-f Lateral (along x axis) Fluid layer Boundary condition.....	44
Figure 4.2-g Finite Element Model of an immersed Structure Half section.	45
Figure 4.2-h Finite Element Model of an immersed Structure.....	45
Figure 4.2-i Finite Element Model of an immersed Structure.....	46
Figure 4.2-j Structure Internal Energy and Radial Displacement (Fluid modelled with MAT Acoustic)	48
Figure 4.2-k Plastic strain at different time steps	49
Figure 4.2-l Energy balance of the numerical simulation	49
Figure 4.2-m Dissipation of the Internal Energy	50
Figure 4.2-n Internal Energy dissipation within early structural response time 0.5 milliseconds	51
Figure 4.2-o Radiation Damping at the fluid element 49237	51
Figure 4.2-p Position of the fluid element 49237 in XY plane at the centre of the impact area of shock wave peak pressure	52
Figure 4.2-q Position of the Fluid element 49237 in YZ plane.....	52
Figure 4.2-r Distribution of total internal energy dissipation.....	53
Figure 4.2-s Cavity flow or flow of low pressure oscillation in MAT Acoustic fluid model SF 1.68.....	54
Figure 4.2-t Structure Internal Energy and the Radial Displacement (Fluid modelled with MAT Acoustic and Cavitation treatment).....	55
Figure 4.2-u Energy balance of the numerical simulation	56
Figure 4.2-v Dissipation of the Internal Energy	56
Figure 4.2-w Internal Energy dissipation within early structural response time 0.5 milliseconds	57
Figure 4.2-x Radiation Damping at the fluid element 49237	58
Figure 4.2-y Distribution of total internal energy dissipation	58
Figure 4.2-z Structure Internal Energy and the Radial Displacement (Fluid modelled with MAT Elastic Fluid).....	59
Figure 4.2-aa Energy balance of the numerical simulation.....	59
Figure 4.2-bb Dissipation of the Internal Energy	60
Figure 4.2-cc Internal Energy dissipation within early structural response time 0.6 milliseconds	60
Figure 4.2-dd Radiation Damping at the fluid element 49237	61
Figure 4.2-ee Distribution of total internal energy dissipation.....	62

Figure 4.2-ff Cavity flow or flow of low pressure oscillation in MAT Elastic Fluid model SF 1.68..... 63

Figure 4.2-gg Fluid mesh flow with structure Shell in MAT Elastic Fluid Model 64

Figure 4.2-hh Structure Internal Energy and the Radial Displacement (Fluid modelled with MAT Elastic Fluid) 65

Figure 4.2-ii Energy balance of the numerical simulation 65

Figure 4.2-jj Dissipation of the Internal Energy 66

Figure 4.2-kk Internal Energy dissipation within early structural response time 0.6 milliseconds 66

Figure 4.2-ll Radiation Damping at the fluid element 49237..... 67

Figure 4.2-mm Distribution of total internal energy dissipation 67

Figure 4.2-nn Structure Internal Energy and the Radial Displacement (Fluid modelled with MAT Acoustic) 68

Figure 4.2-oo Plastic strain at different time steps. 69

Figure 4.2-pp Energy balance of the numerical simulation 69

Figure 4.2-qq Dissipation of the Internal Energy 70

Figure 4.2-rr Internal Energy dissipation within early structural response time 0.5 milliseconds 71

Figure 4.2-ss Radiation Damping at the fluid element 49237..... 71

Figure 4.2-tt Distribution of total internal energy dissipation 72

Figure 4.2-uu Cavity flow or flow of low pressure oscillation in MAT Acoustic SF 2.5 73

Figure 4.2-vv Structure Internal Energy and the Radial Displacement (Fluid modelled with MAT Acoustic & cavitation treatment) 74

Figure 4.2-ww Energy balance of the numerical simulation..... 75

Figure 4.2-xx Dissipation of the Internal Energy 75

Figure 4.2-yy Internal Energy dissipation within early structural response time 0.6 milliseconds 76

Figure 4.2-zz Radiation Damping at the fluid element 49237 77

Figure 4.2-aaa Distribution of total internal energy dissipation 77

Figure 4.2-bbb Structure Internal Energy and the Radial Displacement (Fluid modelled with MAT Elastic Fluid) 78

Figure 4.2-ccc Energy balance of the numerical simulation 78

Figure 4.2-ddd Dissipation of the Internal Energy 79

Figure 4.2-eee Internal Energy dissipation within early structural response time 0.6 milliseconds.....	79
Figure 4.2-fff Radiation Damping at the fluid element 49237.....	80
Figure 4.2-ggg Distribution of total internal energy dissipation.....	81
Figure 4.2-hhh Fluid mesh flow with structure Shell in MAT Elastic Fluid Model.....	81
Figure 4.2-iii Cavity flow or flow of low pressure oscillation in MAT Elastic Fluid SF 2.5.....	82
Figure 4.2-jjj Structure Internal Energy and the Radial Displacement (Fluid modelled with MAT Elastic Element & Cavitation Treatment).....	83
Figure 4.2-kkk Energy balance of the numerical simulation.....	84
Figure 4.2-lll Dissipation of the Internal Energy.....	84
Figure 4.2-mmm Internal Energy dissipation within early structural response time 0.6 milliseconds.....	85
Figure 4.2-nnn Radiation Damping at the fluid element 49237.....	85
Figure 4.2-ooo Distribution of total internal energy dissipation.....	86
Figure 4.2-ppp Effective plastic strain distribution at 50 ms.....	87
Figure 4.2-qqq Plastic strain at different time steps.....	87
Figure 4.2-rrr Structure Internal Energy and the Displacement (Fluid modelled with MAT Acoustic).....	88
Figure 4.2-sss Energy balance of the numerical simulation.....	88
Figure 4.2-ttt Effective plastic strain distribution at 50 ms.....	89
Figure 4.2-uuu Plastic strain at different time steps.....	89
Figure 4.2-vvv Structure Internal Energy and the Displacement (Fluid modelled with MAT Acoustic).....	90
Figure 4.2-www Energy balance of the numerical simulation.....	90
Figure 4.3-a Time evolution of Radial Displacement obtained from different methods of numerical calculation (Simple Decay). Reference for the date LS-DYNA/USA (Brochard, 2018).....	91
Figure 4.3-b Structural response as Radial displacement within a range of 15 ms for simple decay calculation. Reference for the date LS-DYNA/USA (Brochard, 2018).....	93
Figure 4.3-c Structural response as radial displacement for Double decay calculation. Reference for the date LS-DYNA/USA (Brochard, 2018).....	93
Figure 4.3-d Structural response as radial displacement within a range of 10 ms for double decay calculation. Reference for the date LS-DYNA/USA (Brochard, 2018).....	94

Figure 4.3-e Structural response as velocity within a range of 5 ms for simple decay calculation. Reference for the date LS-DYNA/USA (Brochard, 2018) 94

Figure 4.3-f Structural response as velocity for different scenarios of numerical calculation (for simple decay calculation). Reference for the date LS-DYNA/USA (Brochard, 2018) 95

Figure 4.3-g Time evolution of Radial Displacement obtained from different methods of numerical calculation (Simple Decay). Reference for the date LS-DYNA/USA (Brochard, 2018) 96

Figure 4.3-h Structural response as radial displacement within a range of 15 ms for simple decay calculation. Reference for the date LS-DYNA/USA (Brochard, 2018)..... 97

Figure 4.3-i Structural response as radial displacement within a range of 15 ms for double decay calculation. Reference for the date LS-DYNA/USA (Brochard, 2018)..... 98

Figure 4.3-j Structural response as velocity within a range of 5 ms for simple decay calculation. Reference for the date LS-DYNA/USA (Brochard, 2018) 98

Figure 4.3-k Structural response as velocity for different scenarios of numerical calculation (for simple decay calculation). Reference for the date LS-DYNA/USA (Brochard, 2018) ... 99

Figure 5.3-a Description of the material card MAT 54/55 (Osborne, 2012) 105

Figure 5.5-a Plastic strain and failure of the structure at different time steps..... 109

Figure 5.5-b Radial Displacement of the structure 110

Figure 5.5-c Energy balance of the numerical simulation 110

Figure 5.5-d Plastic strain and failure of the structure at different time steps..... 111

Figure 5.5-e Energy balance of the numerical simulation 111

Figure 5.5-f Radial Displacement of the structure..... 112

Figure 5.5-g Plastic strain and failure of the structure at different time steps..... 112

Figure 5.5-h Energy balance of the numerical simulation 113

Figure 5.5-i Radial Displacement of the structure..... 113

Figure 5.5-j Plastic strain distribution at 50 ms..... 114

Figure 5.5-k Radial Displacement of the structure 114

Figure 5.5-l Energy balance of the numerical simulation 115

Figure 5.5-m Dissipation of the internal energy in the simulation (1 indicates Fluid & 2 indicates Structure) 115

List of Tables

Table 2.1-a Equivalent coefficients for similitude equations (Reid, 1996).....	10
Table 3.3-a Typical values of characteristics parameters (Brochard, 2018).....	29
Table 4.2-a Mechanical properties of Steel.....	40
Table 4.2-b Material Properties and options in MAT_01 Card LS-DYNA.....	42
Table 4.2-c Material Properties and options in MAT_90 Card LS-DYNA	43
Table 4.2-d Damage shape of the structure for different simulation scenarios.....	47
Table 5.2-a Available Material Model for modelling composite in LS-DYNA. (LS-DYNA Keyword User's Manual - Volume II, 2014).	104
Table 5.4-a CFRP elastic Properties used in this study	108
Table 5.5-a different plate thickness is applied for the simulation.	109

This page is intentionally left blank

ABSTRACT

Numerical Analysis of Immersed Steel & Composite Cylindrical Shell Structures Submitted to UNDEX.

Author: Md Mahabub Hasan Mousum

Underwater Explosion (*UNDEX*) due to terrorism or accidental incident affects the people and structures causing irreparable loss of life and damage to survivability of the structure. These blast loading due to the explosion is challenging both the civilian and military structures. In order to minimize the effect on the structure, we need to understand the mechanics and the response of the structure submitted to blast loading. After a review of existing methods to simulate the response of a steel and composite structure submitted to dynamic pressure waves, the focus will be on the analysis of naval steel and composite structures when they are submitted to the primary shock wave generated from the underwater explosions. Finite element numerical simulations will be carried out to simulate the dynamic response of a non-stiffened immersed cylindrical shell submitted to such pressure loading. The pressure loading on the structure as a kinetic energy, which is transmitted by the shock wave is calculated from the explosion parameters by using analytical formulation. The assessment of the dynamic response and the fluid structure interaction was performed with explicit finite element solver LS-DYNA. Sensitivity analyses of the response to different parameters like shock factor, treatment of the fluid domain, Anisotropy of material will also be performed.

Keywords

LS-DYNA, Steel Cylinder, Composite Structure, Finite element analysis, fluid structure interaction, UNDEX.

This page is intentionally left blank

1 INTRODUCTION

1.1 Back Ground

Explosions can be the reason of irreparable loss of life and failure or damage of structure which worth millions. UNDERwater EXplosion (UNDEX) or impact is a challenge for both civilian and military marine vessel design to minimize the impact of blast loading on the structure. The extensive studies during the World War II, noted that UNDEX could actually damage the structure without directly impacted by the torpedo or mine (Krueger, 2006). This non-contact concept of UNDEX was especially applicable to submarine warfare. During this era, depth charges were used to destroy submarines. A depth charge can causes catastrophic damage to the submarines without physically touching the target. During and shortly after the World War II numerous studies were conducted for both surface ships and submarines. Most of these studies were focused on the vulnerabilities of floating and submerged structures from UNDEX. Typical weapons (such as torpedo and mine) detonated nearby fluid medium of a floating or submerged structure can damage the vessel in the form of dished hull plating (Wang, 2014).

UNDEX acts as a source of shock wave followed by a series of pressure pulses due to subsequent oscillations of gas bubbles containing the product of detonation. As result of the detonation, it causes a rapid liberation of energy. The dissipation of this energy is divided into three parts. The major part of the detonation energy which is 57% of the total energy is carried away by the shock wave. Followed by 37% of the total energy dissipated for secondary wave pulse generated by UNDEX bubbles and the remaining part (~6%) of the energy is dissipated by heat (Arons, 1948). The initial shock wave produces a severe shock loads to the ship structure and marine vessels (Mouritz, 1995). Not only UNDEX but also striking of a partially submerged object in water (impact) and/or the slamming pressure in the high sea when the forefront of the vessel rises above the free surface (water surface) and rapidly re-enters the water surface with high acceleration. As result the ship structures are facing extremely high strain rates due to the impulse of high pressure from these shock waves over a short period of time. At the same time, the tendency of building lightweight ship structure for increasing payload is also require adequate protection against blast load to be resistant enough against impulsive loads and retain good residual (post-impact) strength (Mouritz, 1996).

Predicting the shock response of the floating and submerged structure from the non-contact UNDEX is essential for the underwater warhead design as well as for naval structure for defending underwater shock. To serve the purpose, engineers must evaluate the damage response and the vulnerability resistance of the naval structure to perform mission in UNDEX environment. However, predicting response of the structures submitted to UNDEX involves quite complex phenomenon and parameters. Detail understanding of the UNDEX phenomenon and the dynamic response of various structural elements are required to design and analyze the structure submitted to UNDEX (Zong, 2013). The key driving incidents are fluid-structure interaction (FSI), material and geometric nonlinearities, high strain rate constitution equations, tensile tearing and rupture et al. There are three major strategies to understand the problem: analytical method, experimental study, and numerical simulation. Analytical solution for the non-contact UNDEX is extremely difficult to develop because the dynamic response of the structure submitted to the UNDEX depends on the propagation of the shock wave, detonation of the high explosive, the bulk and local cavitation as well as the complex fluid-structure interaction and the dynamic behavior of the structure according to the material properties. Due to high expense and time-consuming procedure shock trials of the full-ship are limited and less preferred. On the other hand, numerical methods opened the door to understand the dynamic response of the structure subjected to UNDEX to a greater extend over the past decades. In addition, the feasibility of numerical calculations are frequently verified with small-scale model test.

UNDEX generates initial shock wave in the surrounding water layers which has a spreading velocity greater than the speed of sound in water. The shock wave speed attains a speed close to the speed of sound in water when it spreads into water with about 10 charge radius from the detonation point (Cole, 1946. Shin, 2004). Apart from the incident shock wave, the UNDEX also affects the surrounding fluid medium with wave reflection from the free surface and the seabed, bubble pulse and bulk and local cavitation. The incident shock wave forms a reflected wave in the fluid medium from the structures. Simultaneously, with the movement of the structure the surrounding fluid also moves and produces radiated wave. Together with the reflected wave and radiated wave constitute the scattered wave (Reid, 1996). Therefore it is necessary to consider fluid-structure interaction to elucidate the mechanism of shock response analysis of structures subjected to non-contact UNDEX. Over the past years, numerical simulations have been developed to model the fluid-structure interaction involved in the UNDEX between the structure and the surrounding fluid medium (Felippa, 1980. Geers, 1978).

Structural damage from the UNDEX also depends on standoff distance and explosion weight. The efficient way to reduce the structural damage due to UNDEX is to provide sufficient standoff distance between the structure and the source of explosion. Therefore the effect of the shock wave will not be sufficient enough to cause catastrophic structural damage.

In order to accomplish the objectives, it is necessary to evaluate various scenarios to analyze structural response to blast loading. Scenarios should consider such aspects like structural geometry, explosive magnitude, standoff distance, fluid-structure interaction, structural scantling etc. (Chirica, 2012).

1.2 Scope of Research

In Finite Element Analysis (FEA) a virtual prototype is examined in a virtual environment which is a significant advantage over the experimental method. It allows more concurrent analysis of the design in the pre-designing process and thereby reducing engineering costs and testing while improving product performance. It is necessary to understand the physics of UNDEX to carry out realistic and good numerical analysis.

From the experiment and the literature review, it has been established that the explosion near a submarine or surface vessel generates damaging initial shock wave and oscillating gas bubble in the surrounding fluid medium. The incident shock wave has more influence than the oscillating gas bubble regarding the structural local damage.

A numerical simulation of UNDEX response of a structure consists of obtaining the response of a finite-sized structure (Cylindrical Shell) which is submitted to a blast load when immersed in an infinite fluid medium (Sea or Ocean). In this research work, focus will be on simulation of the dynamic response of a non-stiffened immersed cylindrical shell submitted to primary shock wave from the non-contact UNDEX. In the numerical calculation the pressure loading on the finite-sized structure as a kinetic energy, which is transmitted by the shock wave is calculated from the explosion parameters with the help of analytical formulation. The structure is air-filled and clamed at its extremities.

The scope of this thesis includes the analytical study of primary shock wave from the non-contact UNDEX which strikes the immersed cylindrical shell structure and dynamic response analysis of the structure using explicit finite element solver LS-DYNA. The numerical calculations are verified with the simulation results from the LS-DYNA/USA. LS-DYNA/USA successfully used the boundary element code USA (DeRuntz, 1989) based on the so-called

Doubly Asymptotic Approximation developed by (Geers, 1978). The significant advantage of this method is to eliminate the need for fluid volume elements around the structure. It applies wet-surface response variables to model the surrounding acoustic medium interaction with the structure. Combining the benefit of boundary element and finite element method LS-DYNA, USA allows to simulate the elastoplastic response of floating and submerged structures to UNDEX. A parametric study is conducted to find the effects of different parameters like initial pressure or initial velocity of the primary shock wave, shock factor, treatment of the fluid domain, (Double decay or simple decay), Anisotropy of material. Further an investigation is conducted with low shock factor pressure wave on the laminated and sandwich composite cylindrical shell structure. After reviewing the existing material models available in LS-DYNA material model reference, a suitable material model is selected with the convenience and the capability of the material model to simulate the composite structural response similar to the practical experiment.

The main focus of the study is to provide comprehensive details on the formulation of primary shock wave from the non-contact UNDEX and parameters affecting the dynamic response of steel and composite structure. It is expected that the analysis method and results could be applied to the related developing research in the future.

1.3 Objectives

This study will have two main objectives. *First*, evaluate the appropriate theoretical or analytical methodology to calculate the pressure evolution and the distribution of the primary shock wave from the side-on UNDEX with respect to time neglecting subsequent pressure pulsations from the bubbles. *Secondly*, to perform a non-linear dynamic finite element analysis of the immersed non-stiffened cylindrical shell structure, considering the application of the pressure load distributed over the entire cylindrical shell. To achieve the objectives, the corresponding work is divided into following steps:

1. Review analytical methodologies to calculate and validate the incident primary pressure wave from UNDEX.
2. Develop and Calculate pressure field for incident pressure wave using analytical approach and with different approximations in Scilab Program.
3. Comparing results from different approaches and select the most appropriate one. Here only first shock wave pressure field is considered for incident pressure

evolution during entire explosion.

4. Incorporating Fluid-Structure Interaction to obtain final one sided blast pressure loading to the structure finite elements (Cylindrical Shell) submitted to UNDEX.
5. Validate the calculated pressure field and the methodology by analysing the structural response from LS-DYNA and LS-DYNA/USA.
6. Considering Low and High Shock factors with a given standoff distance the resulting pressure field of primary shock wave from UNDEX is applied on monolithic material structure *i.e.* Steel cylindrical Shell Structure immersed in infinite fluid medium (sea or ocean). Post-Processing the response of the structure and compare the results with the calculation LS-DYNA/USA.
7. Review existing material models available in LS-DYNA for modelling laminated composite structure and influential parameter of the models affecting the results and the response of the structure.
8. A suitable material model is selected with the convenience and the capability of the material model to simulate the composite structural response similar to the practical experiment.
9. Further an investigation is conducted with low shock factor pressure wave on the laminated composite cylindrical shell structure without failure. However, it will be the future work to validate the numerical analysis by experiment and the analysis of the post failure response of the structure.

1.4 Work Flow

The following flow chart is a general guideline for the FEM simulation throughout the numerical process,

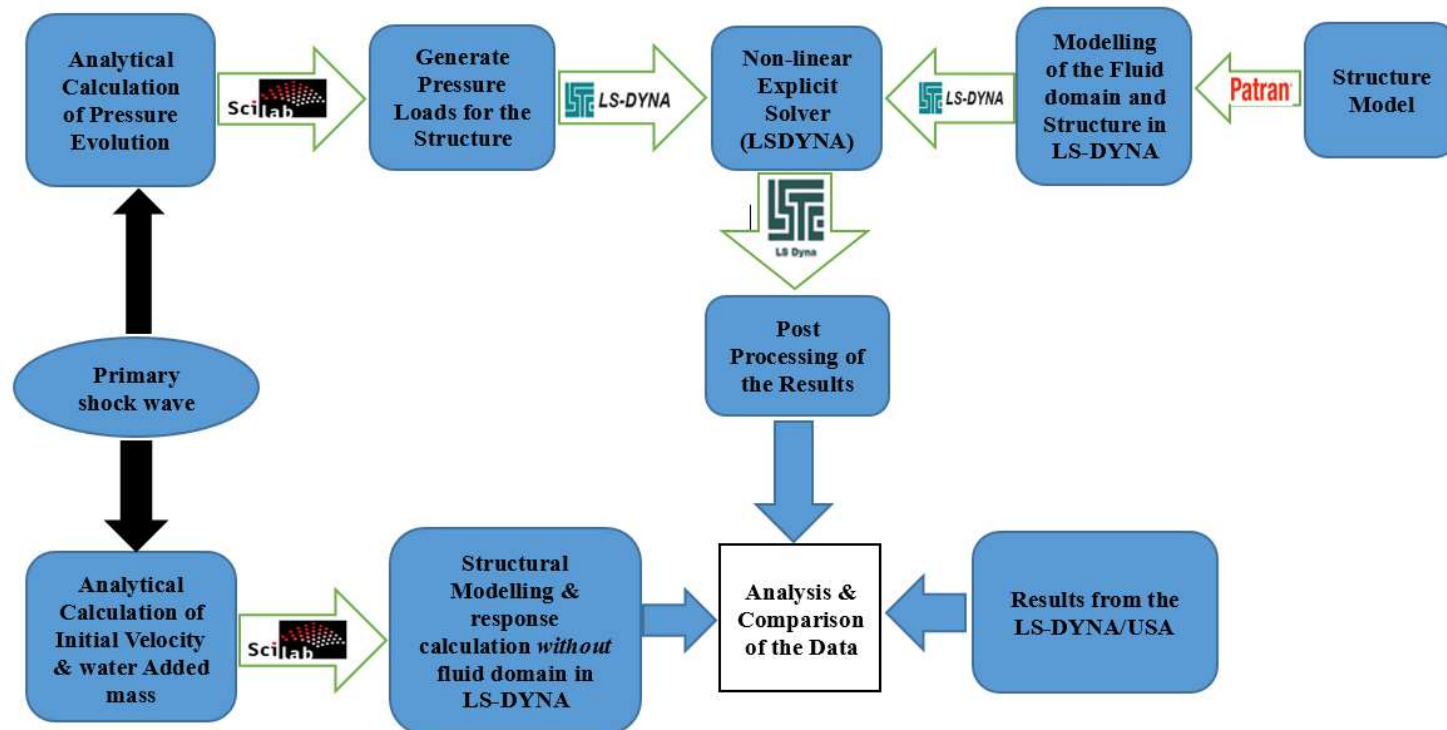


Figure 1.4-a LS-DYNA modelling and simulation process.

The simulation in LS-DYNA will consist of three main steps:

- Creating a model using the MSC PATRAN (the pre-processor of NASTRAN)
- Boundary conditions, Material definition, Prescribing loading on the structure etc. through LS Pre-post.
- Simulating finite element model with non-linear explicit solver LS-DYNA.
- Post-processing with LS-DYNA post-processor LSPOST to obtain/review the simulation results.

In the Scilab Programming software the pressure field coming from the shock wave is calculated with the help of analytical formulation and a keyword file is generated to include in the numerical calculation.

2 UNDERWATER EXPLOSION THEORY AND MODELING

The subsequent reviews have been analysed and collected from Snay (1957), Keil (1961) and Holt (1977). Improvements in computational technology and instrumentation are providing more penetrating insights of dynamic events like underwater explosion and the structural damage due underwater explosion. Complex fluid dynamics associated to underwater explosion is becoming more amenable in the realm of advanced numerical simulation with the advancement of computing power and numerical computing methods (Mair, 1999). Even though, many complexities of underwater explosion is yet to solve, precisely fluid-structure interaction and the bubble dynamics.

2.1 Sequence of events

Reid and Mehaute et. al. (1996) explained the underwater explosion as a highly energetic thermos-chemical reaction in the water. As a result, a superheated, highly compressed gas bubbles are formed and a shock-wave released in the surrounding water. Underwater explosion and the air-blast are comparable with respect to the initial detonation result i.e. release of shock-wave to surrounding medium and the formation fireball of detonation-product of gases. However, due to physically different surrounding medium the structural loading and the subsequent events of underwater explosion is significantly different. The higher density (lower compressibility) of water do not allow the fireball gases to mix immediately into the water. So the isolated gas bubbles contain a substantial amount of energy which later on empowers additional loading mechanisms. It is also obvious that the evolution of bubbles occurs over a slower time than the shock-wave although the whole process is a rapid event. So underwater

explosion produces more catastrophic structural damage if compared to similar size structure at middle air.

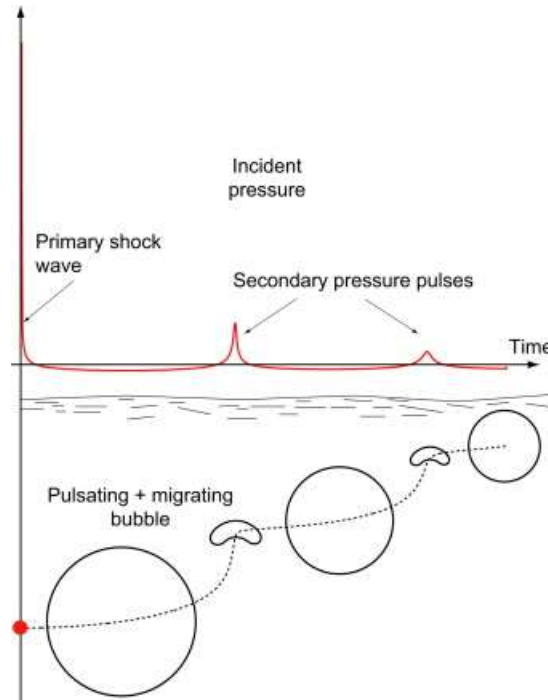


Figure 2.1-a Schematic representation of shockwave and Gas bubble pulsation with respect to time evolution and exponential decay of pressure field of UNDEX. (Keil, 1961).

The exponentially decaying shock wave propagates much faster than the speed of sound as a spherical pressure wave. The propagating velocity drops to acoustic level about 10 charge radius from the detonation point (Cole, 1946. Shin, 2004). Simultaneously, the gas bubbles starts expanding in size and the pressure in the bubble reduces. This expansion of the bubble continues until the hydrostatic pressure in the surrounding fluid medium will impede the expansion. After this stage of bubble growth the surrounding water flows or pressurize (hydrostatic pressure $>$ gas bubble pressure) the bubble to contract inwards and it continues till the energy released from the explosion catches up. This cycle of expanding and contracting is characterized by fluctuation of pressure called pulsations. Due to the influence of gravity the bubble also migrates upward during this pulsation process.

2.1.1 Shock Wave

After the detonation of explosion, the released shock wave attain a peak pressure and exponentially decays up to hydrostatic pressure in the surrounding medium. Primarily the peak

pressure is proportional to velocity (up to 68.95 MPa) (Reid, 1996). The mathematical expression of the peak pressure is explained by Cole (1946),

$$P_0 = f\left(\frac{W}{R}\right) \quad (1)$$

Where W is the weight of charge and R is the standoff distance at the point being measure. The formulation described by (Reid, 1996),

$$P_0 = K_1 \left(\frac{W^{1/3}}{R}\right)^{A_1} \quad (2)$$

P_0 is the **peak pressure** in MPa, W is the weight of charge (TNT) in Kilograms, and R is the Stand-off distance in meters. The pressure follows an exponential decay defined by the equation:

$$P_m(t) = K_1 \left(W^{1/3}/R\right)^{A_1} \cdot e^{-(t-t_0)/\theta} \quad (3)$$

Where, $P_m(t)$ is the free field pressure. t_0 is the initial time when the shock wave arrives at the distance R and t is the time elapsed since the shock wave arrives the distance R . θ is the decay time constant in other words it is equivalent to the time period that required for the pressure to decay ($1/e$).

$$\theta = K_2 W^{1/3} \left(\frac{W^{1/3}}{R}\right)^{A_2} \quad (4)$$

The blast impulse function can be explained as the integral of the pressure along the time lapse of the blast,

$$I(t) = \int_0^t P(t) dt \quad (5)$$

That can also be expressed as:

$$I(t) = K_3 W^{1/3} \left(\frac{W^{1/3}}{R} \right)^{A_3} \quad (6)$$

The shockwave energy can be defined as the energy available per unit of area or the work done over a surface. It can be expressed using the following equation.

$$E(t) = \frac{1}{\rho c} \int_0^t P(t)^2 dt \quad (7)$$

In the same way:

$$E(t) = K_4 W^{1/3} \left(\frac{W^{1/3}}{R} \right)^{A_4} \quad (8)$$

Mathematical expressions for other type of explosive can be obtain from the coefficients listed in the Table 2.1-a. The equivalent equations for other type of explosives are defined as similitude equations.

Table 2.1-a Equivalent coefficients for similitude equations (Reid, 1996).

	Coefficient	HBX-1	TNT	PENT	NUCLEAR
Shock-wave	K1	53.51	52.12	56.21	1.06E4
Pressure	A1	1.144	1.18	1.194	1.13
Decay	K2	0.092	0.092	0.086	3.627
Constant	A2	-0.247	-0.185	-0.257	-0.22
Impulse	K3	7.263	6.52	6.518	4.5E4
	A3	0.856	0.98	0.903	0.91
Energy Flux	K4	106.8	94.34	103.11	1.15E7
Density	A4	2.039	2.155	2.094	2.04
Bubble Period	K5	2.302	2.064	2.098	249.1

Bubble Radius	K6	3.775	3.383	3.439	400.5
---------------	----	-------	-------	-------	-------

The shock wave will propagate from the point of detonation to either its target that is a surface ship or submarine or reflected from the seafloor or air-water interface. Shock wave reflected off the seafloor initially remains compressive and transmit or reflect according to Snell’s law,

$$\frac{C_0}{\sin \alpha} = \frac{C_0}{\sin \alpha'} = \frac{C_0}{\sin \alpha''} \tag{9}$$

Where, C_0 is the speed of sound for a given medium and the three angles are shown in Figure 2.1-b Snell’s law (Shin 2004)Figure 2.1-b below.

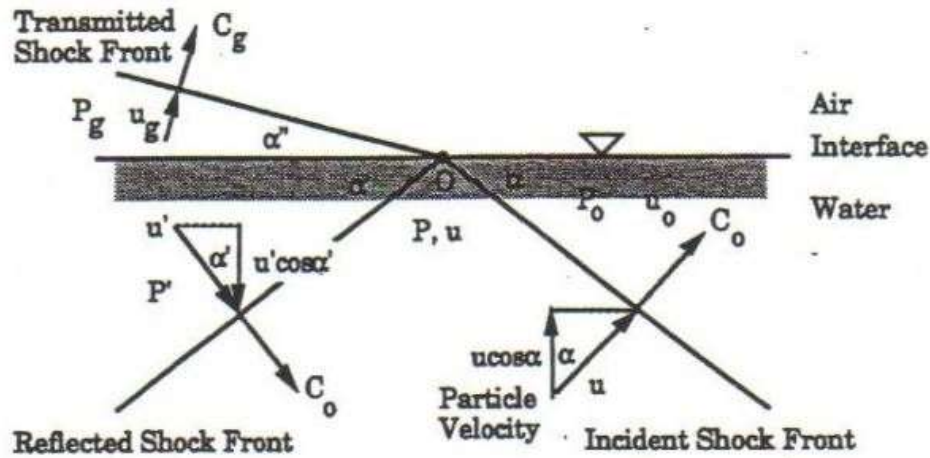


Figure 2.1-b Snell’s law (Shin 2004)

On the other hand, the reflected part from the air-water interface termed as surface reflection or rarefaction waves become tensile in nature. These reflection waves also transmit accordance with the Snell’s law. The direction and magnitude of these waves are estimated by considering a mirror view of the whole scenario below the air-water interface. Here an ‘image’ charge is considered at an equidistant of the charge below the waterline. In Figure 2.1-c the ‘image’ charge and Snell’s law for both reflected waves from the bottom and air-water interface is illustrated.

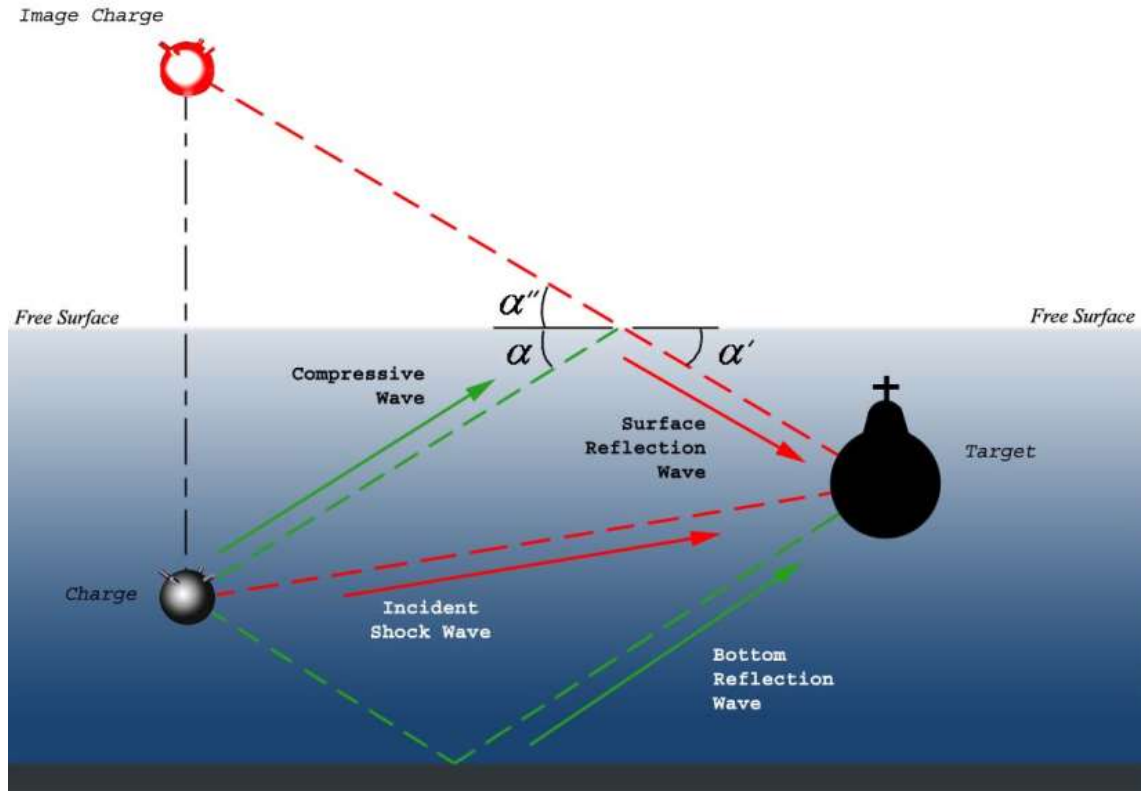


Figure 2.1-c. The 'image' charge and Snell's law for both reflected waves from the bottom and air-water interface (Shin 2004).

It is remarkable that the tensile wave induced tensile force in the water. And consequently it causes a foamy appearance near the air-water interface. This phenomenon is known as Bulk Cavitation, where the pressure of the water is equal to zero. Figure 2.1-d and Figure 2.1-e shows this phenomenon.



Figure 2.1-d Bulk Cavitation as a result of UNDEX

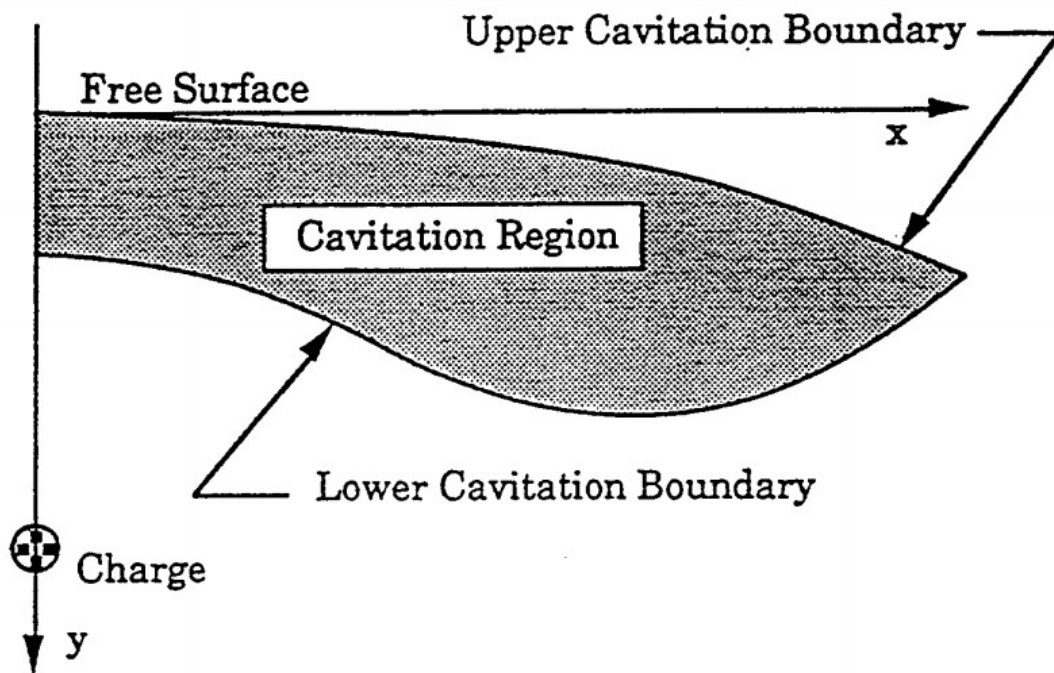


Figure 2.1-e Bulk Cavitation Region

2.1.1.1 Load Modification from Structural Response

Bulk cavitation will directly affect the structure which is close to the water surface. However for rapid deformation of the submerged structure in the response of shock loading will release a tension wave back into the water. The tension wave will cause the water to cavitate. This phenomenon is restricted to the immediate vicinity of the responding structure. So that it is known as local cavitation. The local cavitation will decoupled the structure from the water in the case of bulk cavitation and protect the structure from further loading by the incoming tail of the shock wave. In addition, the collapsing local cavitation can also reload the structure. However, it is worthy to note that local cavitation near the structures is not limited to shallow water depth (Cimpoeru, 2017). Figure 2.1-fF illustrates the formation of local cavitation near the surface of a steel cylinder subjected to the shock wave from the underwater explosion at a standoff distance of 7.5 cm.

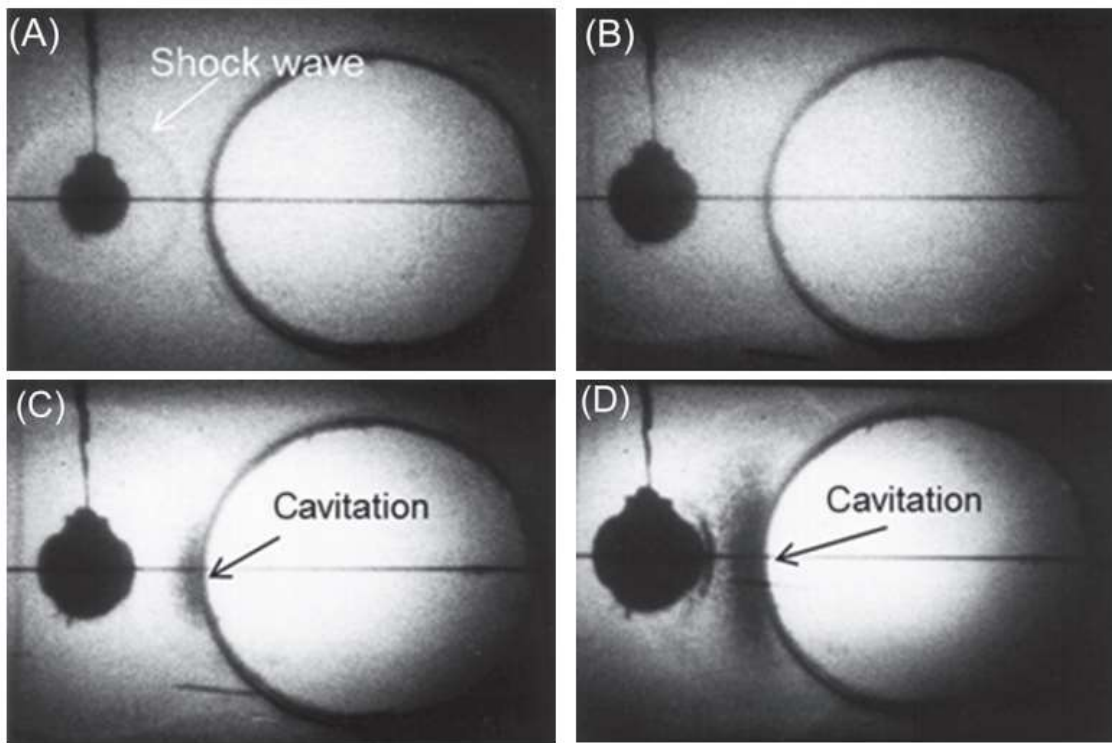


Figure 2.1-f Formation of local cavitation near the surface of a steel cylinder subjected to the shock wave from the underwater explosion (OD 273 mm and wall thickness 2 mm). The images at times (A) 25 μ s, (B) 45 μ s, (C) 55 μ s, and (D) 75 μ s viewed down the axis of cylinder. In the images the dark area at the surface of the cylinder is local cavitation zone. (Cimpoeru, 2017).

2.1.2 Gas Bubble

The time intervals between the propagation of shock wave and the subsequent pulses are the function of charge weight, type of explosive and depth of the charge. After the detonation of the explosives, gaseous products of the charge is released. These gas bubbles starts expanding in size and the pressure inside the bubble reduces as compared to outside. This expansion of the bubble continues until the hydrostatic pressure in the surrounding fluid medium will impede the expansion. After this stage of bubble growth the surrounding water flows or pressurize (hydrostatic pressure > gas bubble pressure) the bubble to contract inwards and it continues till the energy released from the explosion catches up. This cycle of expanding and contracting is characterized by fluctuation of pressure called pulsations. This pulses also create expanding bubbles of lesser magnitude. Now the shock waves are releasing from the oscillating bubbles and thereby the term shock wave is replaced by the term pulse. Compared to initial shock wave the bubble pulses are lower in magnitude but exists with a longer duration.

The maximum radius of the bubble can be obtained by:

$$R_{max} = K_5 \left(\frac{W^{1/3}}{Z_0^{1/3}} \right) \quad (10)$$

The hydrostatic pressure, $Z_0 = (D + 9.8)$ at the point of the explosion. The time to obtain the maximum radius T,

$$T = K_6 \left(\frac{W^{1/3}}{Z_0^{5/6}} \right) \quad (11)$$

Due to the influence of gravity the bubble also migrates upward during this pulsation process with varying speed. This varying speed is as result of drag force on the bubble. In the post detonation phase many bubbles are created and these bubbles dissipate their energy by creating more smaller bubbles or reaches the surface and releases to the atmosphere (Snay, 1957). Depending on the water depth the upward moving bubbles can cause different disruptions of the water surface due to the bubble dynamics. If the depth of the charge is not great enough, a large plume of water can be seen at the water surface.

2.2 Shock Factor

The function of shock factor (SF) is to express the severity of the attack from the underwater explosion to categorise different scenarios of underwater explosions (Keil, 1961). The shock factor takes in to account the standoff distance, the relation between the shock velocity and geometry of the ship, the power of the explosive and the point of detonation. The SF can be determine as:

$$\text{Maximum SF} = \frac{W^{1/2}}{R} \quad (12)$$

If the angle of incidence for shock wave is taken into account then the formula can be rewritten as (Liang & Tai, 2006):

$$SF = \frac{W^{1/2}}{R} \frac{(1 + \cos \theta)}{2} \quad (13)$$

Figure 2.2-a represents the angle of incidence for shock wave on the surface of the structure and the explosion standoff distance.

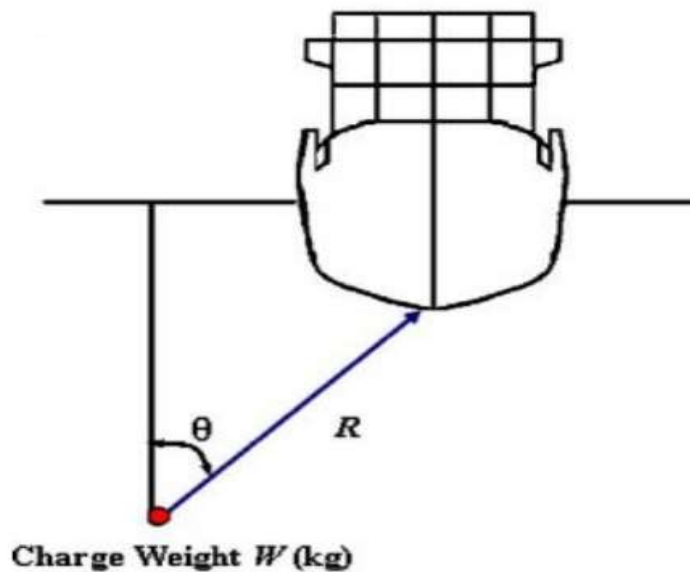


Figure 2.2-a Geometry layout of the problem for angle of incidence for shock wave on the surface of the structure and the explosion standoff distance. (Liang & Tai, 2006).

It is interesting to observe that a small charge near the structure can produce same SF as a much bigger charge further away from the structure. However, the structural response for this two cases will not be same. The bigger charge will have longer impulse time which might create bigger damage (Reid, 1996). Similarly the smaller charge with same SF will induced bigger bending moment as result of its smaller curvature and the difference in lead time at fore and aft part compared to amid ship.

3 REVIEW OF THEORETICAL AND COMPUTATIONAL STUDIES

Under the consideration of the scaling system of the marine structure, the theoretical and computational review on the response of blast loading can be classified in to two major categories.

More specifically,

- a. Modelling of plate/shell-like panels subjected to blast loading which covers a large amount of research work;

Whereas,

- b. Analysis of the full-scale marine structure response under blast loading which cover only a few research efforts.

The ad-hoc developed computational mechanics suites or commercial finite element codes are applied with the basic concept of plate and shell theories for predicting the structural response under the blast load. Full scale structural analysis are obviously conducted with commercially available finite element codes.

3.1 Analysis of Marine Panels

3.1.1 Panel Response to Free Field Blast Loading

Cole et al. (1965) followed a traditional approach for marine structural panel for blast loading. In this effort the panel was subjected to a time dependent uniform pressure blast loading where the peak pressure exponentially decays with time. The pressure in that case,

$$P(t) = P_m e^{-t/\lambda} \quad (14)$$

Where,

P_m = Initial peak pressure

t = Time variable

λ = Time constant of Exponential decay. It is equivalent to the time period that required for the pressure to decay($1/e$).

The relation between the peak pressure and the exponential decay rate of the impulse load can be expressed as,

$$P_m = K_1 \left(\frac{W^{1/3}}{R} \right) \quad (15)$$

$$\lambda = K_2 W^{1/3} \left(\frac{W^{1/3}}{R} \right)^{A_2} \quad (16)$$

Where,

R = Standoff distance (SoD),

W = Explosive charge weight

K_1, K_2, A_1 and A_2 are constants which are dependent on explosive charge.

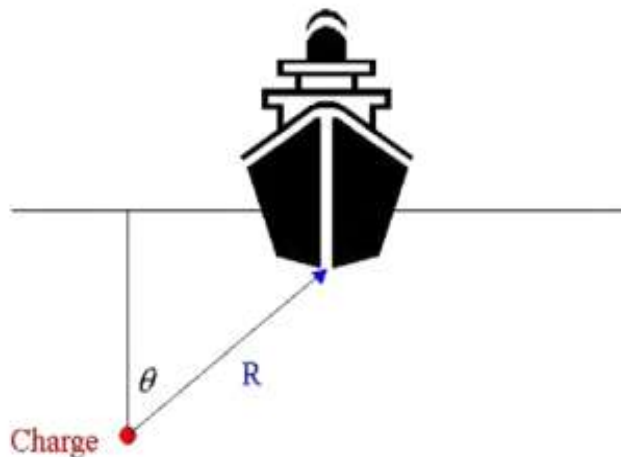


Figure 3.1-a Diagram of a ship structure subjected to underwater explosion (Mouritz, 1995)

The blast pressure accelerates the fluid particles to move away through the blast wave from the detonation source. As a result the fluid behind the blast wave under goes to tensile condition with drop in pressure below the ambient pressure. Therefore, the shock wave deviates from the defined exponential curve after passes of sometime and ultimately reaches to a “negative” pressure region crossing the zero gauge pressure. The modified Friedlander exponential decay equation explains this phenomenon clearly (Gupta, 1987). This is used to analyse the response of the homogeneous panels. A solution of single degree of freedom (DoF) response is obtained for the simply supported plates under the blast loading with the help of classical plate theory and modal analysis. Theoretical results are compared with the finite element simulation using ADINA for both linear and non-linear material and geometric conditions. Linear finite element simulation of single dof panel model accurately predicts the deflection time profile of the plate. Although, the simulation results indicates that the deflection of the centre part of the plate can be reduced under the influence of membrane stretching of the plate and it can be increased due to the early plastic behaviour of the material. Response of the homogeneous cylindrical shell element is also analysed with the modified Friedlander equation (Jiang, 1991).

In the finite element approach a one-dimensional mesh along with shell bending modes are applied to develop reduced order models. With the consideration of beam stiffener effect, the results indicate that it is possible to generate accurate response of the shells even with a single bending mode in blast loading. Simplified Cole exponential decay equation is used to model the blast loading under the effect of stiffening element (Louca, 1998). This equation consists of a single triangular pulse.

On the other hand, von-Karman plate theory is applied for modelling unstiffened plates and the response was investigated by modal analysis. However, finite element codes DYNA3D and ABAQUS/Explicit is used for stiffened plates. Louca et al (Louca, 1998) presented a parametric study to investigate the importance of in-plane boundary conditions, initial imperfection and stiffener buckling effects.

Laminated composite plates are also analyzed with the modified Friedlander exponential decay equation [10]. In this case, the response of the blast loading for the laminated composite plates are compared for different plate theories. To be precise, the linear response of laminated composites with moderate thickness are studied for classical, first order and higher order plate theories in blast loading.

A brief analysis about underwater explosion, failure and damage mechanisms was dealt in the research work of Keil (1956, 1961). In the literature a series of investigation was conducted for air-blast response on the stiffened and unstiffened plates and beams. There is a limited number of work done on the cylindrical panels with underwater explosion. Menkes and Opat (1973) explained three different failure modes a) large deformation, b) tensile tearing and c) shear failure for clamped beams subjected to explosion. Reference (Klaus, 1985, Nurick, 1995) presents the similar failure modes for unstiffened and stiffened plates to air blast loading.

Acceleration and velocity responses of different marine structures such as frigate, cruiser and submarine in different positions are studied in the research work of Harres and Cheneau (1963) from the shock trial data of France Navy. They also studied the measuring equipment for these trials and their fitness. Oleson and Belsheim (1976) reported about the velocity response of large surface naval vessel like aircraft carrier. In recent years, flat plate response from the UNDEX was reported in the systemic experimental investigation of Rajendran et al. (2001, 2006-09). The major damage mode was identified as the ductile failure of rectangular and circular flat plates. These failed samples were examined based on the technology of Scanning Electron Microscopic (SEM) fractography. Rentz (1985) explained the experimental elastic-plastic dynamic response and failure mode analysis of submerged stiffened plate. Comparison of the experimental observations and the Non-linear finite element calculation with ESPA code was conducted. Results showed that the effect of FSI is not significant for water-backed thin plate submitted to UNDEX shock wave. Presented in Ref (Hung, 2009) an experimental study of three types cylindrical shell structure subjected to UNDEX to investigate the transient dynamic responses. Also a number of experiments on a submerged cylindrical shell subjected to bubble collapse loading for UNDEX have been reported in the literature (Brett, 2000, 2008). Despite the fact that, the maximum pressure of the UNDEX bubble pulsation is 10%-20% of the shock wave the bubble pulsation and the collapse jet force may be the most severe structural load. It is generating high accelerations and plastic deformations when bubble pulsation reached the eigen frequency of structure. Most of the discussions are available for far-field and contact UNDEX while there is few related to close-in non-contact UNDEX events. Wardlaw and Luton (2000) adopted the DYSMAS/L (Lagrange method) and GEMINI (high order Godunov method) codes to explain the FSI for close-in explosion. The comparison between explosion experiment conducted with water filled cylinders and the numerical results indicates that there is a significant role of cavitation and the cavitation in cylinder flow field. Zong, Zhao and Li (2013) investigated the close proximity UNDEX shock wave response of a whole ship structure. The numerical analysis with ABAQUS/Explicit code

with acoustic-structure coupling (ASC) method conducted the failure analysis on a verification numerical model. Three potential failure mode was reported such as the dishing deformation, the buckled frame deformation and the bottom-indenting deformation of the ship structure. This close-in torpedo explosion structural damage evolution provides valuable information for naval anti-shock design. However, the bubble pulsation was neglected in this analysis.

A brief analyses of underwater explosion on circular and rectangular plates are conducted with ANSYS/LS-DYNA for elastic and in-elastic response in the research work of Rajendran (2009). Gupta (2010) reported the failure modes of stiffen and unstiffened square plate with isotropic hardening, strain rate effects and fracture criterion. Qiankun and Gangyi (2011) predicted the shock response for a ship section using ABAQUS for non-contact UNDEX. The results point out that the improvement of numerical accuracy strongly influenced from the fluid mesh size and the thickness of the fluid layer around the structure. Rajendran and Narasimhan (2001) reported the damage response of clamped plates subjected to contact underwater explosion. The reference Jacinto et al. (2001) presented the linear dynamic analysis using ABAQUS for a plate model submitted to UNDEX. Zhang et al. (2014) adopted the DAA method coupled with finite element method for explaining the transient dynamic response of a surface ship subjected to UNDEX bubble. The vertical response of the ship due to underwater explosion Bubble is the combination of rigid-body motion and elastic deformation, which is mainly a global response.

Forghani et al. (2007) presented the damage evolution of composite laminates submitted to blast loading in LS-DYNA. The composite laminates are modelled with the Tie-break contact interface to simulate cohesive cracks during the delamination. Chirica and Boazu (2012) investigated the damage development in ship hull laminate plates subjected to the blast loads in COSMOS/M finite element code. They considered various scenarios such as explosive magnitude, distance from source of explosion, and plate thickness to evaluate the response behavior of the laminated plate. A transient dynamic response of a midget submersible vehicle (MSV) pressure hull was analyzed Jen (2009) using ABAQUS when it experiences an acoustic pressure shock wave resulting from an underwater explosion. Jen reported the presence of local cavitation due to the interaction between the midget submersible vehicle structure and the shock wave from the UNDEX. The aim of this study is to improve the dynamic response of a structure subjected to underwater explosion and to design an optimal configuration of a stiffened plate to resist UNDEX shock loading.

An alternative numerical-experimental approach is followed for the response prediction of the composite marine structure in the literature of Houlston et al. (1985, 1991, and 1993). Here rather than using a pre-defined model an in-situ experimental observation is used to modify the pressure profile of the structure. This provide a significant source of validating analytical models where the pressure profile agrees with both experimental measurement and the modified Friedlander exponential decay rate in both cases of stiffened and unstiffened plates. A comparison of the experimental measurements and the predictions from the numerical results (finite element code ADINA) based on the linear classical plate theory and von-Karman plate theory for a square steel plate (*Dimensions: length of 508 mm and thickness of 3.4 or 1.5 mm*) and a full scale stiffened plate (*in-plane dimensions of 4.57× 2.44 m and thickness 6.35 mm*) is presented in the research work of Houlston et al. (1985). For unstiffened *square plate*, the numerical result with linear classical plate theory shows close agreement with experimental computation although the full scale stiffened panel has reasonable response with respect to membrane stretching. The detail review work of finite element procedure presented in the scientific literature of Houlston et al. (1985), can be useful for enhancing the accuracy of the numerical solution with respect to the experimental result.

Batra et al. (2007) explains the blast pressure evolution in the fiber reinforced laminated composites subjected to blast loading by using comprehensive nonlinear model. This model elucidate the mechanics such as matrix cracking, fibre/matrix deboning, fibre breakage and delamination/sliding from the point of view of continuum damage mechanics. Classical exponential decay equation is applied for modelling the blast and a parametric study is conducted to with an in-house developed 3D finite element code in Fortran to investigate the effect of composite energy dissipation with respect to geometric and material properties of the composites (Hassan, 2008). Some response observation of the *rectangular four-ply laminate* composite specimen subjected to the blast loading,

- I. *Specimen's centroid*: fibre breakage is concentrated near the centroid of the specimen
- II. *Centre of the specimen's back surface*: initiation of matrix cracking initiates at the centre of the back side of the specimen's surface.
- III. *Along the fibre of the laminate*: fibre and matrix separation or deboning takes place along the fibre.
- IV. *Delamination or sliding of the plies*: Delamination or sliding of the plies absorb insignificant amount of energy from the blast pressure on the structure.

- V. *Maximum portion of energy absorption:* It is found that the stacking sequence of the plies is the significant parameter for influencing major energy absorption.
- VI. *Failure Mode prediction:* thickness of the plies is the dominant parameter that directs to the relevant mode of failure.

Gupta et al. (2007) studied the circular homogeneous plate response against the blast with different support configuration and blast loading is modelled as a uniform pulse. It also considers the large plastic deformation. For numerical technique, ANSYS computer code results for clamped plates are compared with experimental observations and precisely with respect to the different failure modes, large plastic deformation, shear and tensile stresses. The significant finding is the improvement of the plate energy absorption due to the presence of ring support and allows large plastic deformation before failure. Shear hinges are also studied as additional failure mode (Li QM, 1999).

3.1.2 Fluid–Structure Interaction in Sandwich Composites

In this literature review so far, the interactions of shock wave and the structure are not taken in to account whereas the impulsive loading is a separate input to the structural model. But it is not the ideal case to neglect the fluid marine structure interaction in blast loading. As reflection and the transmission of energy incidents are key role playing characteristics while investigating the panel deformation through the thickness in the fluid and sandwich structure interaction. Hayman et al (1995) describe the uniform pressure on the front facing panel as the sum of following contributions,

- I. Free-field pressure, it is as a result of incident wave
- II. Pressure reflected on the front face and Pressure transmitted through the panel
- III. Pressure reflected by the rear face of the panel and travels back to the fluid.

Batra et al. (2008) discussed an equivalent pressure (maximum pressure) term as the Free-field pressure (incident pressure) and the magnitude of the other pressure can be calculated from a one dimensional wave propagation problem. These competing terms in the blast loading problem can lead to the cavitation zone in the vicinity and away from the structure.

Librescu et al. (2006) followed the approach of Hayman et al. (1995) to investigate the response of sandwich structure in-air and underwater explosion. The model is adopted with classical laminated theory and membrane stretching is considered through the von-Karman nonlinearity. The remarkable observation was the influence of the core material characteristics

on the time history of the pressure distribution due to the blast loading. Weak core material can significantly alter the pressure time history. So it is possible to maximize the time history or the delay between the shock wave impact and the cavitation by tailoring the core material properties. Thereby it is an essential parameter to consider Anisotropy of face sheets and core material. Considering the modified Friedlander exponential decay equation, the core material property is insignificant in the case of in-air blast. This is evident in the study of sandwich structure composed of graphite/epoxy face sheets and PVC foam core material. *Slamming* impact on the *sandwich composite hulls* are studied with the identical framework in the literature of Qin et al. (2009) and fluid structure interaction on thick *cylindrical shells* are observed in the research work of McCoy et al. (1997).

Makinen et al. (1999) use a distributed one-dimensional model for both fluid and composite structure to analyze the response of the sandwich panel. In this model the fluid motion in terms of pressure and velocity in the direction of thickness was elucidated with one-dimensional linearized acoustical formulation, see for example (Taylor, 1963). As a vibrating segmented bar the transverse motion of the panel was modelled. From the results it is evident that the potential delamination is the consequence of the significant oscillation of the composite face sheet leading to considerable rate of strain in transverse direction.

3.2 Full-Scale Marine Structures Analysis

Liang et al. (2006) presented the transient dynamic response of full-scale steel and aluminum petrol boats under the blast loading (underwater explosions). In the Figure 3.2-b, the finite element solution considers the elastoplastic response and large deformations. And the fluid structure interaction is taken into account by coupling a boundary element formulation from fluid dynamics problem with the finite element analysis. The scattered wave pressure acting on the wetted surface of the ship is determined by the doubly asymptotic approximation. KSF (keel shock factors) are used to measure the shock severity. KSF depends on the explosive charge weight W , the standoff distance (SoD) from the charge to the structure R , and the angular distance between the perpendicular to the water surface and the line drawn from the charge location and the keel of the ship θ .

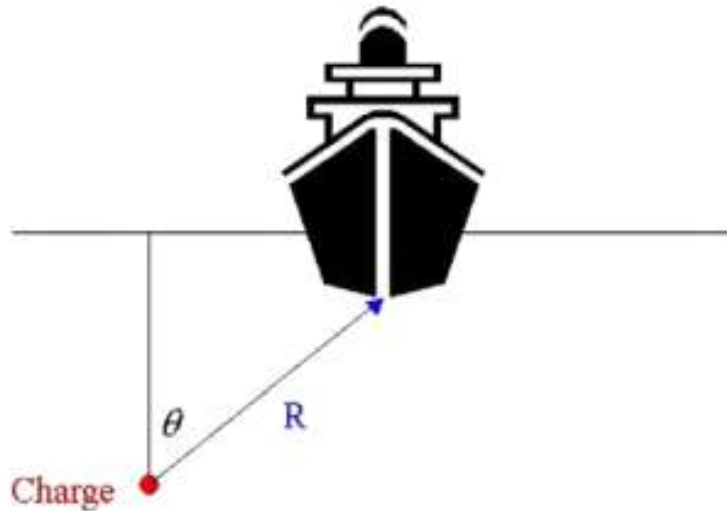


Figure 3.2-a Diagram of a ship structure subjected to underwater explosion (Mouritz, 1995)

More specifically,

$$KSF = 0.5(1 + \cos \theta) \sqrt{W/R} \quad (17)$$

In this investigation the ship geometric dimensions and specification is taken from the real design to simulate the numerical response to underwater explosion. For given KSF that means for a definite scenario such as if the charge is small and the SoD distance is long then it is more likely to damage the ship hull. Another scenario, when the charge is large and the SoD is shorter then it is more likely to damage the ship equipment. A similar approach is followed for a submersible composite hull of glass–epoxy to present the transient response to underwater explosion (Gong, 1998).

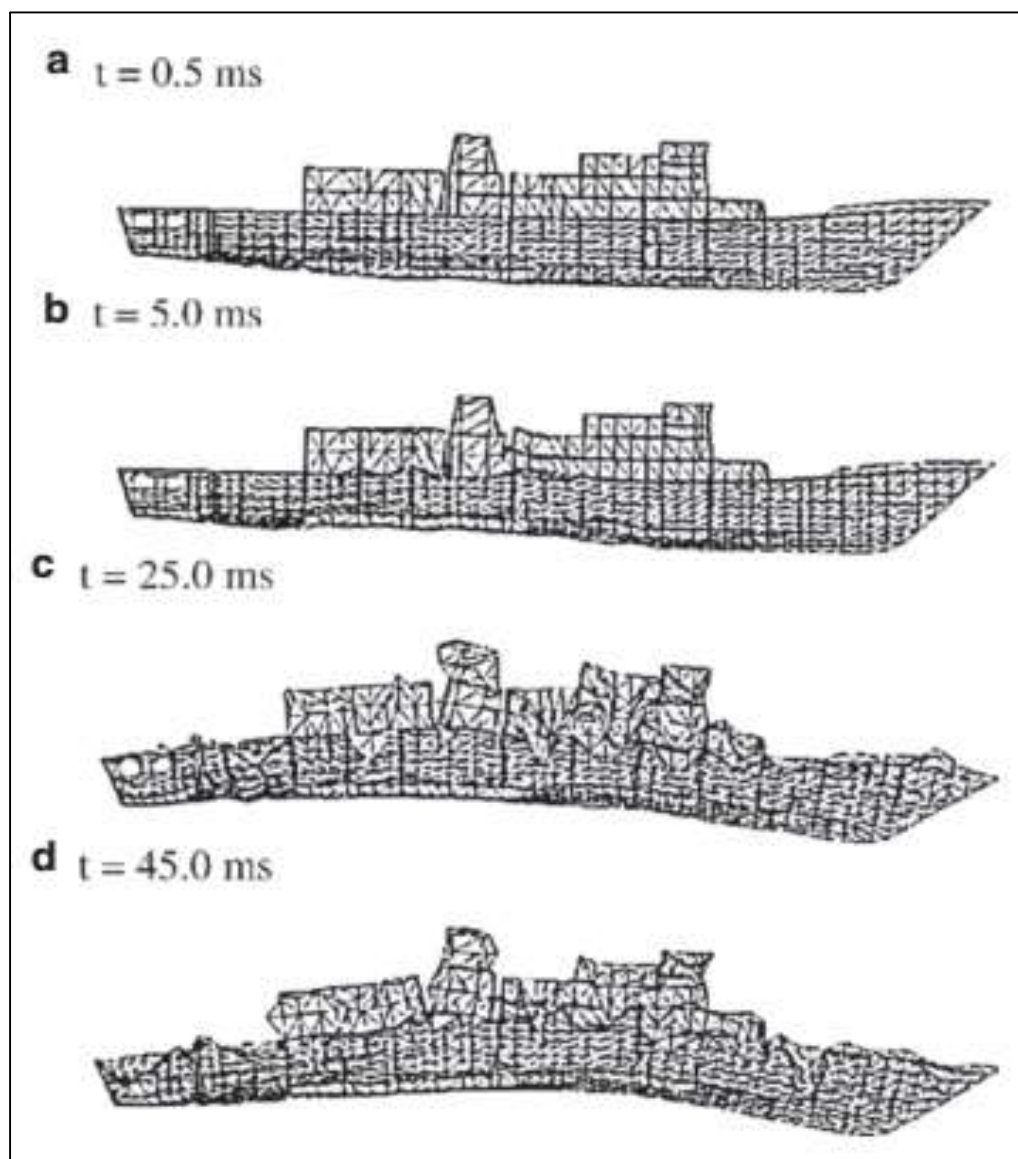


Figure 3.2-b The response of a full-scale petro boat model subjected to underwater explosion (Liang, 2006)

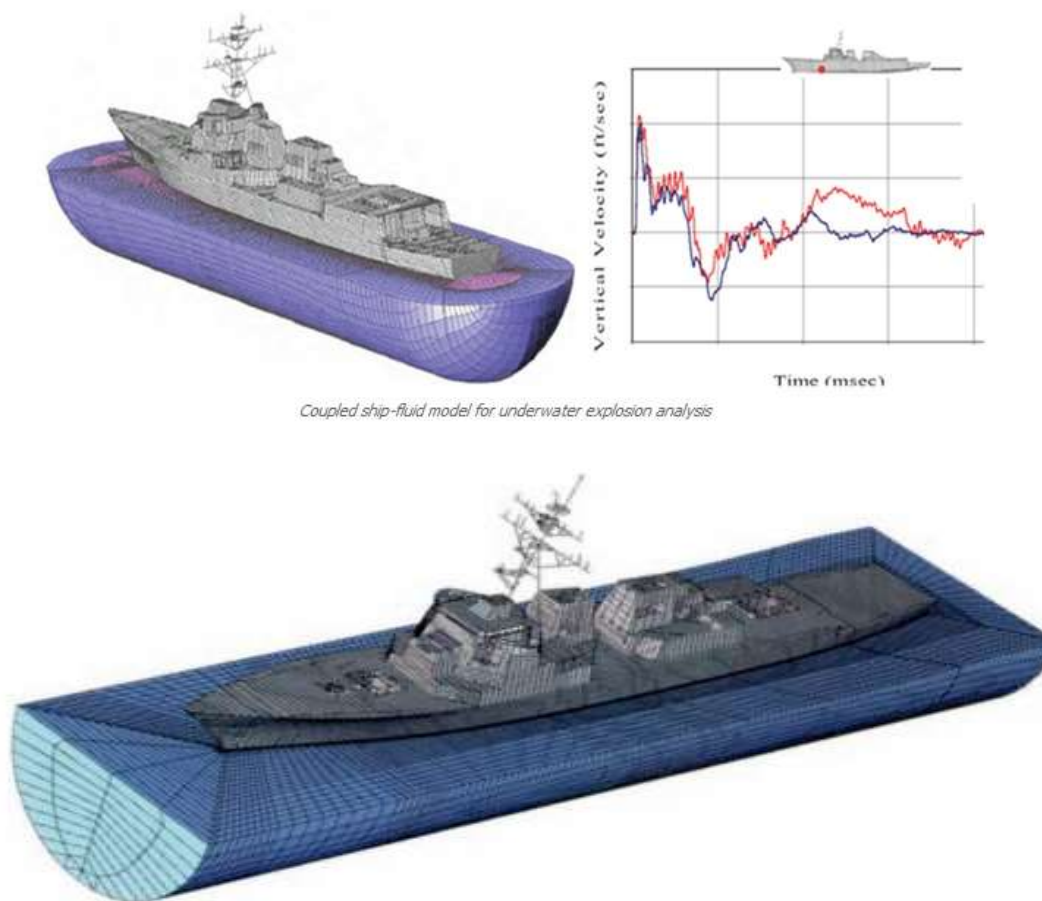


Figure 3.2-c Coupled Ship-fluid model for underwater explosion response analysis (Liang, 2006)

Moreover, Shin et al. (2006) consider the fluid perturbation due to the blast such as bubble pulse loading, fluid cavitation and gas bubble behavior to analyze the full scale ships response for the underwater explosion. LS-DYNA computer code is used to study the fluid and structure interaction near the hull (show in Figure 3.2-c) (Shin, 2006). In this numerical analysis the fluid response away from the structure is modelled by USA (Underwater Shock Analysis) code. USA code is based on the doubly asymptotic approximation. The presence of the far field infinite fluid medium beyond the finite element meshed fluid structure system is modelled with this boundary element code USA as a radiation boundary. The bulk and hull cavitation can be described by the fluid response, which is modelled by the simultaneous use of finite element and boundary element methods. At the early time the results obtain in the experimental ship shock test and the simulated velocity at the bulkhead and keel shows strong agreement but it deviates from it with the elapse time or with the time increases.

For sub-sea oil pipelines and stiffened shell elements are simulated with a similar approach based on the LS-DYNA/USA computer codes in the scientific review of Kwon et al. (Kwon, 1998) respectively to study the response for underwater explosion. In the reference (Zong, 1999) a classical Euler-Bernoulli beam theory based close form solution is used as the comparison criteria with the numerical results under low-frequency excitations. Then a probabilistic failure analysis is developed from the analytical and numerical results which is potentially extended to the ship structure. In the literature (Kwon, 1998), the dynamic response of the stiffened panel structure is analyzed with recommended smeared finite element models to develop a numerically efficient and accurate procedures for analyzing the response of marine structure. Kwon et al. (Kwon, 2008) introduce an alternative the Lattice Boltzmann Method to replace the traditional boundary and finite element methods for fluid structure interaction to investigate the fluid flow.

3.3 The UNDEX Loading for Numerical Analysis

In this study the primary shock wave released from the underwater explosion is considered as the main UNDEX loading on the submerged structure for analyzing the dynamic response. The Pressure field generated by the initial shock wave is calculated with the help of analytical formulation equation (14) and (15) with out considering fluid-structure interaction.

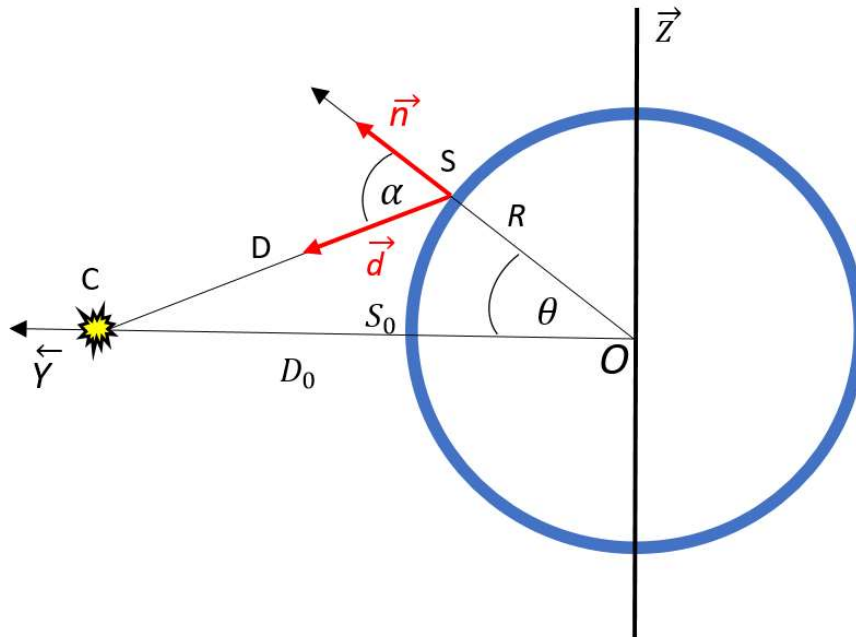


Figure 3.3-a Configuration of an Immersed Cylinder Subjected to an UNDEX.

A cylindrical Shell structure subjected to underwater explosion is considered for the numerical analysis. To calculate the UNDEX loading on the structure, the simplified formulations are described in the following discussion taking into account the geometrical configuration of the structural. The length of the cylindrical shell L , radius R and thickness h , clamped at both ends. The cylinder is filled with air and fully submerged in the Sea or Ocean. The mass of the explosive charge C detonates at a distance of D_0 from the standoff point S_0 as show in Figure 3.3-a. The incident pressure at point S from shock wave can be calculated with the following expression.

$$P_I = P_S e^{-t/T_S} \tag{18}$$

With

$$P_S = K_P \left(\frac{C^{1/3}}{D} \right)^{A_P} \tag{19}$$

$$T_S = K_T C^{1/3} \left(\frac{C^{1/3}}{D} \right)^{A_T} \tag{20}$$

Here,

P_I = Incident Pressure with an exponential decay in free field

P_S = Peak pressure in MPa

D = Distance between S and the charge location or Standoff distance (SoD)

C = Explosive charge weight

t = Time variable

T_S = Time constant of Exponential decay, it is equivalent to the time period that required for the pressure to decay(1/e).

K_P, K_T, A_P and A_T are characteristics parameters which are dependent on explosive charge. For the calculation, the typical values of these coefficient are used from the Table 3.3-a.

Table 3.3-a Typical values of characteristics parameters (Brochard, 2018)

Explosive characteristics parameters		Typical Values
K_P	Explosive characteristics coefficient	6.84E+7

K_T	Explosive characteristics coefficient	8.9E-5
A_P	Peak Pressure coefficient, (Pa)	1.178
A_T	Time constant coefficient, (Sec)	-0.284

For the further development, the fluid is considered as the inviscid, incompressible and infinite. So a potential flow can be assumed. Considering a point P located far enough from the charge, the pressure field inside the fluid also complies the Bernoulli linear equation. After the detonation the shock wave released from the underwater explosion and propagates through the water to impact on the shell structure. Due to the incoming shock wave through the water the interaction between the fluid and structure leads to a pressure which can be defined by the following mathematical expression (Cole, 1965),

$$\mathbf{p}(t) = \mathbf{p}_I(t) + \mathbf{p}_S(t) \quad (21)$$

Where, \mathbf{p} total pressure at point P, \mathbf{p}_I is the incident pressure at point P and \mathbf{p}_S is the scattered pressure at point P, which is the combination of a reflected wave on the cylinder when the structure is assumed to be fixed and rigid, and a radiated wave due to cylinder wall acceleration.

First of all, to calculate the applied pressure on each element of the finite element model, consider a single element at S in the Figure 3.3-a and the applied pressure on this element can be written as equation (22) (Hollyer, 1995). Equation (22) is derived by considering spherical wave approximation, where the incoming shock wave is assumed to be in spherical profile.

$$P_{element} = 2P_I(t) - \frac{\rho c v_s}{\sin \alpha} \quad (22)$$

Here,

ρ = Density of liquid, (kg/m³)

c = speed of sound in liquid

Assuming that the thick of the shell is uniform. Now introducing a non-dimensional number

$$\beta_s = \frac{\rho c T_s}{m \sin \alpha} = \frac{\beta}{\sin \alpha} \quad (23)$$

Here β_s represents the mass unit displacement by the shock wave in the normal direction of the shell element and $T_s = (D - D_0)/c$ is the time delay to reach the shock wave to the point S. Neglecting the time delay then the general solution of the equation for the velocity at point S can be written as,

$$v_s = \frac{2 \sin \alpha P_s}{m} \frac{T_s}{1 - \beta_s} (e^{-\beta_s t/T_s} - e^{-t/T_s}) \quad (24)$$

Thus, equation 22 can be rewritten as:

$$P_{element}(t) = 2P_I(t) - \frac{2\rho c T_s P_s}{m(1 - \beta_s)} (e^{-\beta_s t/T_s} - e^{-t/T_s}) \quad (25)$$

The second term of the equation (25) has a small value compared to the first term $2P_I(t)$, which makes it obvious that it has a negligible influence on the result (Tsai, 2017). So the second term on the right side of the equation can be ignored. Now the final simplified expression for the applied pressure on the each element can be written as,

$$P_{element}(t) = 2P_I(t) \quad (26)$$

The similitude relation is an accurate representation of the far field shock wave pressure profile (Cole, 1946. Farley and Snay, 1978. Price, 1979). Equation (18) calculates the pressure blast loading where the peak pressure exponentially decays with time. Here the peak pressure profile is decaying with single exponential fit. The single exponential fit is not capable to extend the pressure profile up to the start of oscillation phase (Geers, 2002). So double exponential fit is applied which extends up to the time when pressure is reduced approximately 5% of the peak.

Two good choices for $f(\tau)$ are,

$$\tau = \frac{t}{T_s} \quad (27)$$

$$f(\tau) = e^{-\tau}, \quad \tau \leq 1 \quad (28)$$

$$f(\tau) = 0.8251e^{-1.338\tau} + 0.1749e^{-0.1805\tau}, \quad \tau \leq 7. \quad (29)$$

With exception of small oscillation in the experimental profile the two fits are good in their respective ranges. This oscillation is a clear evidence of wave effects in the gas bubble (Geers, 2002). A higher order polynomial fit was constructed to the oscillation but the influence on these subsequent bubble motion was negligible. So the equation (29) was satisfactory for $\tau \leq 7$ (Geers, 2002). The equations (28) and (29) explain the condition for double decaying pressure profile, which is combined with the equation (18) and (26) to calculate the pressure field.

To simulate appropriate blast loading on the cylindrical shell, it is essential to take into account the angle of incidence for the incoming pressure wave on the cylindrical shell. Figure 3.3-a describes the geometrical configuration for the angle of incidence on the structure and the equation (26) can be re-write as,

$$P_{element}(t) = 2p_I(t) \left(\frac{1 + \cos \alpha}{2} \right) \quad (30)$$

Figure 3.3-b & Figure 3.3-c Presents the pressure profile induced by the initial shock wave from the UNDEX for SF 1.68 and 2.5 i.e. is for the charge of 0.5 kg and 1.1 kg respectively with consideration of Single Exponential Decay.

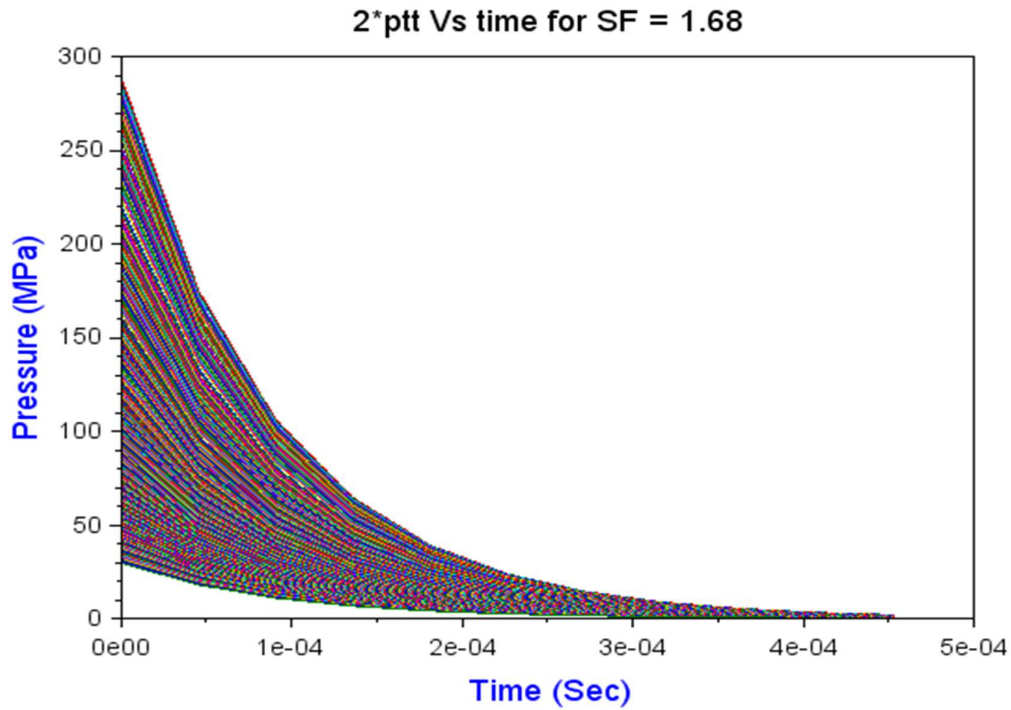


Figure 3.3-b Pressure profile for SF 1.68 with Single Exponential Decay

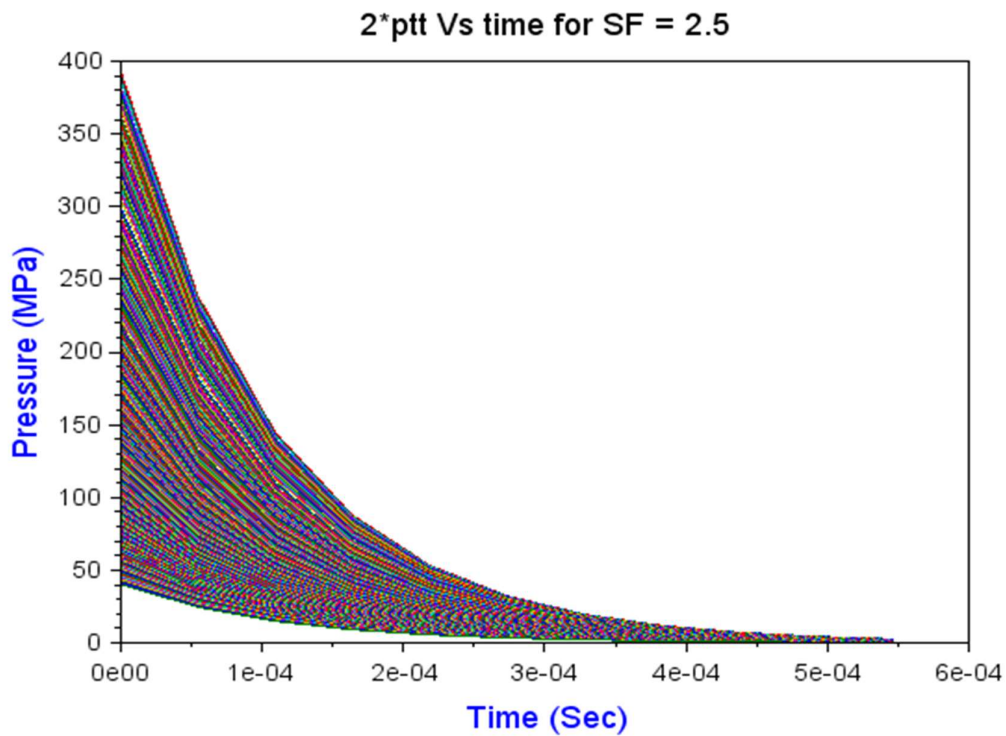


Figure 3.3-c Pressure profile for SF 2.5 with Single Exponential Decay

Figure 3.3-d & Figure 3.3-e Presents the pressure profile induced by the initial shock wave from the UNDEX for SF 1.68 and 2.5 i.e. is for the charge of 0.5 kg and 1.1 kg respectively with consideration of Double Exponential Decay and Time Delay.

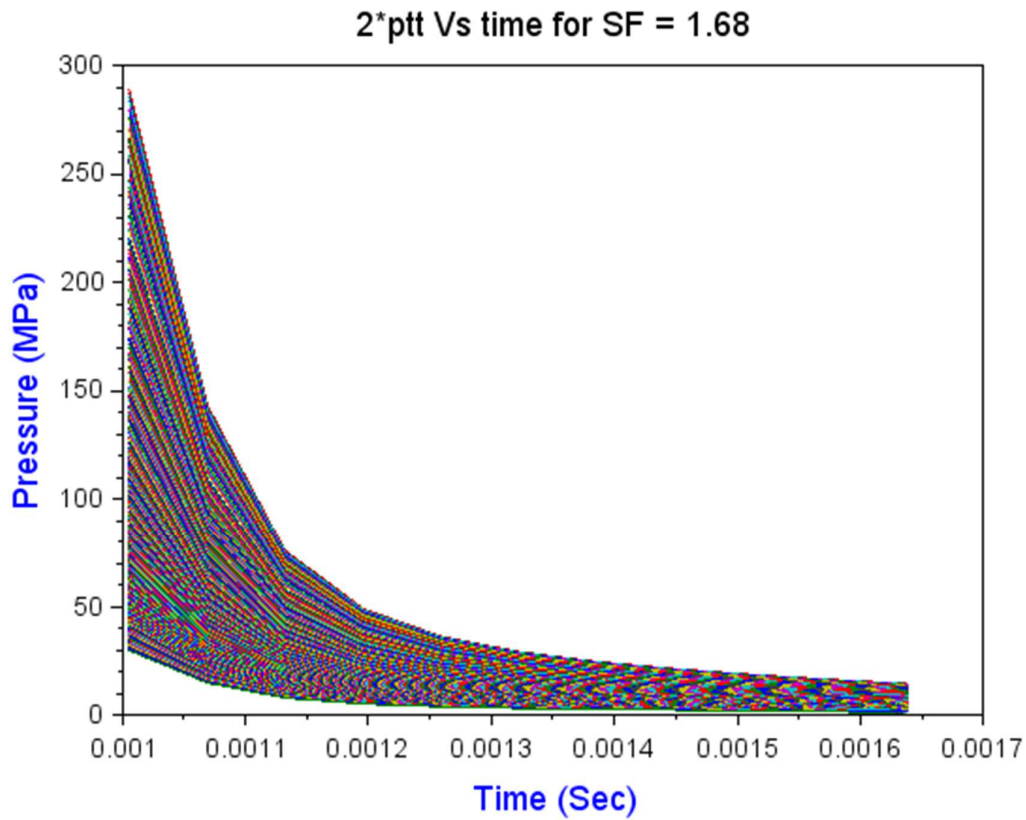


Figure 3.3-d Pressure profile for SF 1.68 with Double Exponential Decay & Time Delay

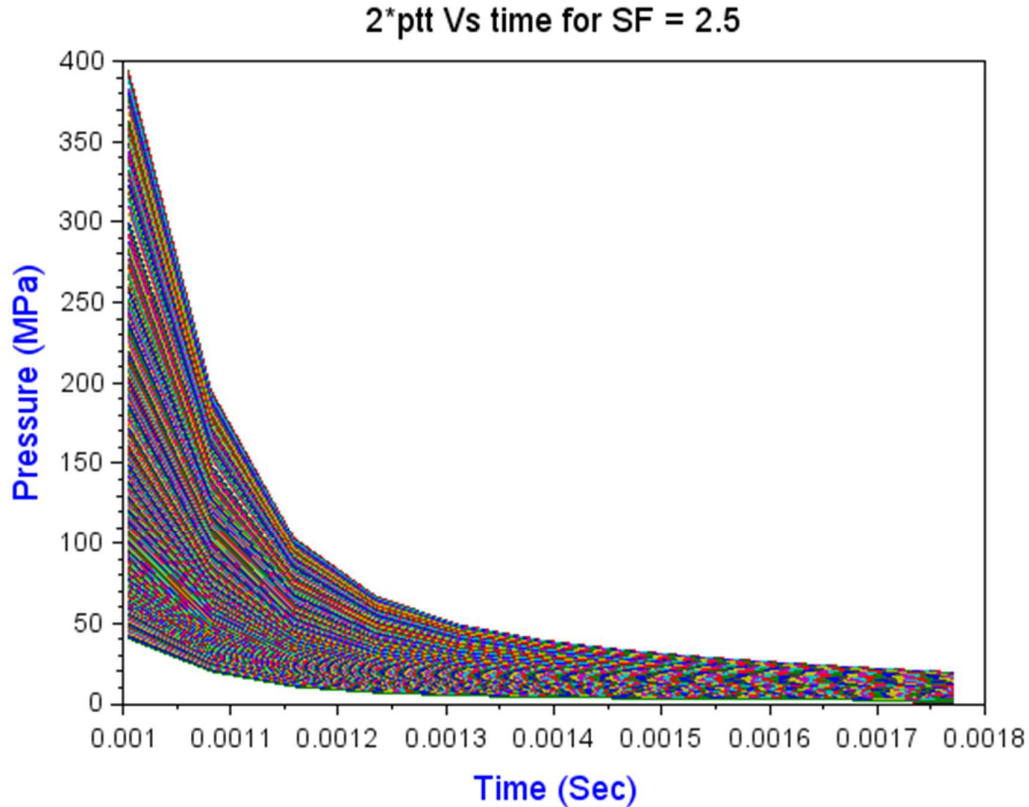


Figure 3.3-e Pressure profile for SF 2.5 with Double Exponential Decay & Time Delay

3.4 Simulation strategies and validation tools

As a chain of events which are explosive detonation, pressure wave propagation, fluid structure interaction, and finally the structural response are considered in a simulation in order to execute an underwater explosion simulate correctly (ISSC, 2006). Among all the events, fluid structure interaction (FSI) is the most studied one and significantly influenced the simulation results. Double Asymptotic Approximation (DAA) (DeRuntz Jr, 1994) is one of the way to model the surrounding fluid on the wet surface in contact with the fluid as a membrane. LS-DYNA, AUTODYN, NASTRAN, ABAQUS, etc. coupled with USA (Underwater Shock Analysis) solver (DeRuntz Jr, 1994) are the available codes which are capable of modelling FSI as a result of UNDEX. The general equation acting during this sort of simulation on a flexible structure (Nu, Zhi, & Wepeng, 2014),

$$M\ddot{X} + C\dot{X} + KX = F \tag{31}$$

Where M , C and K are refereed as the mass, damping and stiffness matrices of the model, and F denotes the external forces the degrees of freedom of the structure being analyzed. The variables

$$\mathbf{F} = -\mathbf{G}\mathbf{A}_f(\mathbf{p}_i + \mathbf{p}_s) \quad (32)$$

Where p_i and p_s represents the nodal wet surface and nodal pressure respectively to the incident flow and scattered flow. The value A_f is the diagonal matrix associated with an element in the fluid mesh, and G represents the transformation matrix relating the structural fluid and nodal surface forces.

DAA is based on the acoustical differential relations between the fluid pressure and its velocity on the surface of a submerged structure which is the uncoupling motion of the structure from the fluid. The fluid acts as a damping force in early time and as an added mass in the later time,

$$\mathbf{M}_f \dot{\mathbf{P}}\mathbf{s} + \rho c \mathbf{A}_f \mathbf{p}\mathbf{s} = \rho c \mathbf{u}_s \quad (33)$$

M_f is an ($N \times N$) fluid mass matrix, where N if the number of degrees of freedom ρ and C are the fluid density and the sound speed in the fluid respectively and U_s is the velocity of the fluid particles normal to the structural surface.

Structure and fluid speed vectors follows the equation defined below,

$$\mathbf{G}^T \dot{\mathbf{X}} = \mathbf{u}_i + \mathbf{u}_s \quad (34)$$

Where u_i is the speed of the incident flow. Using equations (31) and (32) as the same way as (33) and (34), the coupled fluid-structure interaction equations can be written:

$$\mathbf{M}\mathbf{X}' + \mathbf{C}\mathbf{X}' + \mathbf{K}\mathbf{X} = -\mathbf{G}\mathbf{A}_f(\mathbf{p}_i + \mathbf{p}_s) \quad (35)$$

$$\mathbf{M}_f \dot{\mathbf{P}}\mathbf{s} + \rho c \mathbf{A}_f \mathbf{p}\mathbf{s} = \rho c (\mathbf{G}^T \dot{\mathbf{X}} - \mathbf{u}_i) \quad (36)$$

4 NON-LINEAR FINITE ELEMENT ANALYSIS OF MONOLITHIC MATERIAL STRUCTURE

4.1 LS-DYNA

LS-DYNA is a commercial software developed by Livermore Software Technology Corporation. It is generally used by the automobile, aerospace, bioengineering, construction and manufacturing industries. LS-DYNA is developed to solve highly nonlinear transient dynamic finite element analyses using explicit time integration but it is also capable of adding more options. Simulation capabilities like failure analysis, rigid body dynamics, non-linear dynamics, thermal analysis, crack propagation, fluid analysis, multi-physics coupling etc. can be performed by LS-DYNA and many other fields can be tailored to match. It is also facilitated with implicit solver. LS-DYNA requires a single executable file to run simulation and it is entirely a command line driven software. The input file is called Key file (.key) and written on ASCII format. The keyword file can be prepared or edited in the text editor but dedicated preprocessors are most frequently used.

4.2 Numerical Analysis with LS-DYNA

After conducting a brief on the underwater explosion and suitable method to calculate the blast loading on the structure, a set of *Scilab* program is developed to be used considering two different shock factors. The detail mathematical calculation is discussed in the section 3.3. The available Figures (Figure 3.3-b to Figure 3.3-e) illustrate the pressure field applied on the cylindrical shell structure. Incorporating the blast load on the structure, the dynamic response of the structure is calculated by using non-linear finite element solver LS-DYNA.

The different categories of structural analysis and calculation have been performed depending on various conditions and approximations in this thesis work are as follows:

- Different Shock Factors with a fixed standoff distance
- Pressure profile with Single and Double Exponential Decay
 - High Shock Factor
 - Pressure profile with Single Exponential Decay
 - Pressure profile with Double Exponential Decay & Time Delay
 - Low Shock Factor
 - Pressure profile with Single Exponential Decay
 - Pressure profile with Double Exponential Decay & Time Delay

- Modelling the surrounding fluid layer with different Material Model available in LS-DYNA.

MAT_01 Fluid Modelled with MAT_ELASTIC_FLUID

MAT_90 Fluid Modelled with MAT_ACOUSTIC

- Treatment of the surrounding fluid layer for cavitation.

4.2.1 Analysis procedure

In order to simulate the dynamic response of a submerged cylindrical shell structure submitted to an underwater explosion, Scilab Program was developed to calculate the blast load and structural analysis and finite element simulations were carried out using LS-DYNA. Following steps were successively performed during the analysis process:

- I. Model preparation: A cylindrical shell finite element model is prepared in MSC Patran. The model information such as nodes and element lists as *.keyword files is exported to Scilab and LS-DYNA.
- II. Pressure load calculation: Calculate the pressure time evolution to be applied on each wetted finite element of the shell structure by means of analytical formulation using programming software Scilab.
- III. Structural response analysis: Apply the pressure loads to the shell structural model in LS-DYNA, and run the simulations for different conditions.
- IV. Check results: In the post-processing stage, it is important to check the structural response behaviour, such as vertical displacement, vertical velocity, acceleration, pressure in fluid elements adjacent to the structure, damaged shape of the structure, energy dissipated by both the fluid and the structure, effective plastic strain of the structure and total energy in the system.

4.2.2 Model and loads

In this investigation the following unit system is applied: stress in N/m^2 , force in Newton [N], distance in meter [m], energy in Newton-Meter [Nm] and time in Second [S].

4.2.2.1 Structure Model

The structure which is under the scrutiny of this investigation, considered as a part of a cylindrical shell structure bounded by two bulkheads (considered as rigid) at its extremities i.e. like a submarine section hull. Figure 4.2-a illustrates the geometry and the boundary conditions for the deformable cylindrical hull. The air filled cylindrical shell is clamped at its both ends and it is 2.8 m long with a diameter of 1.4 m. The plate thickness is 15 mm and the structural material is *Steel*. The mechanical properties of the material used in this study is presented in Table 4.2-a. The steel structure is modelled with MAT_PLASTIC_KINEMATIC (MAT 03) material model in LS-DYNA. The boundary conditions imposed on the two edges are clamped by restraining all the translation motions T_X, T_Y, T_Z and the rotations R_X, R_Y, R_Z . The steel structure is modelled with under integrated 4 node shell elements with element formulation options (ELFORM = 2) Belytschko-Tsay. The mesh size for the shell element is 0.025 X 0.0249 m (Figure 4.2-b).

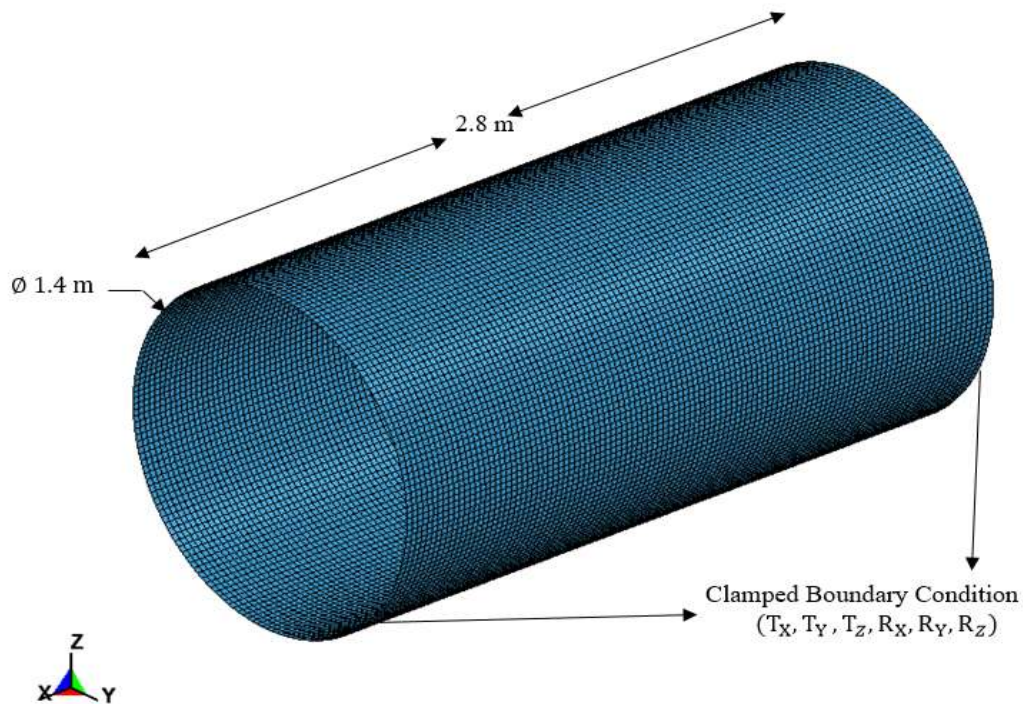


Figure 4.2-a Finite Element model of the structure

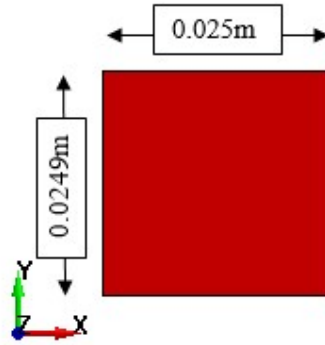


Figure 4.2-b Shell Element mesh size

Table 4.2-a Mechanical properties of Steel

Material Model	Mass density, ρ kg/m^3	Young's modulus, E GPa	Poisson's ratio, PR	Yield stress, σ (SIG) MPa	Tangent modulus, TAN MPa
MAT_03	7800	200	0.3	355	415
MAT_PLASTIC_KINEMATIC					

4.2.2.2 *Fluid Model*

In order to simulate the response of an immersed structure, a layer of fluid is modelled around the structure. The thickness of the fluid layer 0.7 m (half diameter of the cylinder) and it is modelled with 8 node solid elements presented in the Figure 4.2-c and Figure 4.2-d. The fluid layer around the structure is modelled with two different material model available in LS-DYNA.

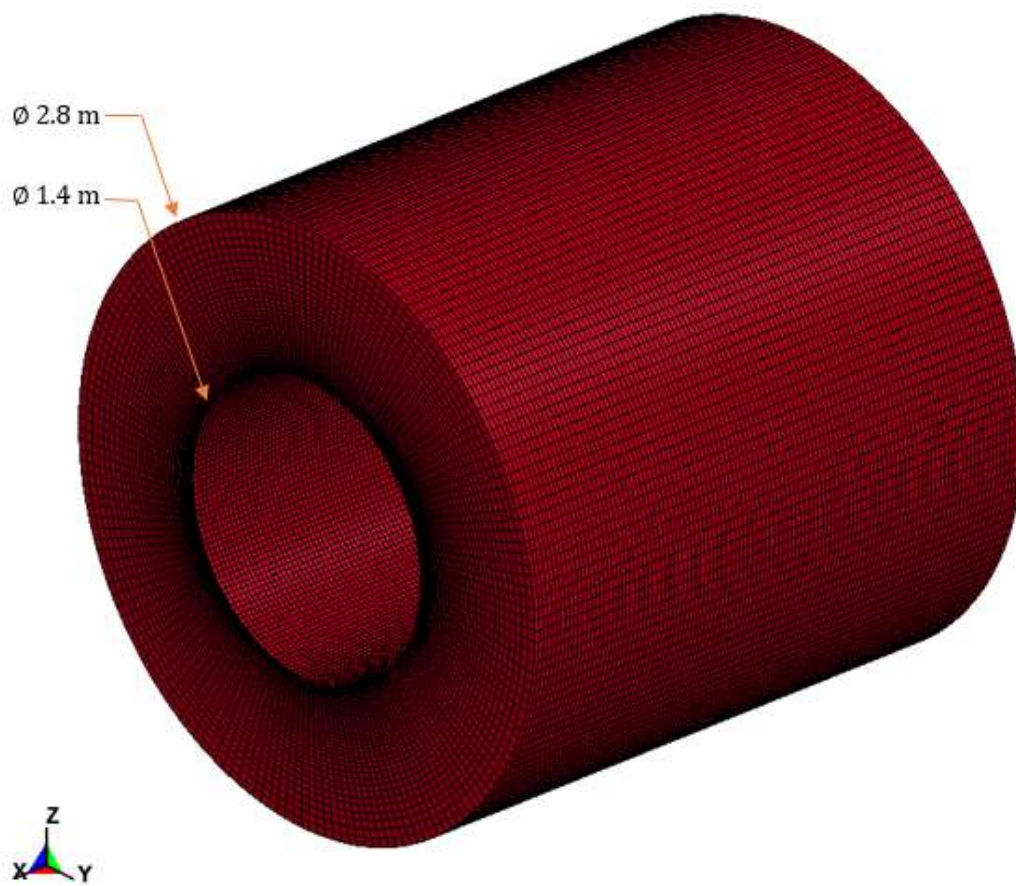


Figure 4.2-c Finite Element model of the structure and fluid around it

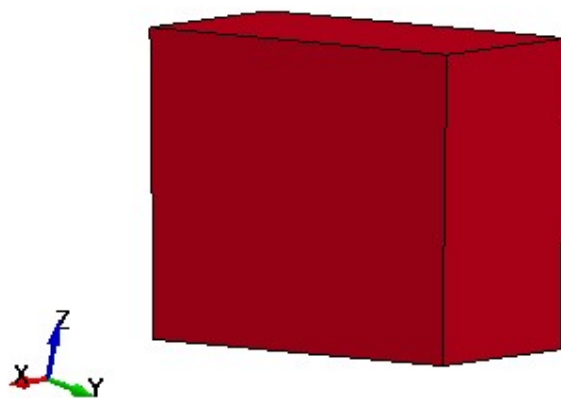


Figure 4.2-d Solid Element mesh size

- **Material-01 (MAT ELASTIC FLUID)**

MAT ELASTIC is used for modelling inviscid, irrotational flow of fluid material. This is an option of elastic material in LS-DYNA and suitable for modelling fluid-structure interaction spread out from far-field underwater explosion. This is available for beam, shell, and solid elements in LS-DYNA. MAT_01 has a numerical viscosity coefficient rather than a physically meaningful and it is useful where viscosity is not of interest. The material model is a flexible as model where it can be applied for both Euler and Lagrangian meshes. Moreover, the ALE (Arbitrary Lagrangian Euler) capabilities of MAT_01 allows to model relatively large structural motions (ie. at the fluid-structure interface) as compared to Material 90 (MAT Acoustic) (Hammond, 1999).

Table 4.2-b Material Properties and options in MAT_01 Card LS-DYNA

Material Model	Mass density	Young's modulus	Poisson's ratio	Axial damping factor	Bending damping factor
	ρ kg/m^3	E, MPa	PR	DA	DB
MAT_01 MAT ELASTIC FLUID	1000	0	0.0	0.0	0.0

Bulk Modulus,	Tensor viscosity coefficient	Cavitation pressure	Cavitation Treatment
K GPa	VC	CP	
2.2	0.0	I. 1E+20	NO
		II. 0.01	YES

- **Material-90 (MAT ACOUSTIC)**

MAT Acoustic is a linear, Eulerian and acoustic element specially formulated for modelling low-pressure, acoustic shock wave propagation in a fluid domain. It is limited to track only small structural displacements since it is restricted to linear and Eulerian mesh. In this material model only pressure information is unknown and calculated with respect to the meshes. It is useful for modelling large volume of fluid as it is cheap in terms of CPU time. MAT_90 can

be easily understood when Eulerian fluid nodes are shared by the Lagrangian structural nodes at the fluid structure interface. So if there is a large deformation or motion of structure, then the fluid elements immediately close to the structure will be distorted or stretched. As a result, the calculations in those elements can produce wrong results. So this material model is only useful for linear and small amplitude structural response (Hammond, 1999). Table 4.2-c presents different options and material properties for this material model.

Table 4.2-c Material Properties and options in MAT_90 Card LS-DYNA

Material Model	Mass density, ρ kg/m^3	Sound Speed, C	Damping Factor, Beta	Cavitation flag, CF	Cavitation Treatment
MAT_90	1000	1480	0.5	I. EQ.0.0: off	NO
MAT_Acoustic				II. EQ.1.0: on.	YES

- **Non-Reflecting Boundary conditions For Fluid Model**

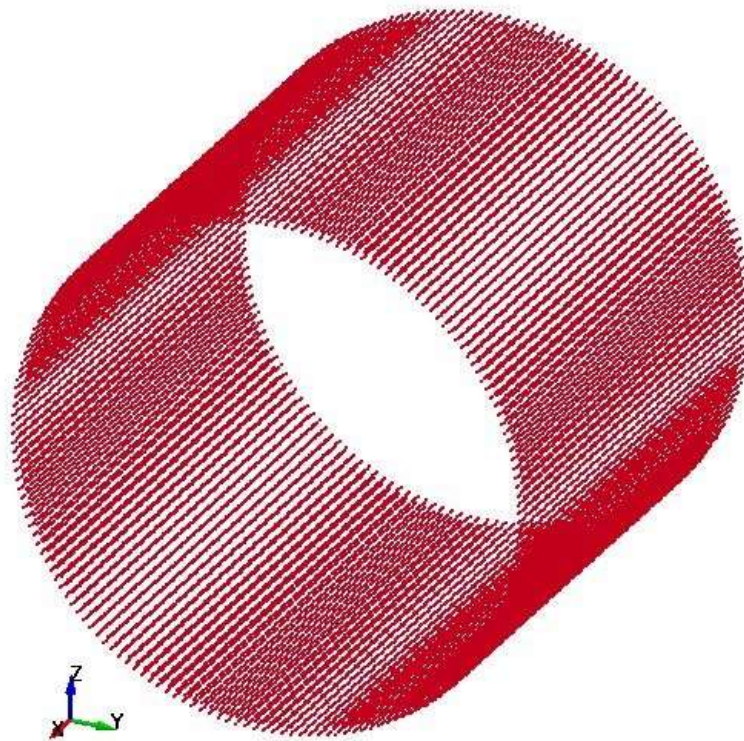


Figure 4.2-e Non-Reflective Boundary Condition for fluid

Non-Reflecting boundaries (NRBCs) are usually used for modelling an infinite domain in a finite element problem. Here in this simulation NRBCs are applied at the outer surface of the fluid layer as illustrated in the Figure 4.2-e. The purpose of applying NRBC to the wave propagation problem is for eliminating the reflections created by the outer surface of the fluid layer. In this simulation problem the structure is impacted by the shock wave coming from the UNDEX and part of the shock wave energy is reflected on the surface of the structure. This reflected wave travels through the fluid layer up to the outer surface of the fluid layer, where the outer surface creates a reflections which can pollute the shock wave propagation from the detonation. So to prevent energy being reflected back into the model at the finite boundary of the model, the NRBC is applied to act all energy radiating toward infinity.

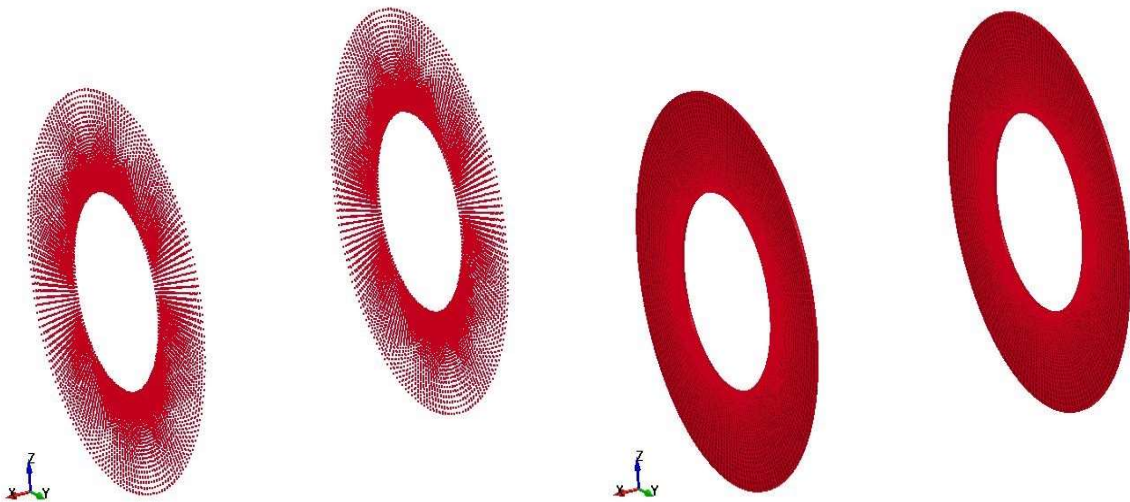


Figure 4.2-f Lateral (along x axis) Fluid layer Boundary condition

- **Lateral (along x axis) Fluid layer Boundary condition**

The fluid particles at the both ends are restrained of being flowing out of the cylindrical region along the x axis. So the movement of the fluid particles through the planes presented in the Figure 4.2-f along the x axis is restrained.

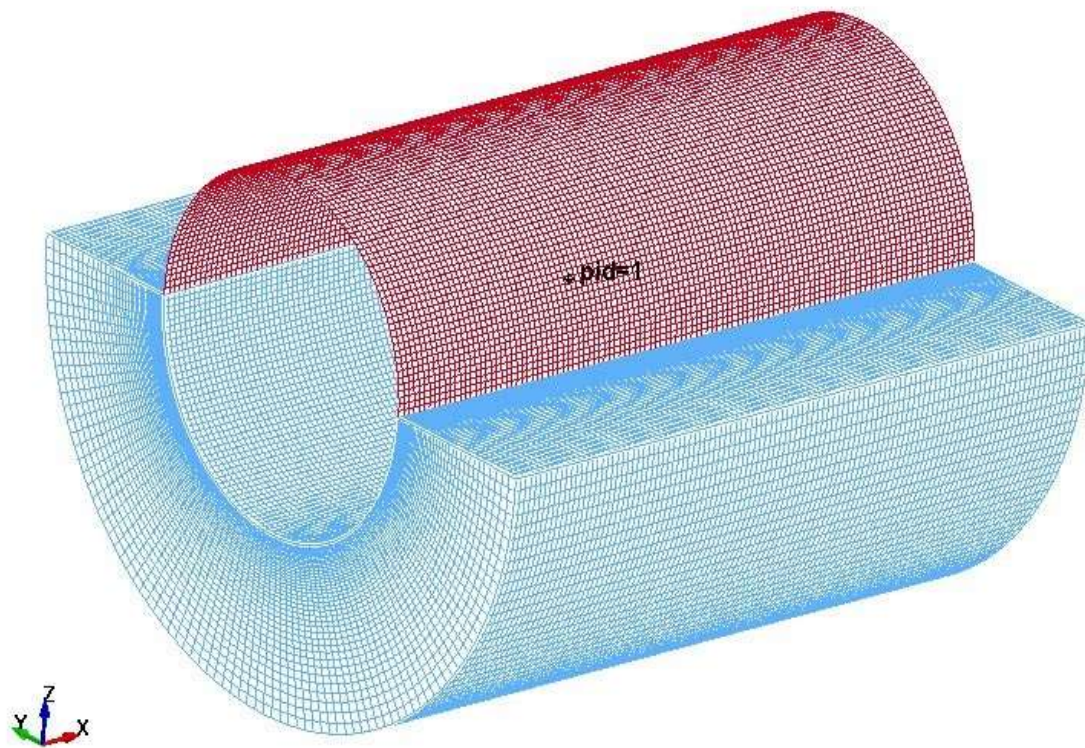


Figure 4.2-g Finite Element Model of an immersed Structure Half section.

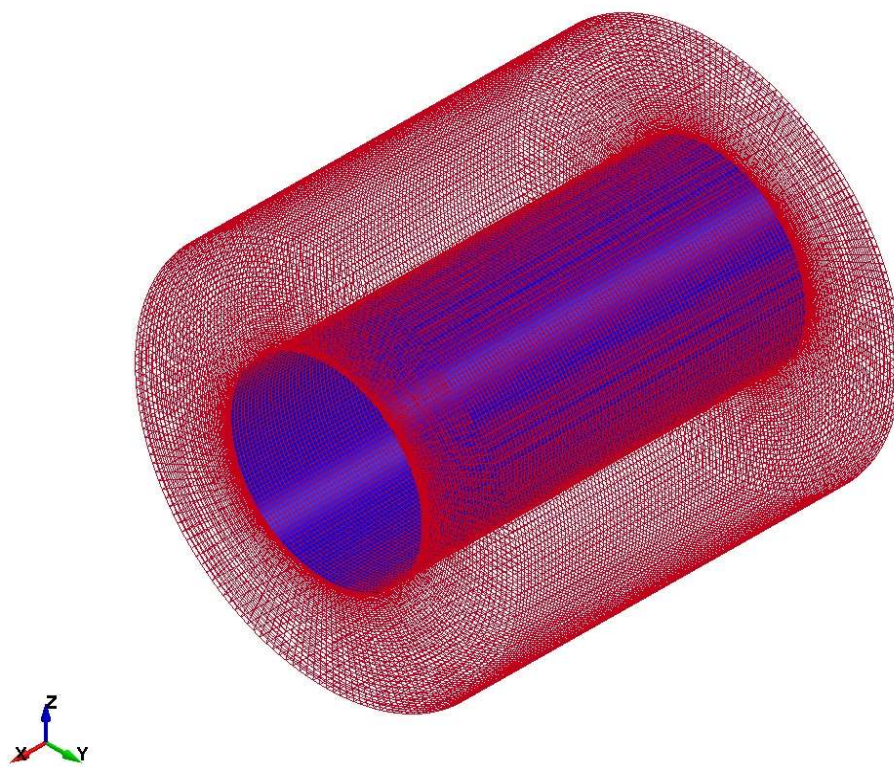


Figure 4.2-h Finite Element Model of an immersed Structure

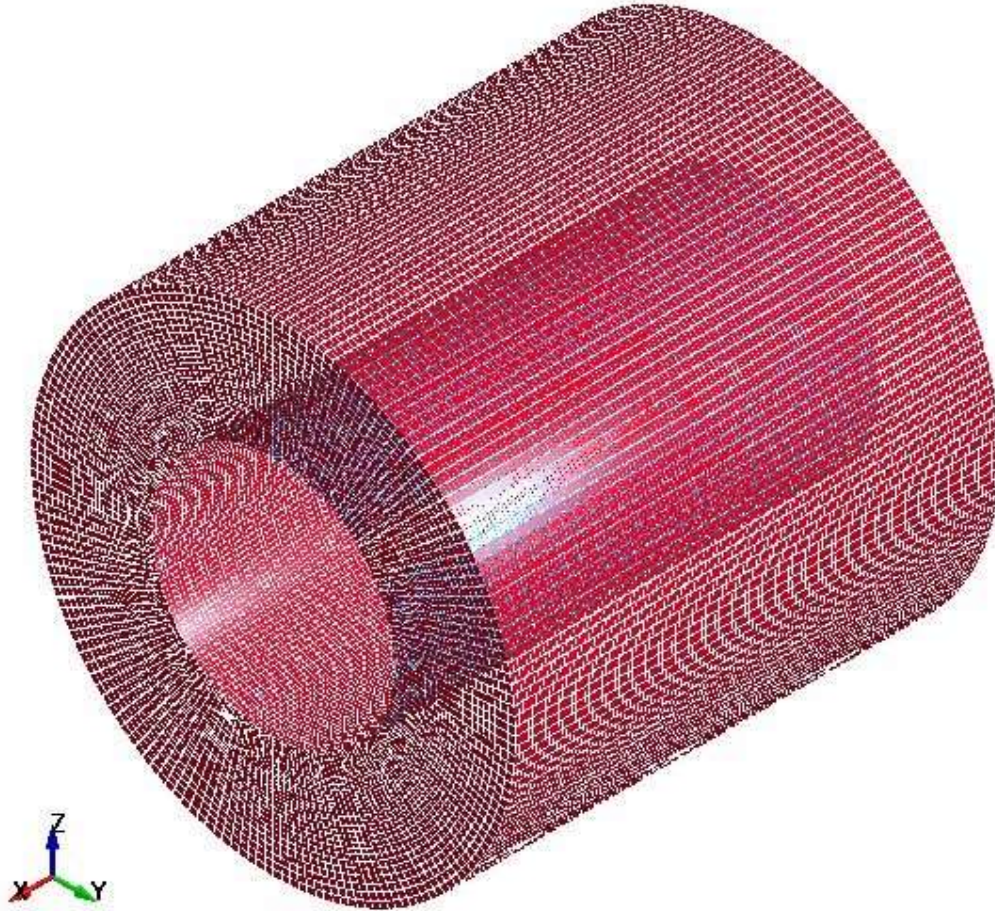


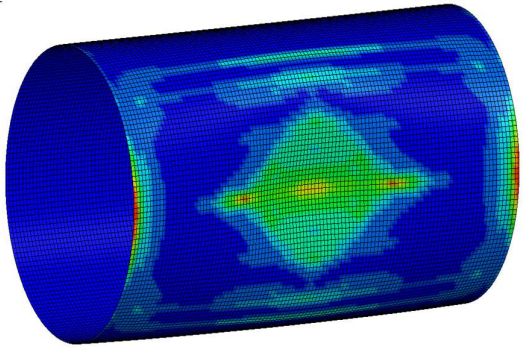
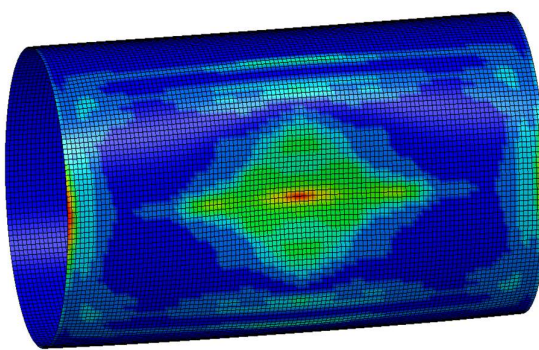
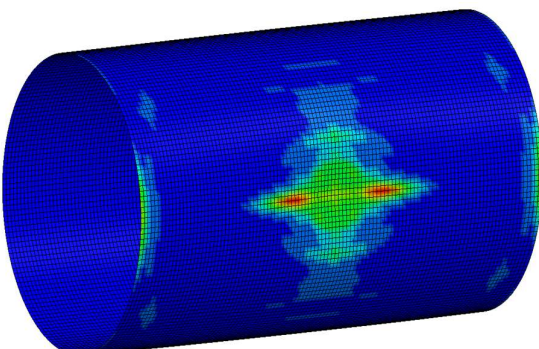
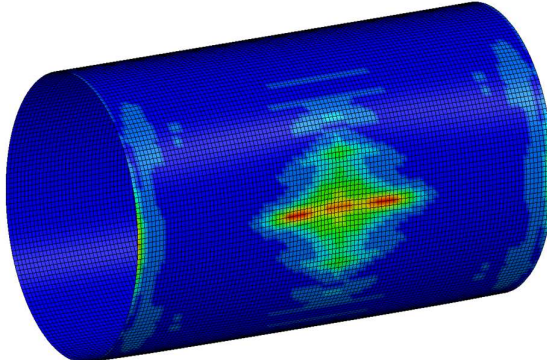
Figure 4.2-i Finite Element Model of an immersed Structure

4.2.3 Response Analysis of a Monolithic Material Structure

4.2.3.1 Deformed Shape

From the literature review plating (Wang, 2014) and also from the experimental test results of the reference Brochard (2018), it has been observed that the damage shape of the cylindrical shell can be dished hull plating submitted to one sided noncontact UNDEX. In the Table 4.2-d a complete comparison of the damaged shape is presented for different scenarios of calculation.

Table 4.2-d Damage shape of the structure for different simulation scenarios

SF 2.5	
Fluid Modelled with MAT_ACOUSTIC	Fluid Modelled with MAT_ELASTIC_Fluid
	
SF 1.68	
	

4.2.3.2 Shock Factor 1.68

Shock factor is defined by the equation 12 and rewriting the equation as follows, here the charge weight is $C = 0.5$ kg and $D = 0.42$ m is the distance of the charge. The shock factor $SF = 1.68$.

$$SF = \frac{C^{1/2}}{D} \tag{37}$$

1. Structure immersed in Fluid modelled with Acoustic behaviour law

After simulating the numerical model with MAT_PLASTIC_KINEMATIC (MAT 03) for structure and MAT_ACOUSTIC for the fluid, the maximum radial displacement was reported to be 0.098 m at the internal energy level of 116 kJ.

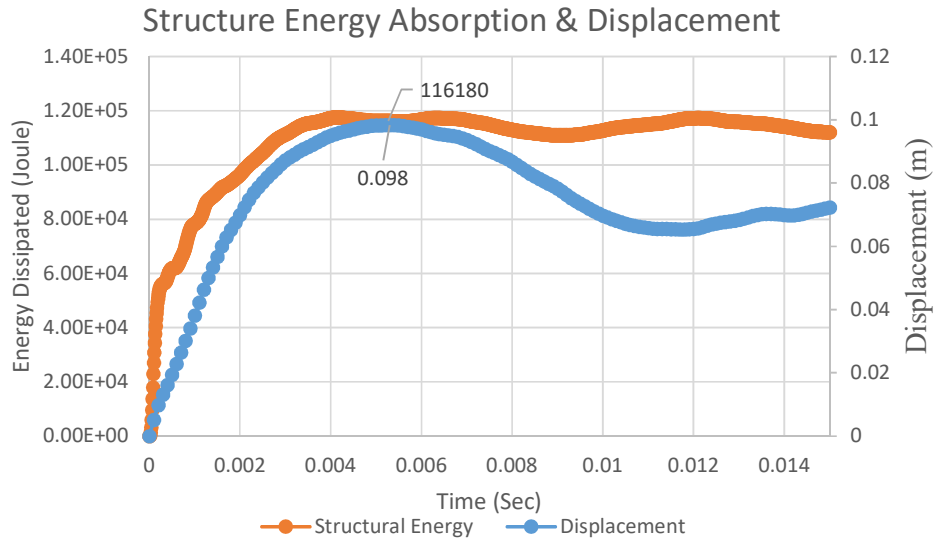


Figure 4.2-j Structure Internal Energy and Radial Displacement (Fluid modelled with MAT Acoustic)

The energy balance for the numerical calculation is presented in the Figure 4.2-j where in the beginning of the calculation, the maximum amount of total energy was reported 219.8 kJ. This energy was supplied by the shock wave as a result of underwater explosion near the structure.

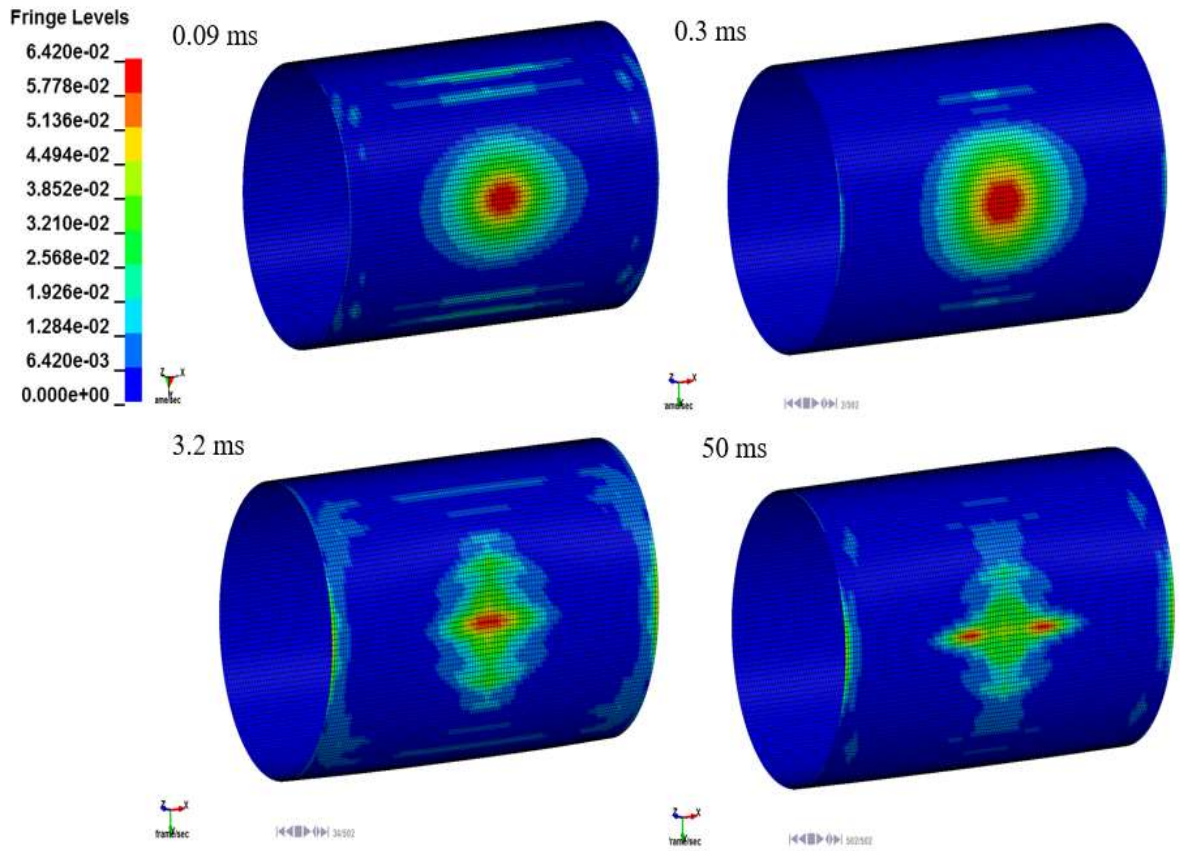


Figure 4.2-k Plastic strain at different time steps

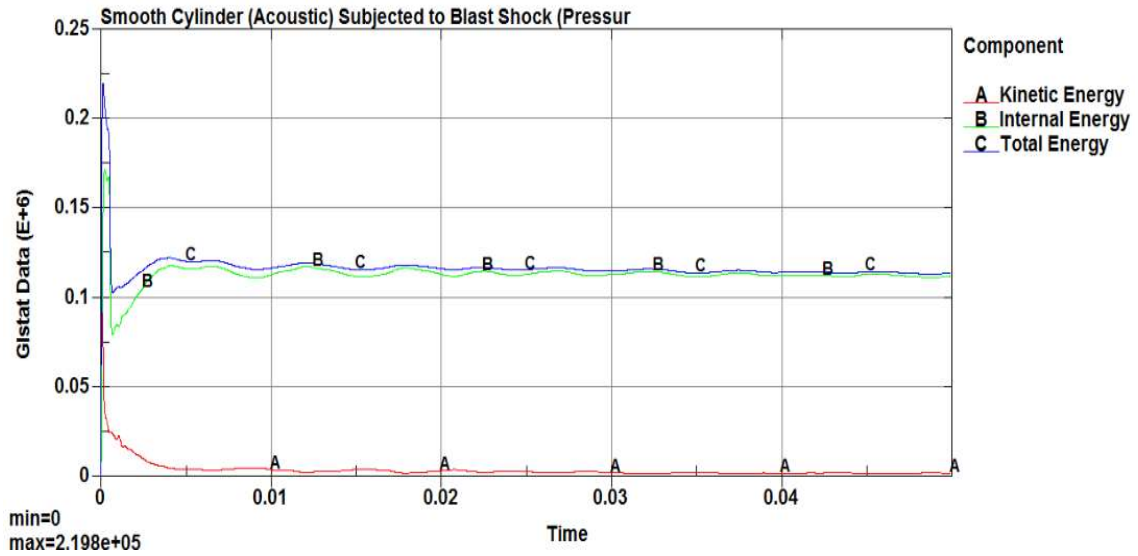


Figure 4.2-l Energy balance of the numerical simulation

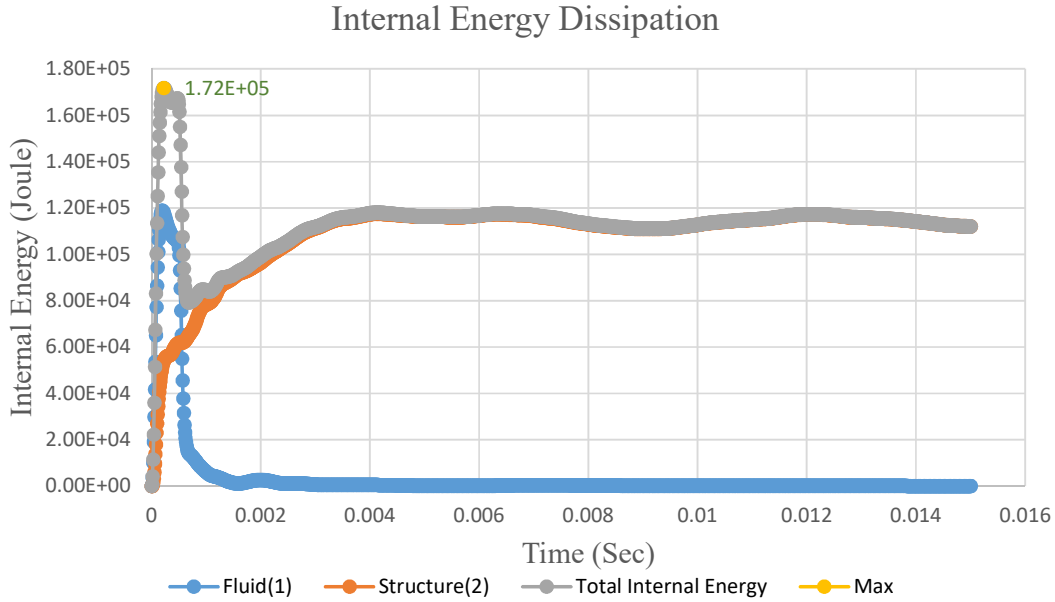


Figure 4.2-m Dissipation of the Internal Energy

Figure 4.2-m presents the level of energy dissipated separately by structure and fluid layer close to the submerged structure. It is also noted that the level of energy dissipation in the fluid layer is significant. For underwater explosion analysis, it is very important to observe early stage phenomenon within few micro-seconds. It is also remarkable to observe that at the primary phase of the structural response, the combine total amount of internal energy supplied to fluid and structure was 172kJ.

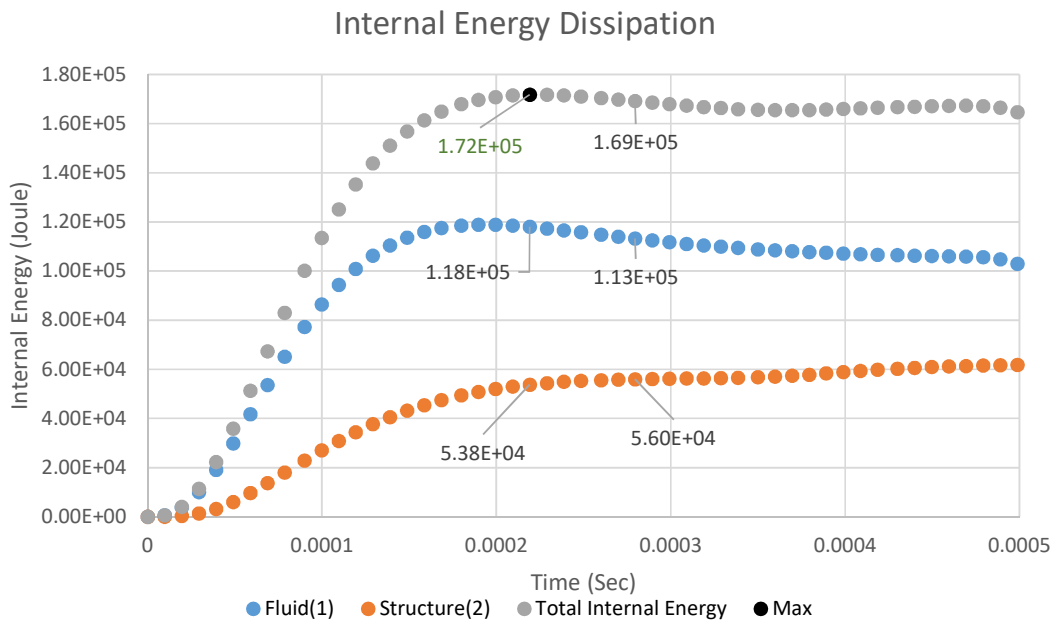


Figure 4.2-n Internal Energy dissipation within early structural response time 0.5 milliseconds

Here it can be observed that at the beginning of the blast pressure applied to the structure, the structure starts to move and generating a negative pressure (Figure 4.2-o) in the fluid elements adjacent to the structure. As a result the fluid starts to absorb more energy, here the energy is coming from the blast pressure. The fluid absorbs almost 67% (*At time 0.2 ms fluid has 118 kJ, structure has 53.8 kJ and the total energy 172 kJ*, Figure 4.2-n) of the total energy supplied by the blast pressure to gain zero pressure or equilibrium from the negative pressure, which is radiation damping by the fluid in this situation. And the deformation of the structure absorbs the rest of the energy to resist the underwater blast shock.

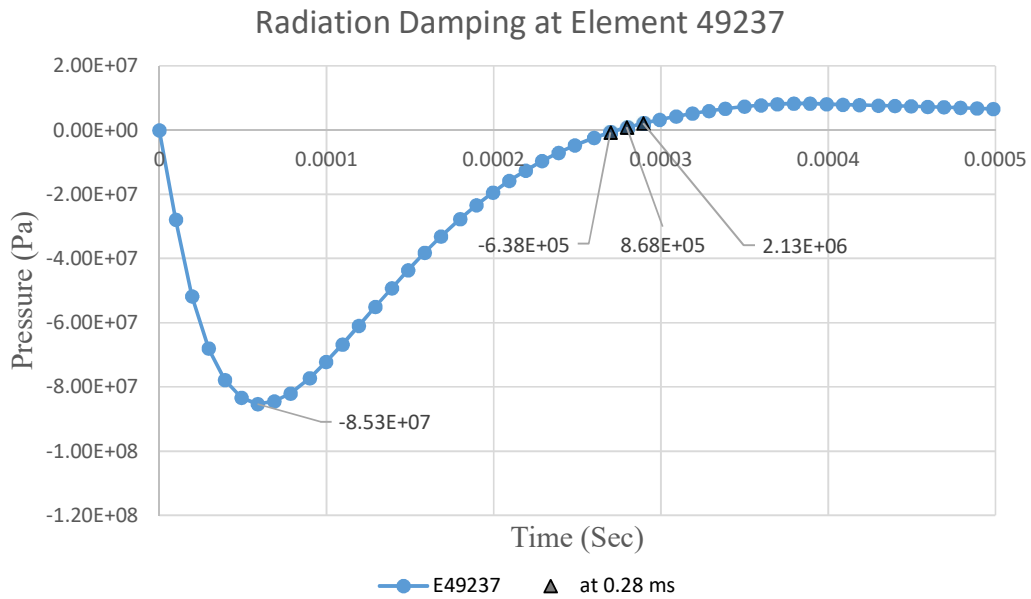


Figure 4.2-o Radiation Damping at the fluid element 49237

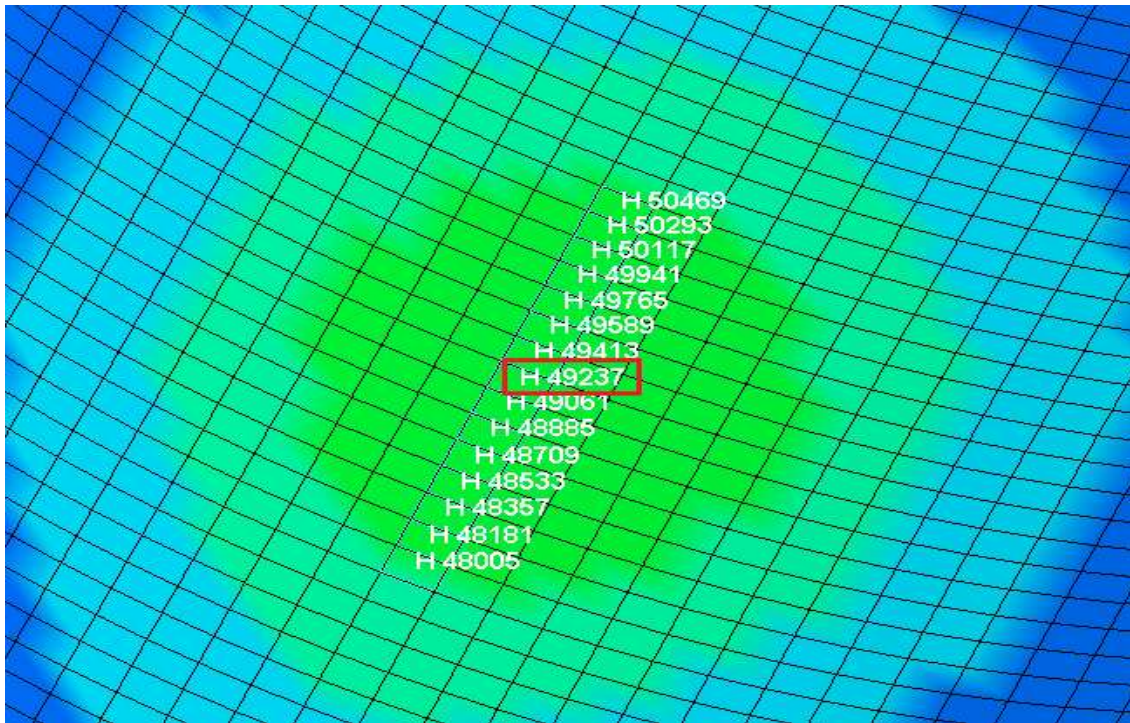


Figure 4.2-p Position of the fluid element 49237 in XY plane at the centre of the impact area of shock wave peak pressure

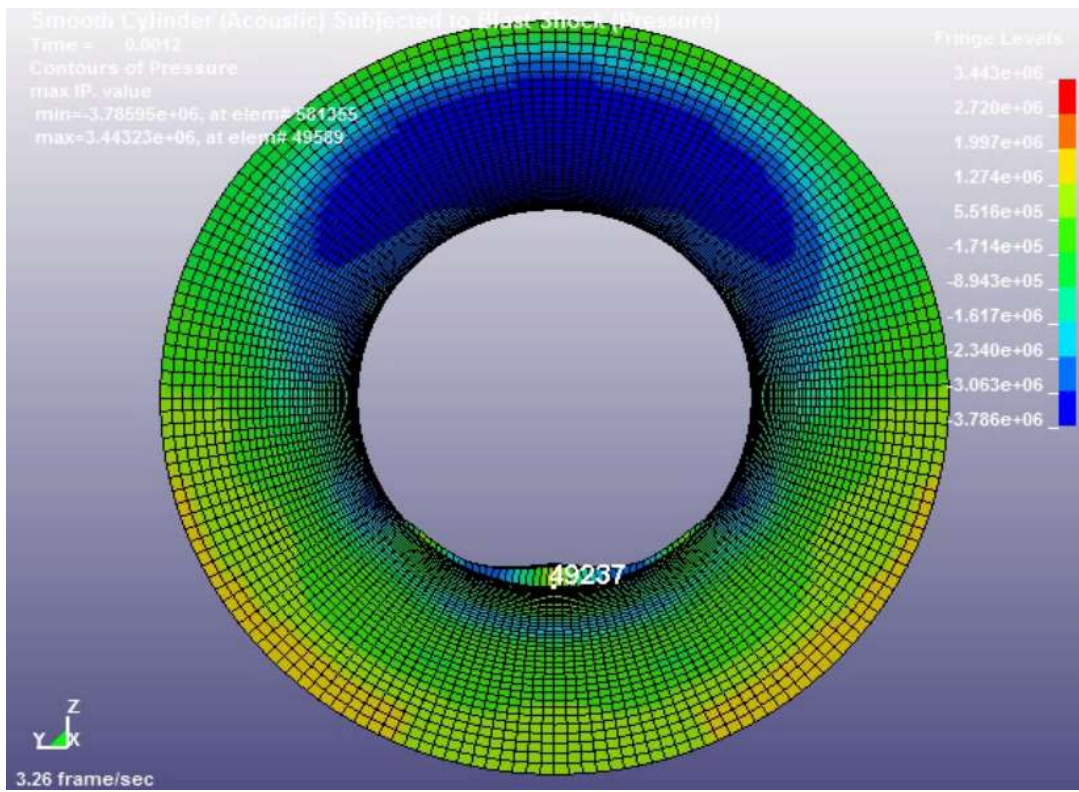


Figure 4.2-q Position of the Fluid element 49237 in YZ plane

INTERNAL ENERGY AT 0.28MS

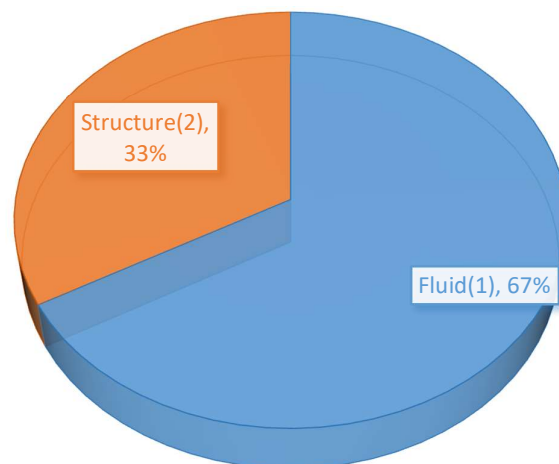


Figure 4.2-r Distribution of total internal energy dissipation

Figure 4.2-s represents the evolution of the low pressure region in the fluid layer near the structure as a result of complex fluid structure interaction during the post phase of underwater explosion. This phenomenon can be seen frequently for surface ships as close to the water surface and the influence of hydrostatic pressure is less than deep in the sea or ocean. So for the structures submerged in the deep sea state, it is less likely to observe cavitation near the structure due to the influence of high hydrostatic pressure. The other effect of stretching of the fluid mesh near the shell is due to the fact that Eulerian fluid nodes are shared by the Lagrangian structural nodes at the fluid structure interface. As here the fluid model is modelled with MAT_90 (MAT ACOUSTIC). So due to the large deformation or motion of structure, the fluid elements immediately close to the structure are distorted or stretched. But it is not affecting the calculated pressure close to that region as in the previous simulations already reported approximately same level of results (Energy, Pressure and deformation) as MAT_01 (MAT ELASTIC Fluid). The fluid mesh in MAT_01 has the capability to follow the structure whenever there is a large deformation or motion of structure.

Cavitation in the Fluid domain - Fluid modelled with MAT_ACOUSTIC (SF 1.68)

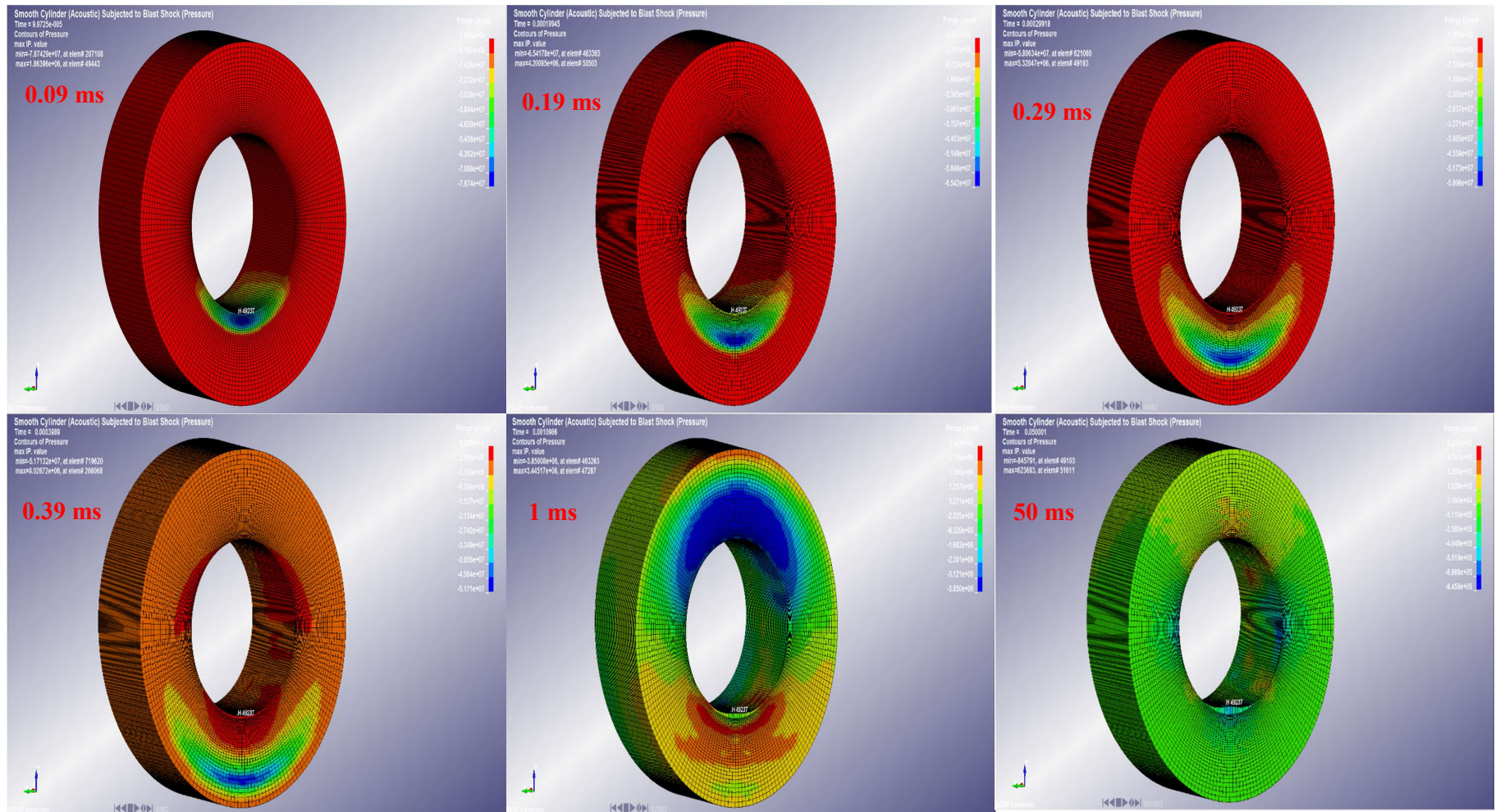


Figure 4.2-s Cavity flow or flow of low pressure oscillation in MAT Acoustic fluid model SF 1.68

2. Structure immersed in Fluid modelled with Acoustic behaviour law & Cavitation Treatment

In this section, the cavitation option was activated in MAT_ACOUSTIC (MAT 90) behaviour law in order to prevent negative pressure inside the fluid by allowing the occurrence of cavitation. MAT_PLASTIC_KINEMATIC (MAT 03) is still used to model the elastic plastic behavior of the structure. In this case, the maximum radial displacement was reported to be 0.223 m at the internal energy level of 573.9 kJ. The cavitation treatment was considered by LS-DYNA with the simulation parameters described in Table 4.2-c.

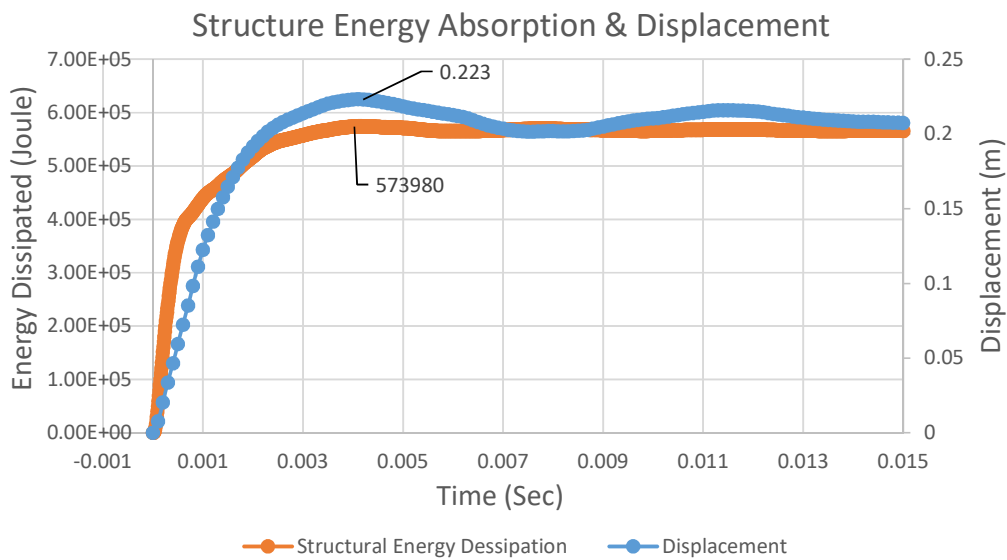


Figure 4.2-t Structure Internal Energy and the Radial Displacement (Fluid modelled with MAT Acoustic and Cavitation treatment)

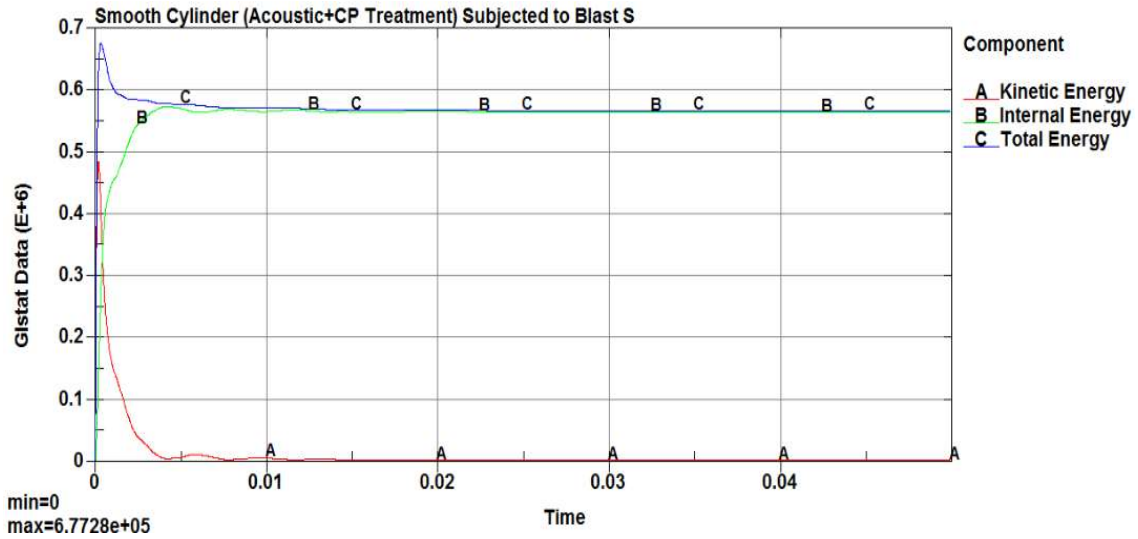


Figure 4.2-u Energy balance of the numerical simulation

The energy balance for the numerical calculation is presented in the Figure 4.2-u where in the beginning of the calculation, the maximum amount of total energy was reported 677 kJ. Here the total energy supplied by the shock wave is larger than the numerical calculation without cavitation treatment. It is due to the absence of negative pressure in the fluid layers near the structure which indeed resists to the structure deformation.

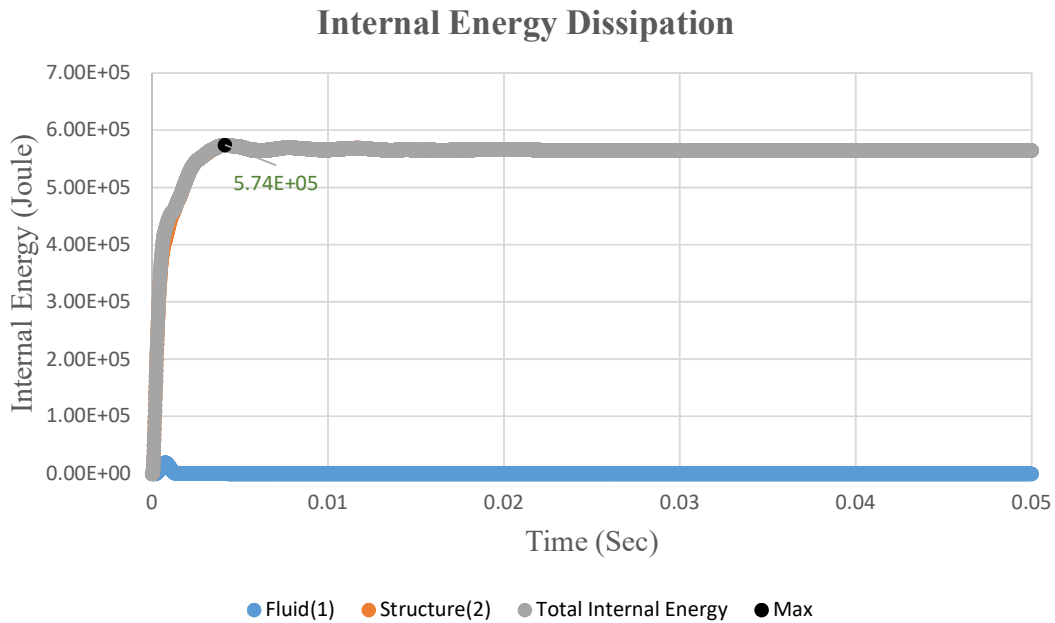


Figure 4.2-v Dissipation of the Internal Energy

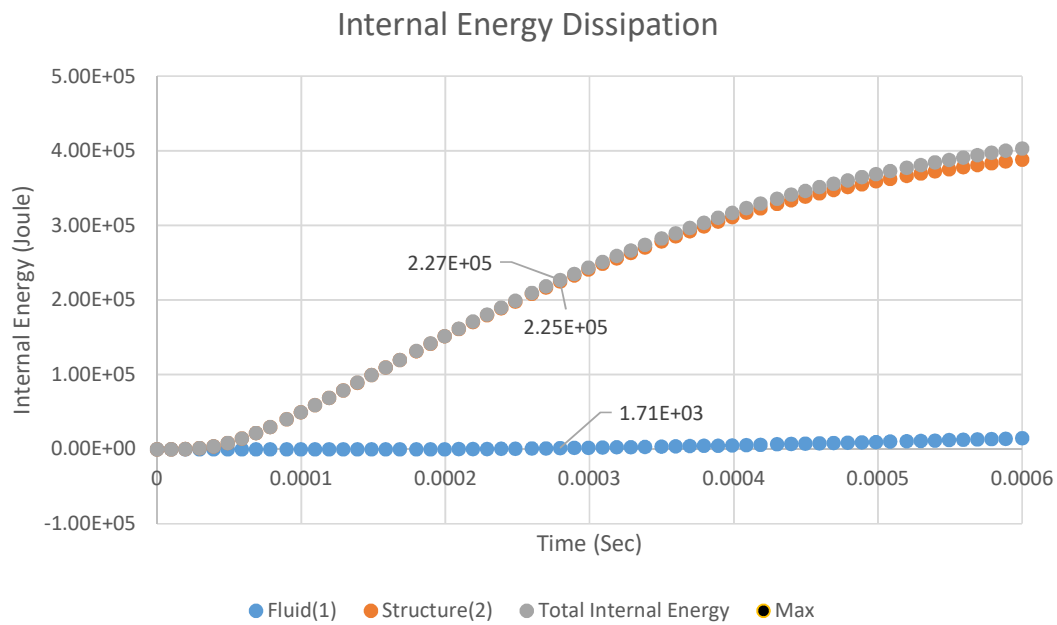


Figure 4.2-w Internal Energy dissipation within early structural response time 0.5 milliseconds

Figure 4.2-v presents the level of energy dissipated separately by structure and fluid layer close to the submerged structure. It is also noted that the level of energy dissipation in the fluid layer is insignificant when fluid domain is treated with cavitation treatment. It is also remarkable to observe that at the primary phase of the structural response, all the supplied energy is absorbed by the structure. Consequently, the radiation damping is almost zero in this circumstance.

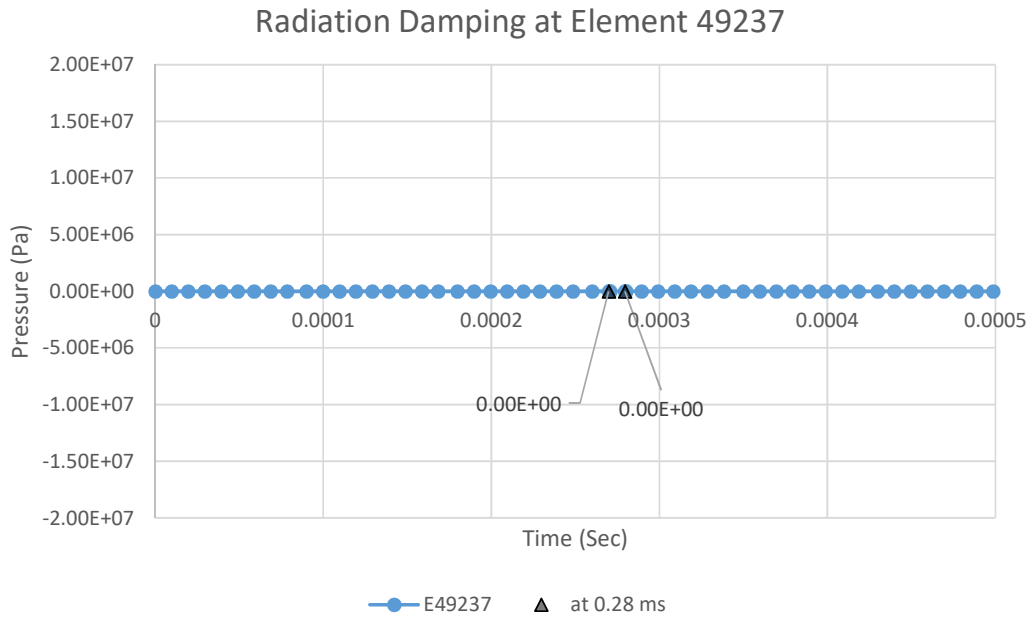


Figure 4.2-x Radiation Damping at the fluid element 49237

INTERNAL ENERGY AT 0.28MS

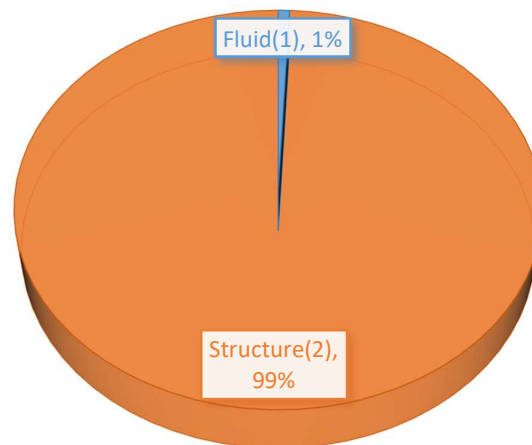


Figure 4.2-y Distribution of total internal energy dissipation

3. Structure immersed in Fluid modelled with Fluid Elastic behaviour law

After simulating the numerical model with MAT_PLASTIC_KINEMATIC (MAT 03) for structure and MAT_ELASTIC_FLUID for the fluid, the maximum radial displacement was reported to be 0.099 m at the internal energy level of 117 kJ. This structural response is quite similar to the simulation with Acoustic Element.

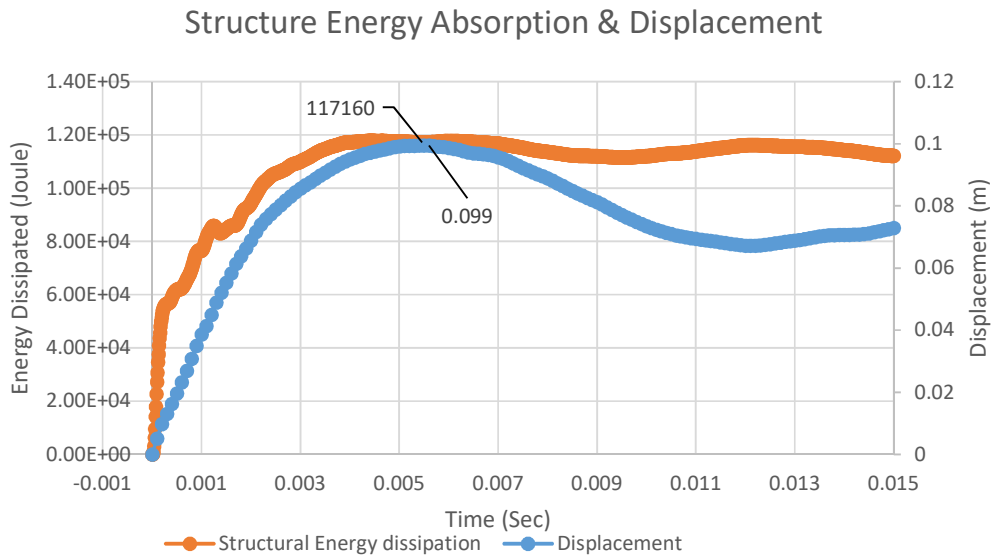


Figure 4.2-z Structure Internal Energy and the Radial Displacement (Fluid modelled with MAT Elastic Fluid)

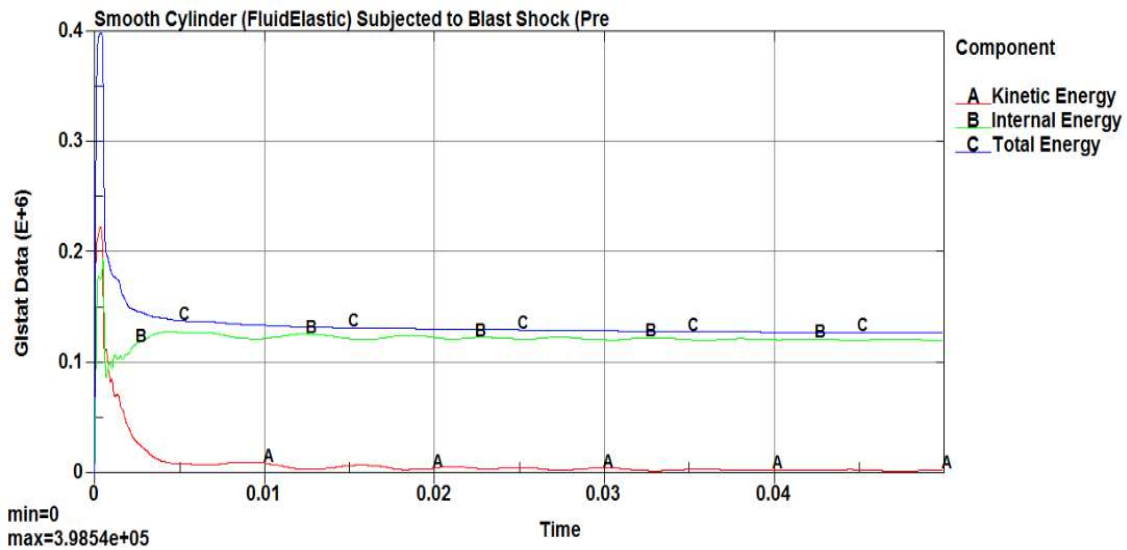


Figure 4.2-aa Energy balance of the numerical simulation

The energy balance for the numerical calculation is presented in the Figure 4.2-aa where in the beginning of the calculation, the maximum amount of total energy was reported 398.5 kJ. This energy was supplied by the shock wave as a result of underwater explosion near the structure.

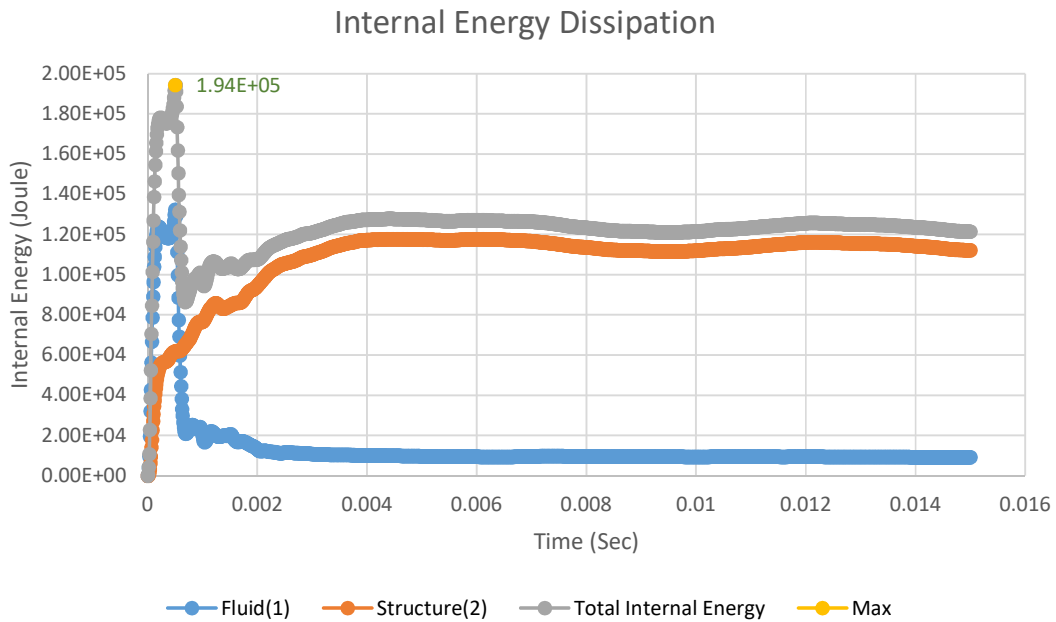


Figure 4.2-bb Dissipation of the Internal Energy

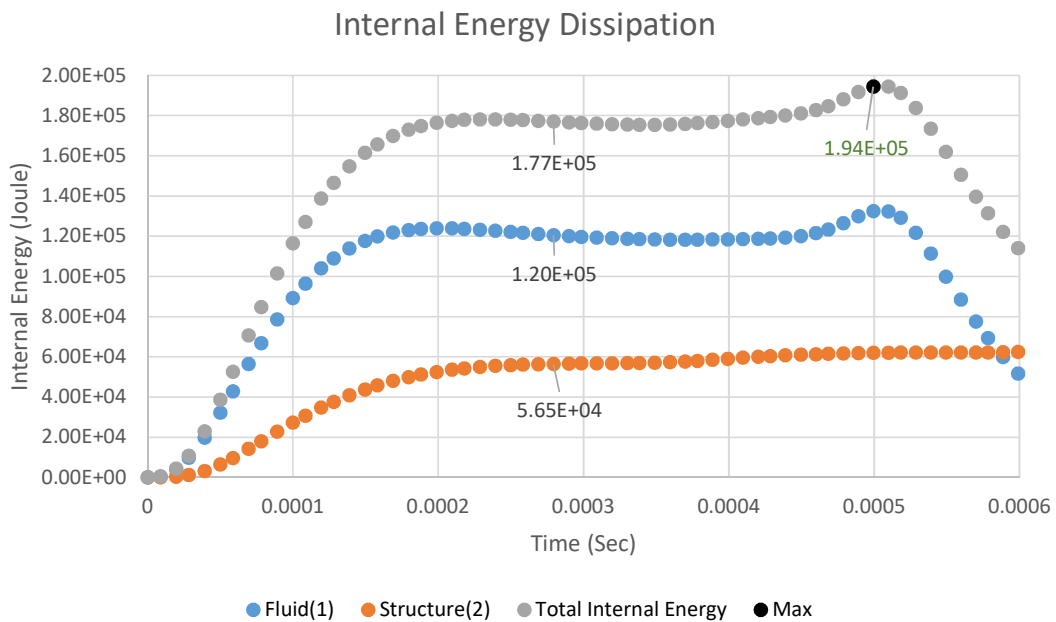


Figure 4.2-cc Internal Energy dissipation within early structural response time 0.6 milliseconds

Figure 4.2-bb presents the level of energy dissipated separately by structure and fluid layer close to the submerged structure. It is also noted that the level of energy dissipation in the fluid layer is significant. For underwater explosion analysis, it is very important to observe early stage phenomenon within few micro-seconds. It is also remarkable to observe that at the

primary phase of the structural response, the combine total amount of internal energy supplied to fluid and structure was 194 kJ.

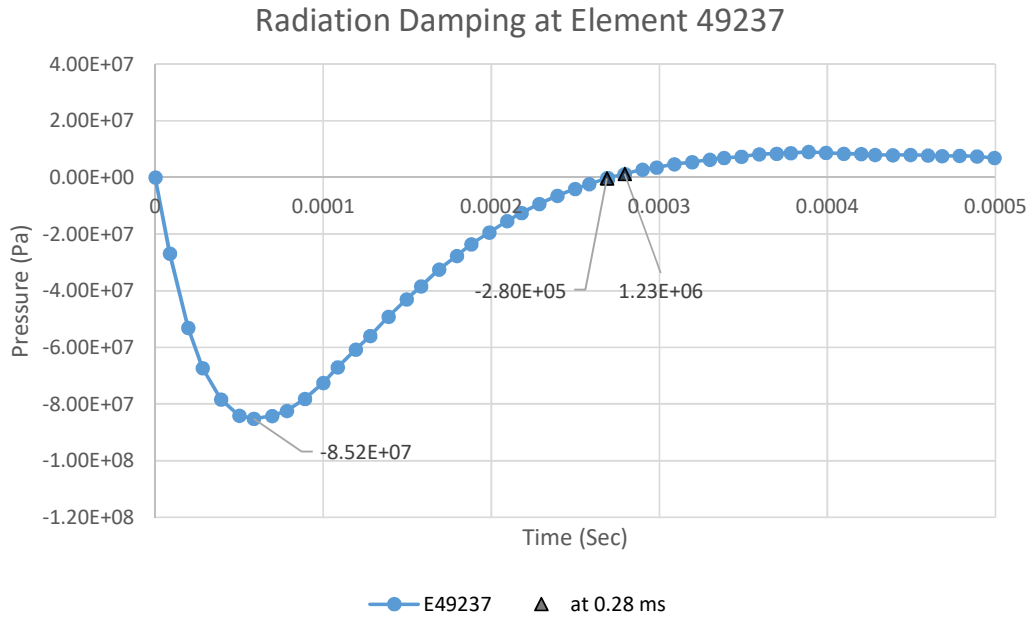


Figure 4.2-dd Radiation Damping at the fluid element 49237

Here it can be observed that at the beginning of the blast pressure applied to the structure, the structure starts to move generating a negative pressure (Figure 4.2-dd) in the fluid elements adjacent to the structure. As a result the fluid starts to absorb more energy, here the energy is coming from the blast pressure. The fluid absorbs almost 68% (*At time 0.28 ms fluid has 120 kJ, structure has 56.5 kJ and the total energy 177 kJ, Figure 4.2-cc*) of the total energy supplied by the blast pressure to gain zero pressure or equilibrium from the negative pressure, which is radiation damping by the fluid in this situation. And the deformation of the structure absorbs the rest of the energy to resist the underwater blast shock.

INTERNAL ENERGY AT 0.28MS

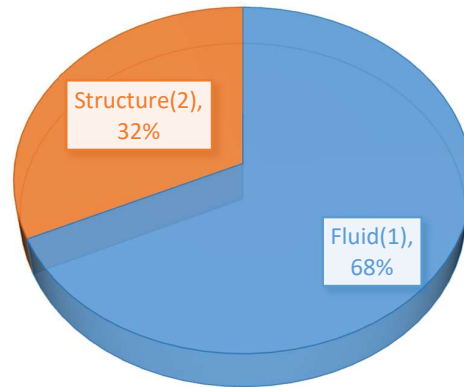


Figure 4.2-ee Distribution of total internal energy dissipation

Figure 4.2-ff illustrates the evolution of the low pressure region in the fluid layer near the structure as a result of complex fluid structure interaction during the post phase of underwater explosion. Figure 4.2-gg presents the capability of MAT ELASTIC Fluid elements to flow the fluid mesh with the large deformation or motion of the structure. So there is no stretching or distortion of the fluid mesh like MAT Acoustic in the previous scenario.

Cavitation in the Fluid domain - Fluid modelled with MAT_ELASTIC_Fluid (SF 1.68)

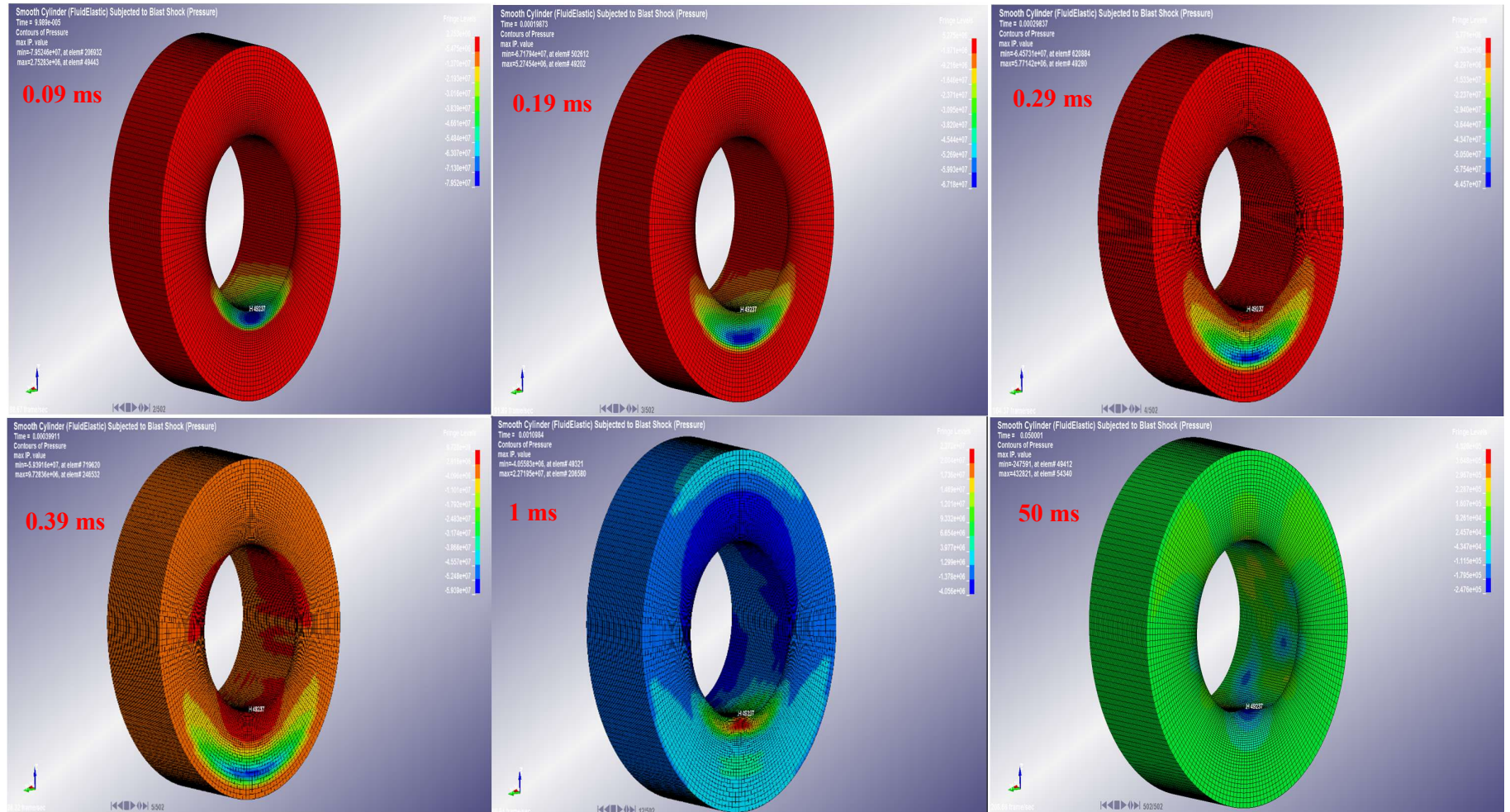


Figure 4.2-ff Cavity flow or flow of low pressure oscillation in MAT Elastic Fluid model SF 1.68

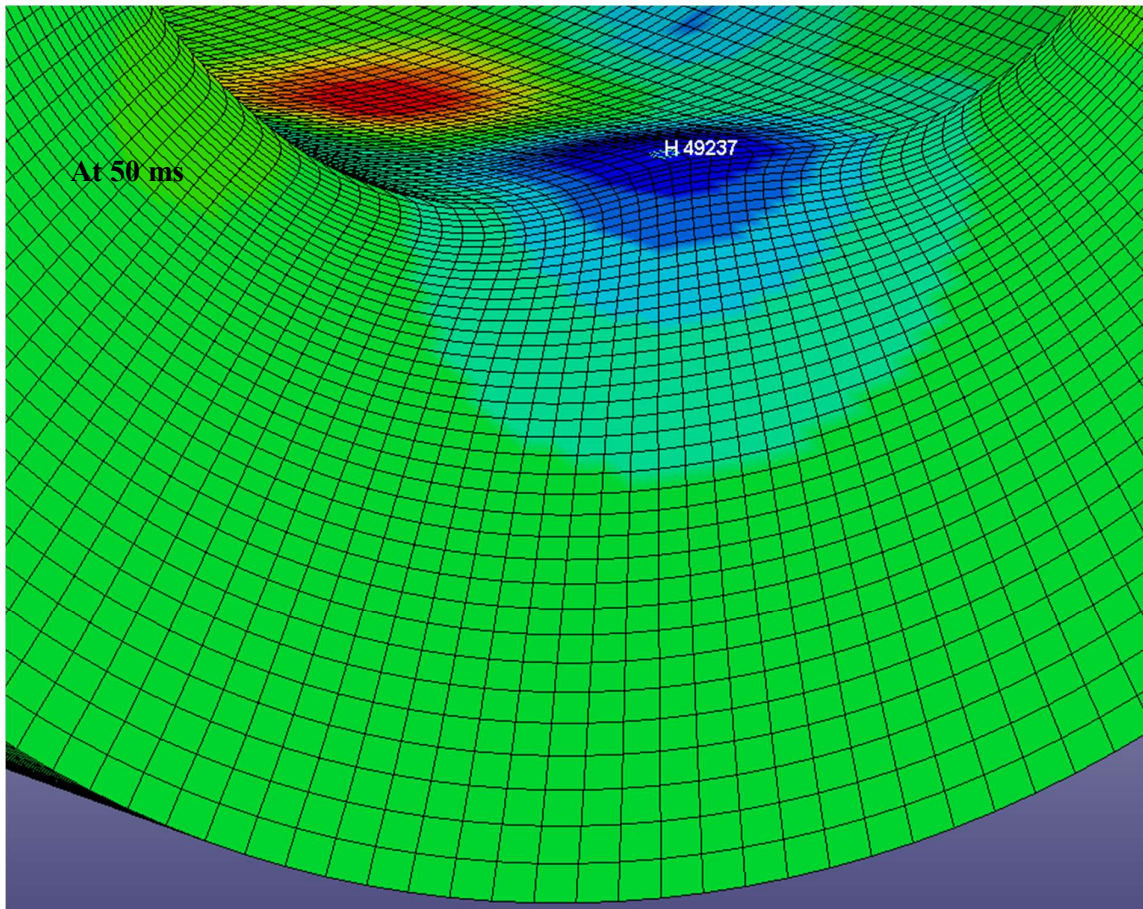


Figure 4.2-gg Fluid mesh flow with structure Shell in MAT Elastic Fluid Model

4. Structure immersed in Fluid modelled with Fluid Elastic behaviour law & Cavitation Treatment

After simulating the numerical model with MAT_PLASTIC_KINEMATIC (MAT 03) for structure and MAT ELASTIC FLUID for fluid with cavitation treatment to prevent any negative pressure in the fluid domain, the maximum radial displacement was reported to be 0.219 m at the internal energy level of 559.6 kJ. The cavitation treatment was considered by LS-DYNA with the simulation parameters described in Table 4.2-b.

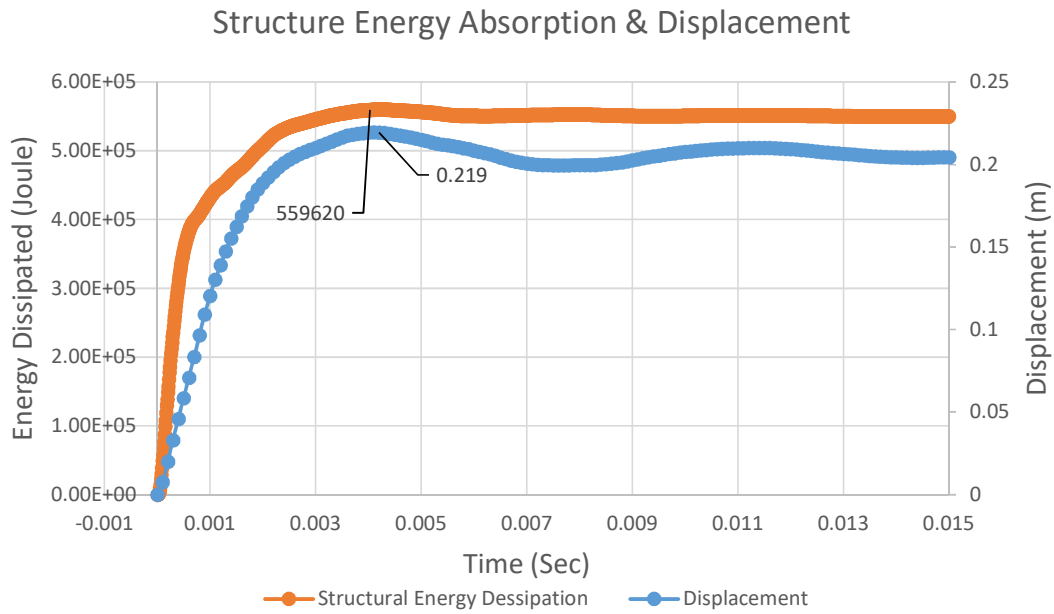


Figure 4.2-hh Structure Internal Energy and the Radial Displacement (Fluid modelled with MAT Elastic Fluid)

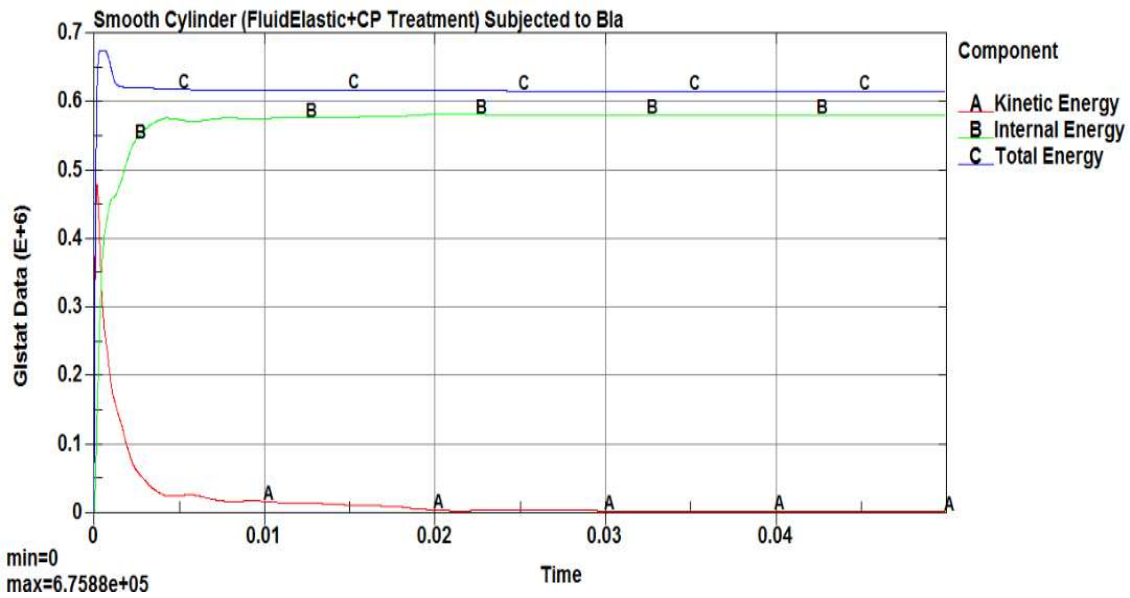


Figure 4.2-ii Energy balance of the numerical simulation

The energy balance for the numerical calculation is presented in the Figure 4.2-ii where in the beginning of the calculation, a maximum amount of total energy of 675.8 kJ was reported. Here the total energy supplied by the shock wave is larger than the numerical calculation without cavitation treatment and also quite close to the calculation where fluid is modelled with

MAT Acoustic including cavitation treatment behaviour law. It is again due to the absence of negative pressure in the fluid layers near the structure.

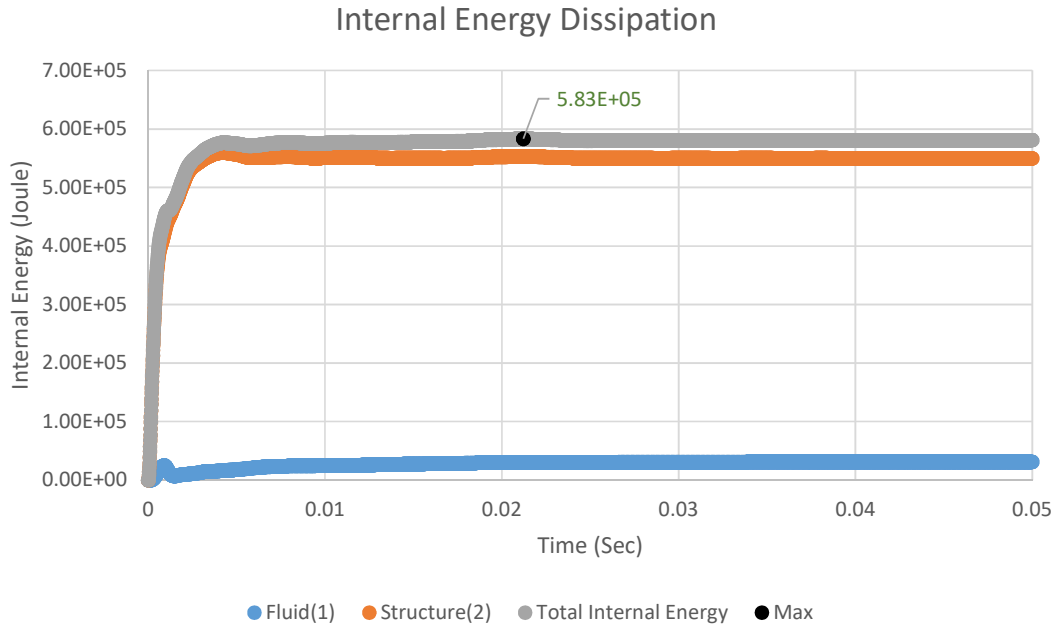


Figure 4.2-jj Dissipation of the Internal Energy

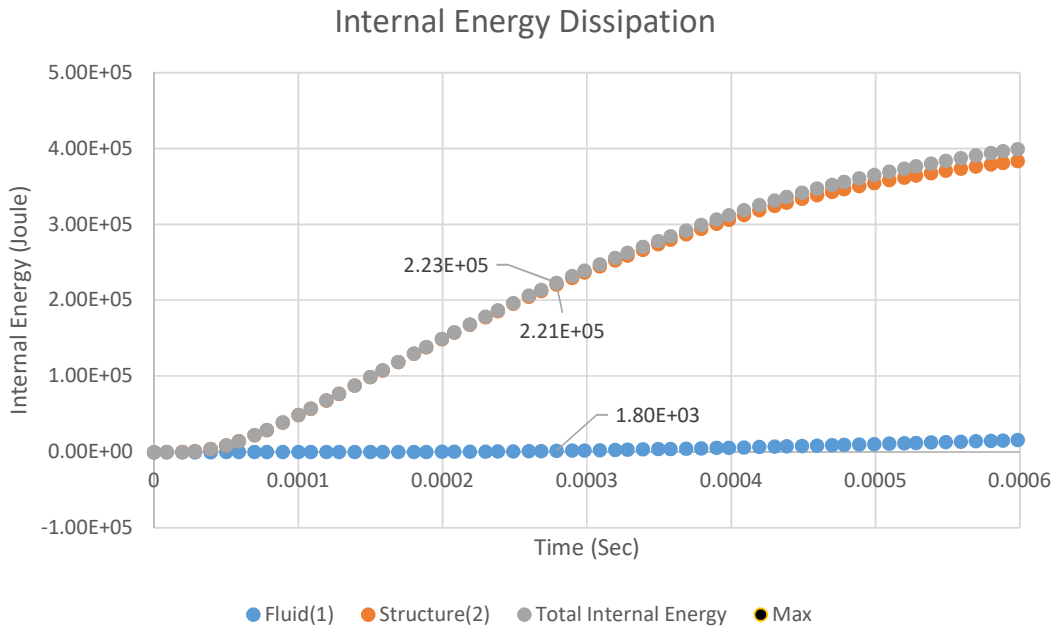


Figure 4.2-kk Internal Energy dissipation within early structural response time 0.6 milliseconds

Figure 4.2-jj presents the level of energy dissipated separately by structure and fluid layer close to the submerged structure. It is also noted that the level of energy dissipation in the fluid layer is insignificant when fluid domain is treat with cavitation treatment. It is also remarkable to observe that at the primary phase of the structural response, all the supplied energy is absorbed by the structure. Consequently, the radiation damping is almost zero in this circumstance.

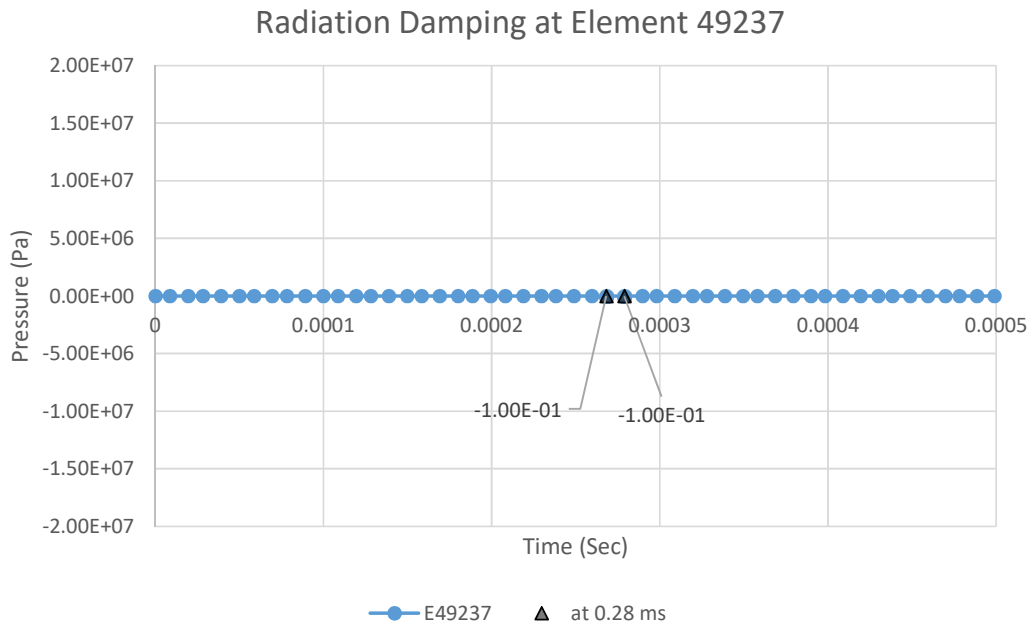


Figure 4.2-ll Radiation Damping at the fluid element 49237

INTERNAL ENERGY AT 0.28MS

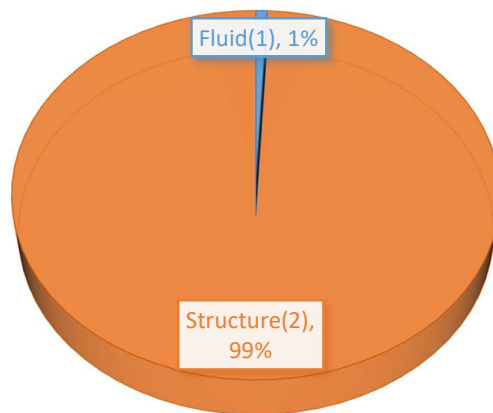


Figure 4.2-mm Distribution of total internal energy dissipation

4.2.3.3 Shock Factor 2.5

Shock factor is defined by the equation 12 and rewriting the equation as follows, here the charge weight is $C = 1.1$ kg and $D = 0.42$ m is the distance of the charge. The shock factor $SF = 2.5$.

$$SF = \frac{C^{1/2}}{D} \quad (38)$$

1. Structure immersed in Fluid modelled with Acoustic Behaviour Law

After simulating the numerical model with MAT_PLASTIC_KINEMATIC (MAT 03) for structure and MAT_ACOUSTIC for the fluid, the maximum radial displacement was reported to be 0.182 m at the internal energy level of 332.1 kJ.

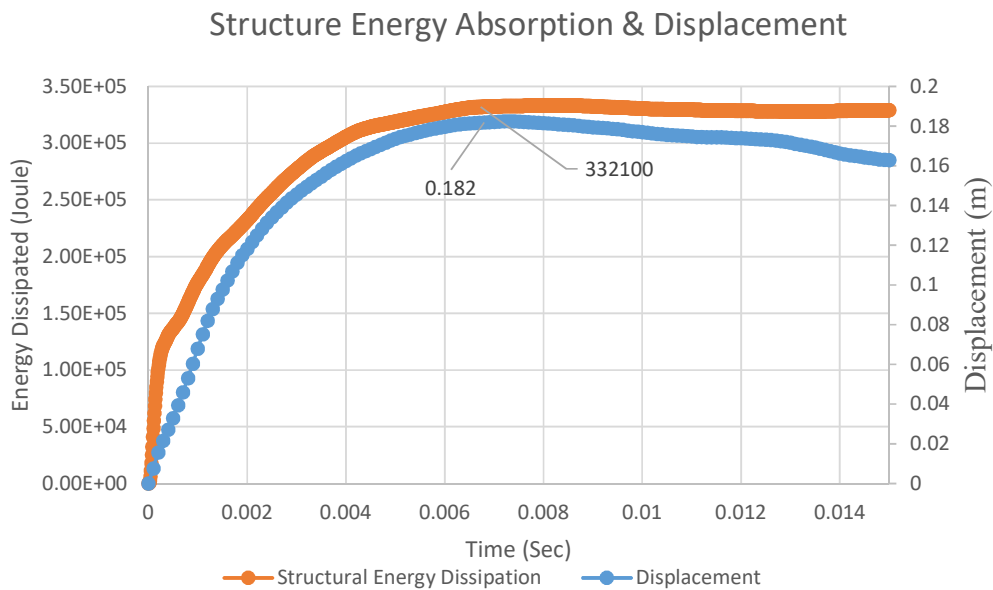


Figure 4.2-nn Structure Internal Energy and the Radial Displacement (Fluid modelled with MAT Acoustic)

The energy balance for the numerical calculation is presented in Figure 4.2-pp where in the beginning of the calculation, the maximum amount of total energy was reported 522.3 kJ. This energy was supplied by the shock wave as a result of underwater explosion near the structure.

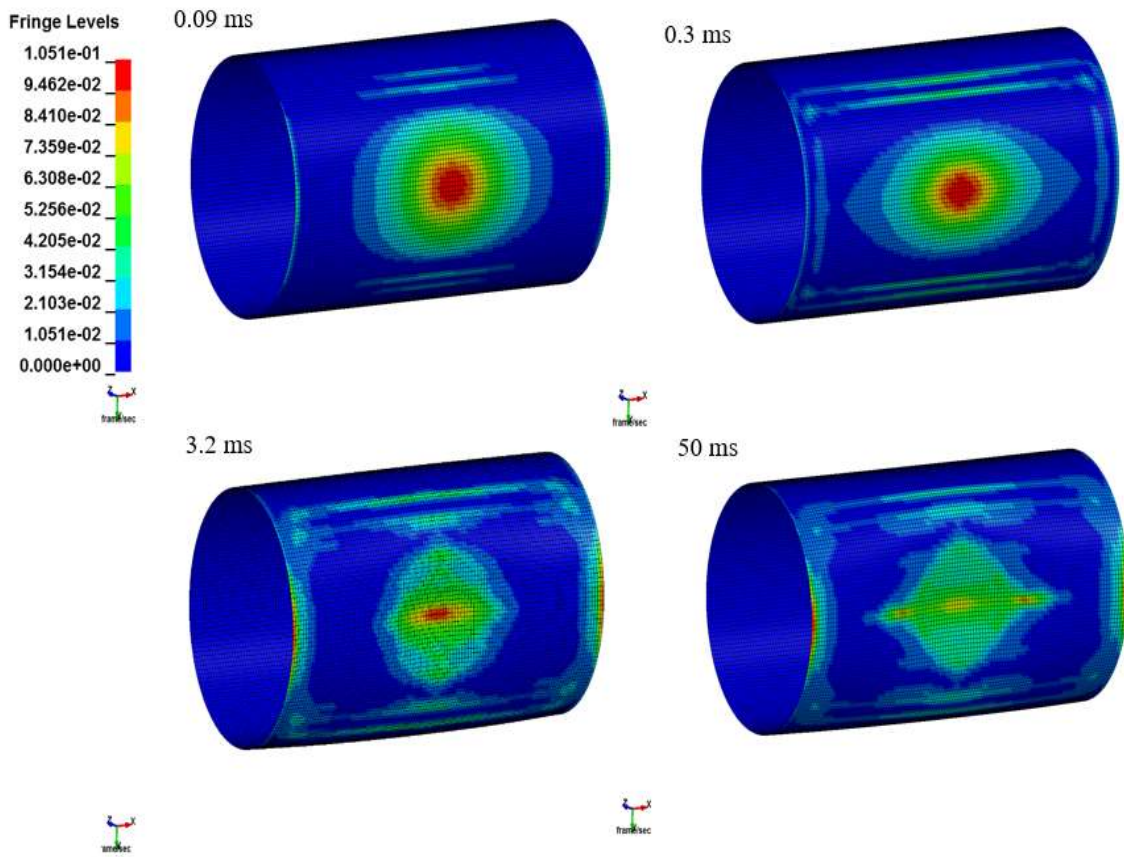


Figure 4.2-oo Plastic strain at different time steps.

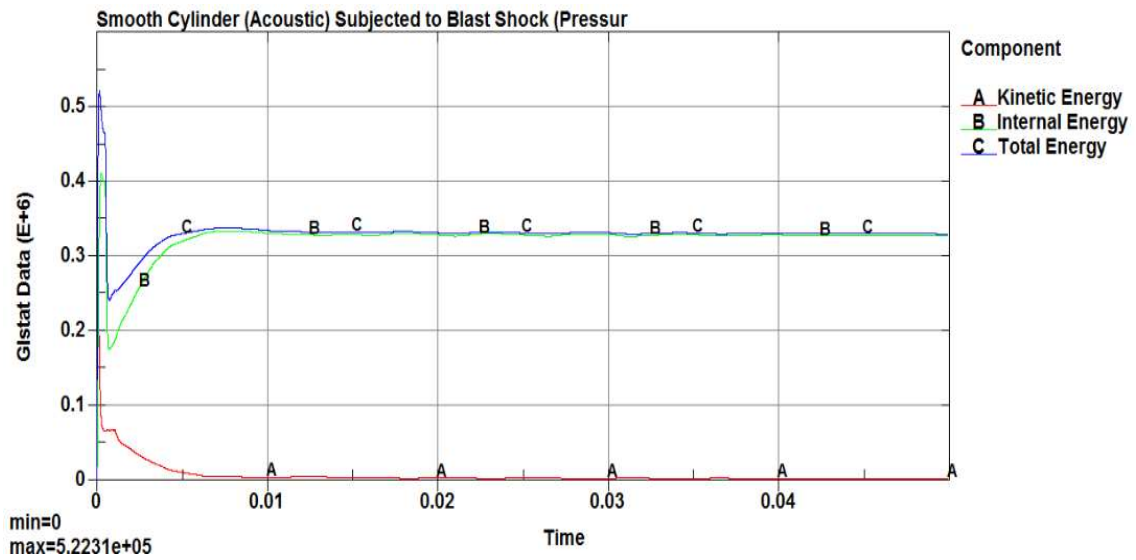


Figure 4.2-pp Energy balance of the numerical simulation

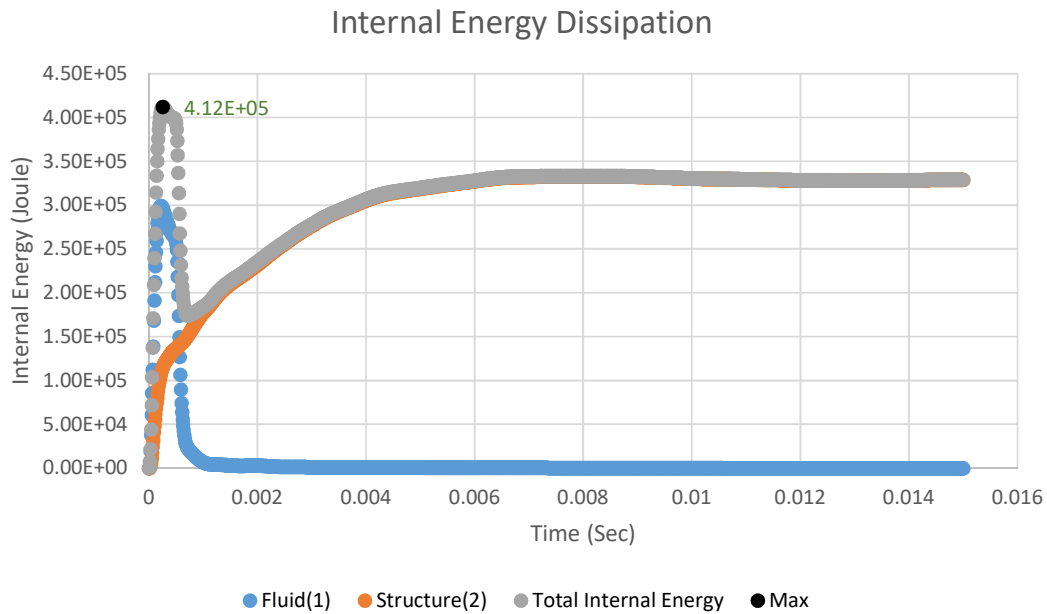


Figure 4.2-qq Dissipation of the Internal Energy

Figure 4.2-qq presents the level of energy dissipated separately by structure and fluid layer close to the submerged structure. It is also noted that the level of energy dissipation in the fluid layer is significant. For underwater explosion analysis, it is very important to observe early stage phenomenon within few micro-seconds. It is also remarkable to observe that at the primary phase of the structural response, the combine total amount of internal energy supplied to fluid and structure was 412 kJ.

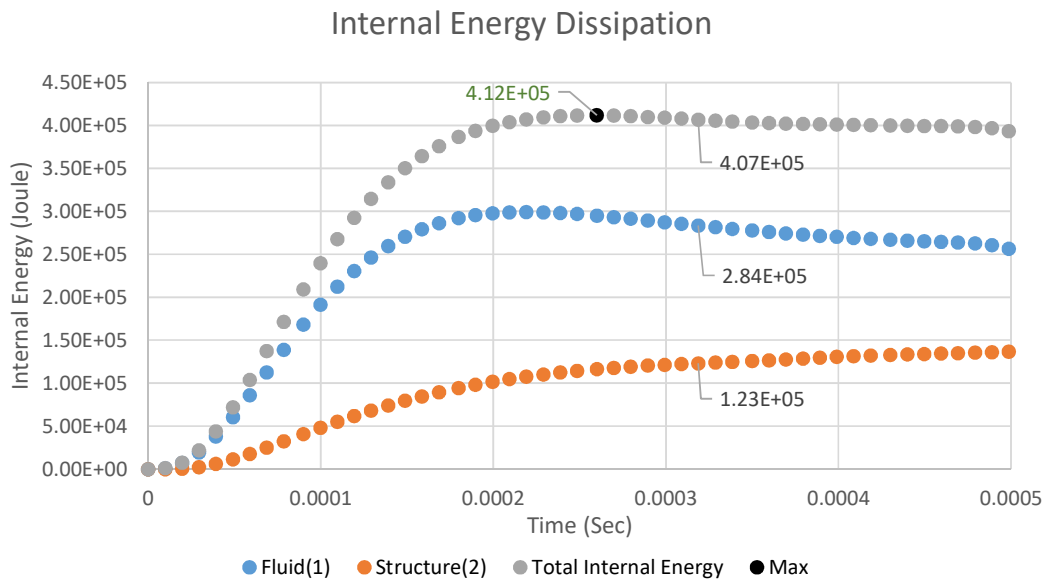


Figure 4.2-rr Internal Energy dissipation within early structural response time 0.5 milliseconds

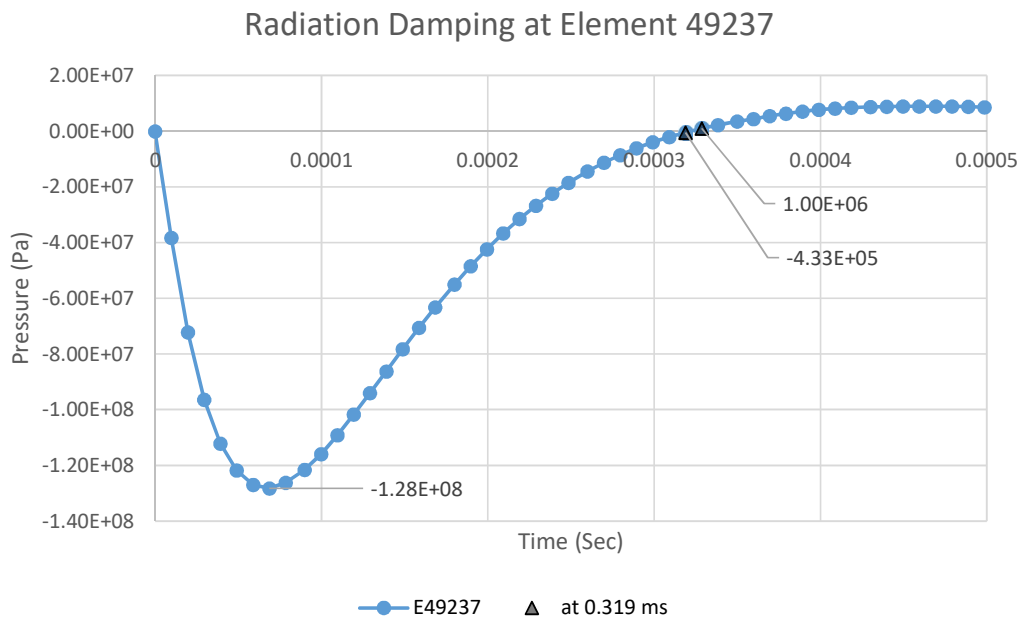


Figure 4.2-ss Radiation Damping at the fluid element 49237

Here it can be observed that at the beginning of the blast pressure applied to the structure, this latter starts to move, generating a negative pressure (Figure 4.2-ss) in the fluid elements adjacent to the structure. As a result the fluid starts to absorb more energy, here the energy is coming from the blast pressure. The fluid absorbs almost 67% (At time 0.2 ms fluid has 53.8 kJ, structure has 118kJ and the total energy 172 kJ, Figure 4.2-rr) of the total energy

supplied by the blast pressure to gain zero pressure or equilibrium from the negative pressure, which is radiation damping by the fluid in this situation. And the deformation of the structure absorbs the rest of the energy to resist the underwater blast shock.

INTERNAL ENERGY AT 0.319MS

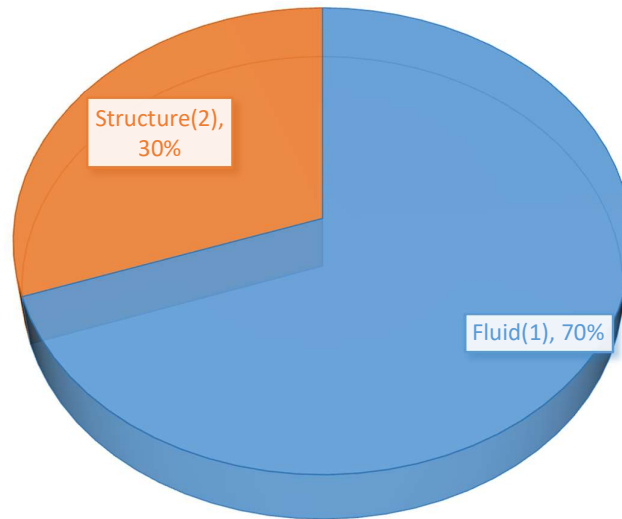


Figure 4.2-tt Distribution of total internal energy dissipation

Figure 4.2-uu represents the evolution of the low pressure region in the fluid layer near the structure as a result of complex fluid structure interaction during the post phase of underwater explosion. This phenomenon can be seen frequently for surface ships as close to the water surface and the influence of hydrostatic pressure is less than deep in the sea or ocean. So for the structures submerged in the deep sea state, it is less likely to observe cavitation near the structure due to the influence of high hydrostatic pressure. The other effect of stretching of the fluid mesh near the shell is due to the fact that Eulerian fluid nodes are shared by the Lagrangian structural nodes at the fluid structure interface. As here the fluid model is modelled with MAT_90 (MAT Acoustic). So due to the large deformation or motion of structure, the fluid elements immediately close to the structure are distorted or stretched. But it is not affecting the calculated pressure close to that region as in the previous simulations already reported approximately same level of results (Energy, Pressure and deformation) as MAT_01 (MAT Elastic Fluid). The fluid mesh in MAT_01 has the capability to follow the structure whenever there is a large deformation or motion of structure.

Cavitation in the Fluid domain - Fluid modelled with MAT_ACOUSTIC (SF 2.5)

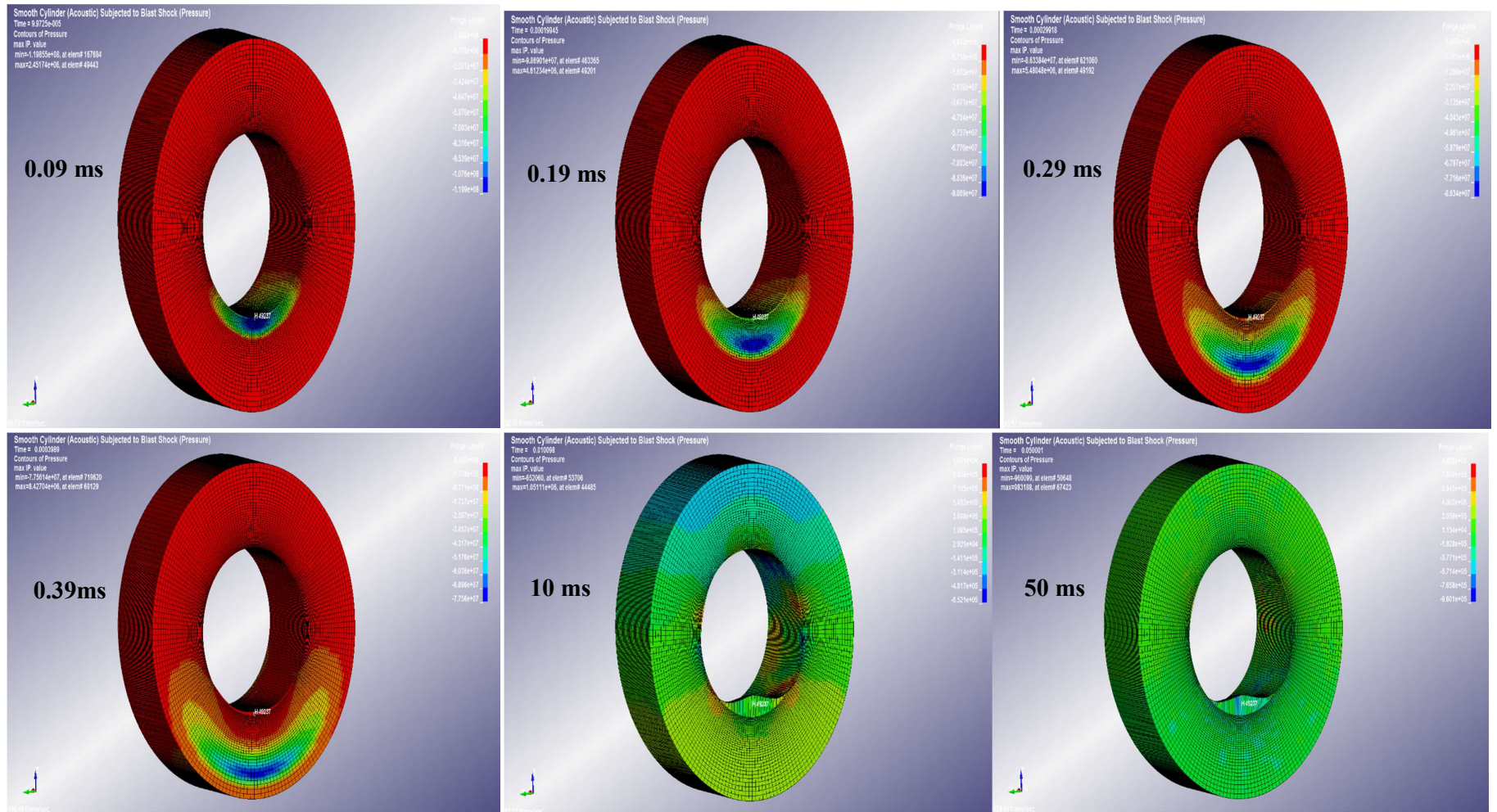


Figure 4.2-uu Cavity flow or flow of low pressure oscillation in MAT Acoustic SF 2.5

2. Structure immersed in Fluid modelled with Acoustic behaviour law & Cavitation Treatment

In this section, the cavitation option was activated in MAT_ACOUSTIC (MAT 90) behaviour law in order to prevent negative pressure inside the fluid by allowing the occurrence of cavitation. MAT_PLASTIC_KINEMATIC (MAT 03) is still used to model the elastic plastic behavior of the structure. In this case, the maximum radial displacement was reported to be 0.51 m at the internal energy level of 1.74 MJ. The cavitation treatment was considered by LS-DYNA (negative pressures are set to zero) with the simulation parameters described in Table 4.2-c.

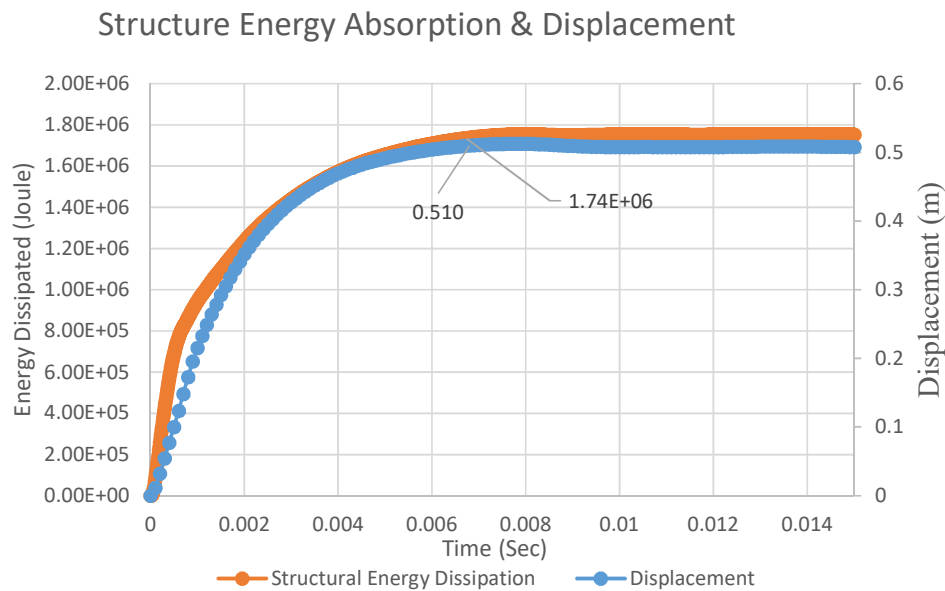


Figure 4.2-vv Structure Internal Energy and the Radial Displacement (Fluid modelled with MAT Acoustic & cavitation treatment)

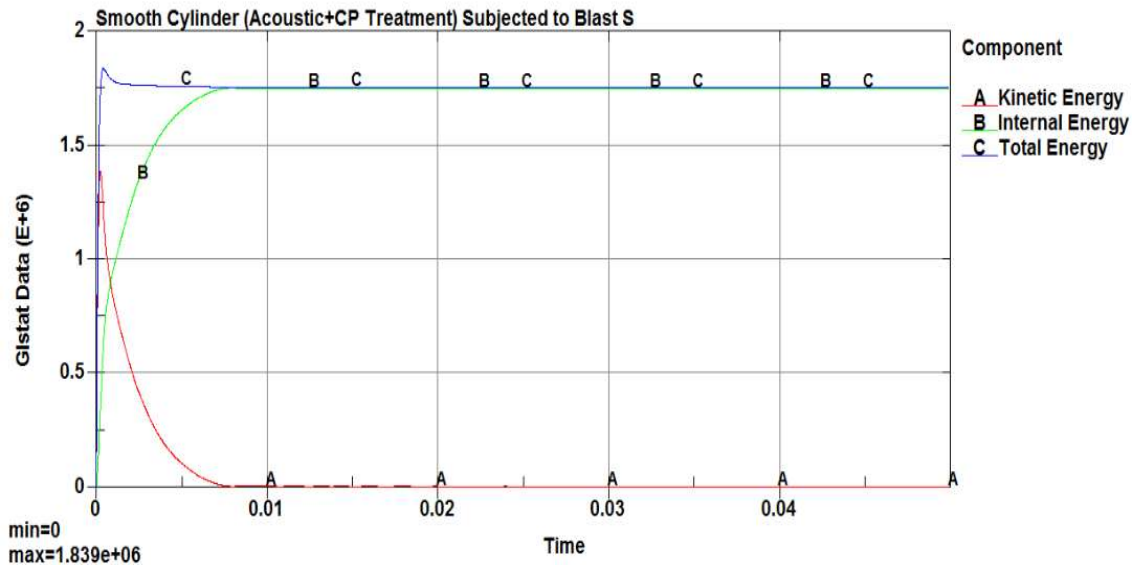


Figure 4.2-ww Energy balance of the numerical simulation

The energy balance for the numerical calculation is presented in the Figure 4.2-ww where, in the beginning of the calculation, a maximum amount of total energy of 1.83 MJ was reported. Here the total energy supplied by the shock wave is larger than the numerical calculation without cavitation treatment. It is due to the absence of negative pressure in the fluid layers near the structure which indeed resists to the structure deformation.

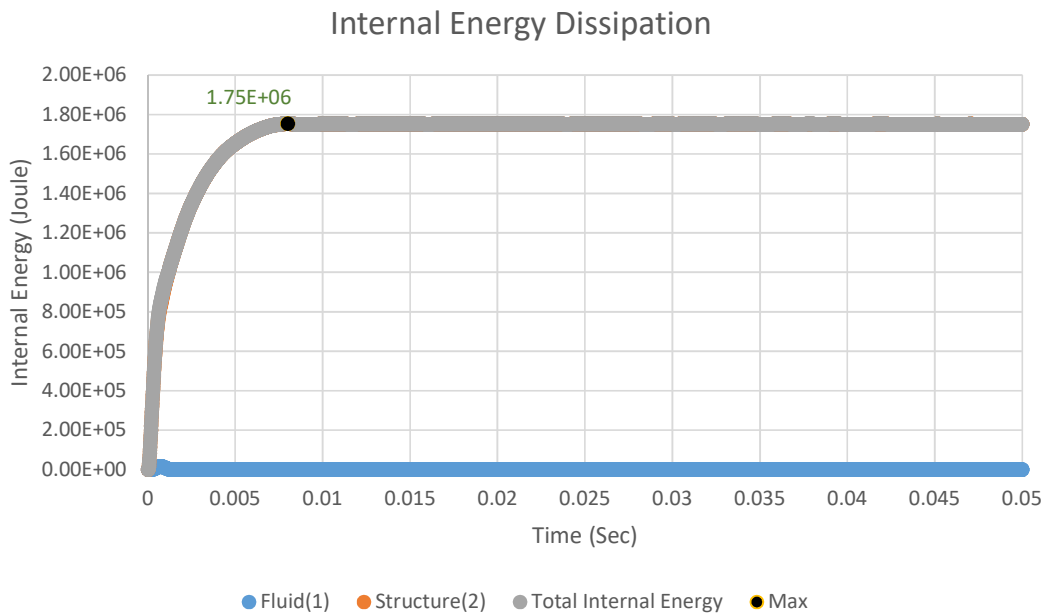


Figure 4.2-xx Dissipation of the Internal Energy

Figure 4.2-xx presents the level of energy dissipated separately by structure and fluid layer close to the submerged structure. It is also noted that the level of energy dissipation in the fluid layer is insignificant when fluid domain is treat with cavitation treatment. It is also remarkable to observe that at the primary phase of the structural response, all the supplied energy is absorbed by the structure. Consequently, the radiation damping is almost zero in this circumstance.

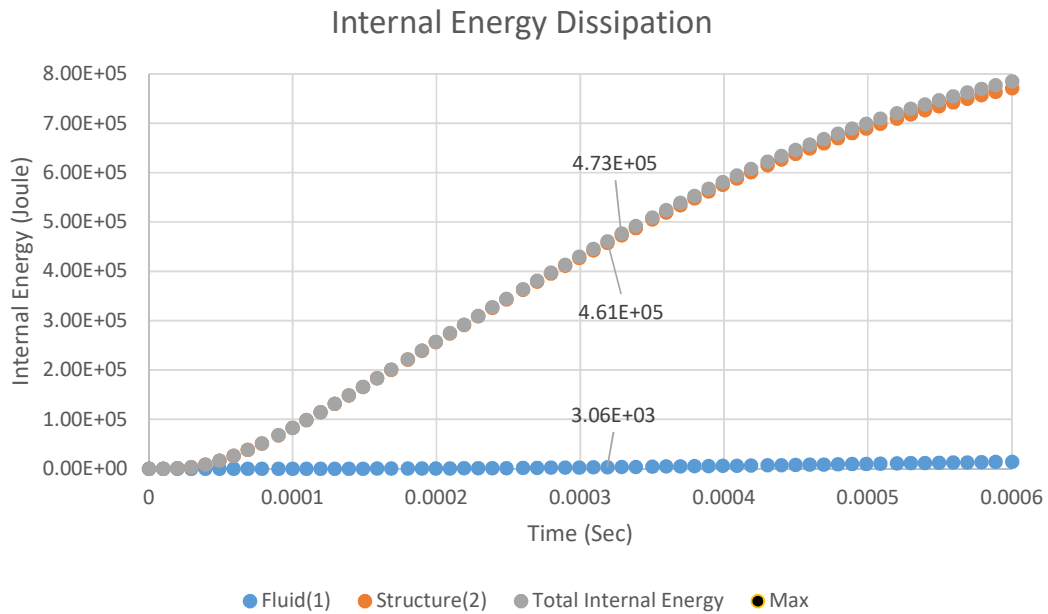


Figure 4.2-yy Internal Energy dissipation within early structural response time 0.6 milliseconds

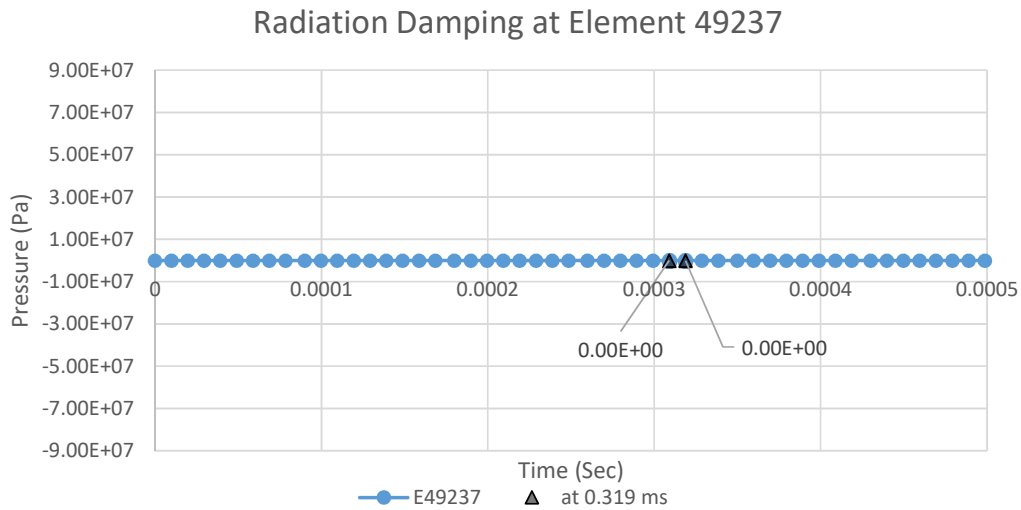


Figure 4.2-zz Radiation Damping at the fluid element 49237

INTERNAL ENERGY AT 0.3MS

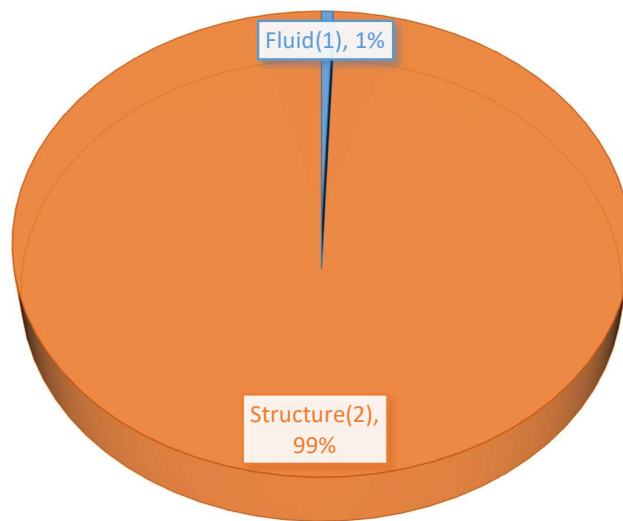


Figure 4.2-aaa Distribution of total internal energy dissipation

3. Structure immersed in Fluid modelled with Fluid Elastic behaviour law

After simulating the numerical model with MAT_PLASTIC_KINEMATIC (MAT 03) for structure and MAT_ELASTIC_FLUID for fluid, the maximum radial displacement was reported to be 0.176 m at the internal energy level of 320 kJ. The results are quite similar to the simulation with MAT Acoustic for SF 2.5.

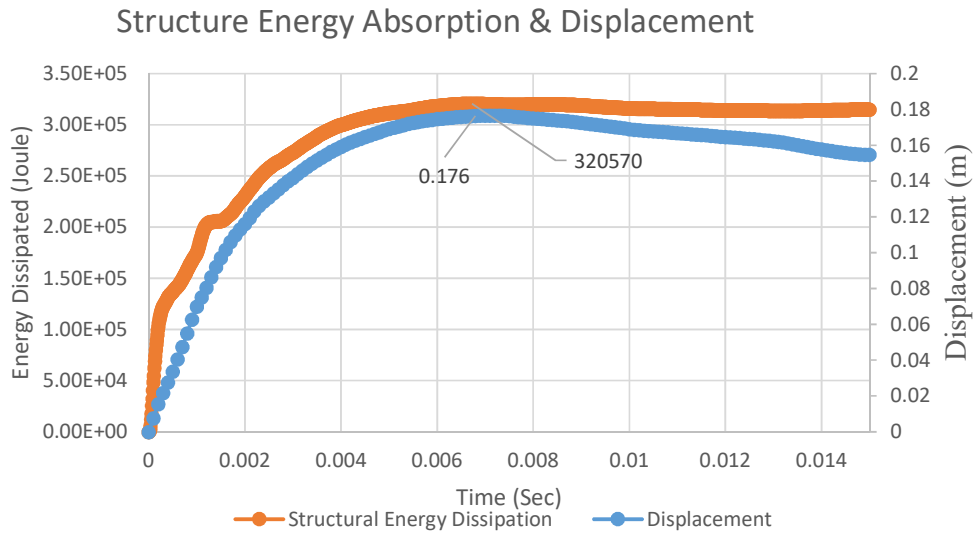


Figure 4.2-bbb Structure Internal Energy and the Radial Displacement (Fluid modelled with MAT Elastic Fluid)

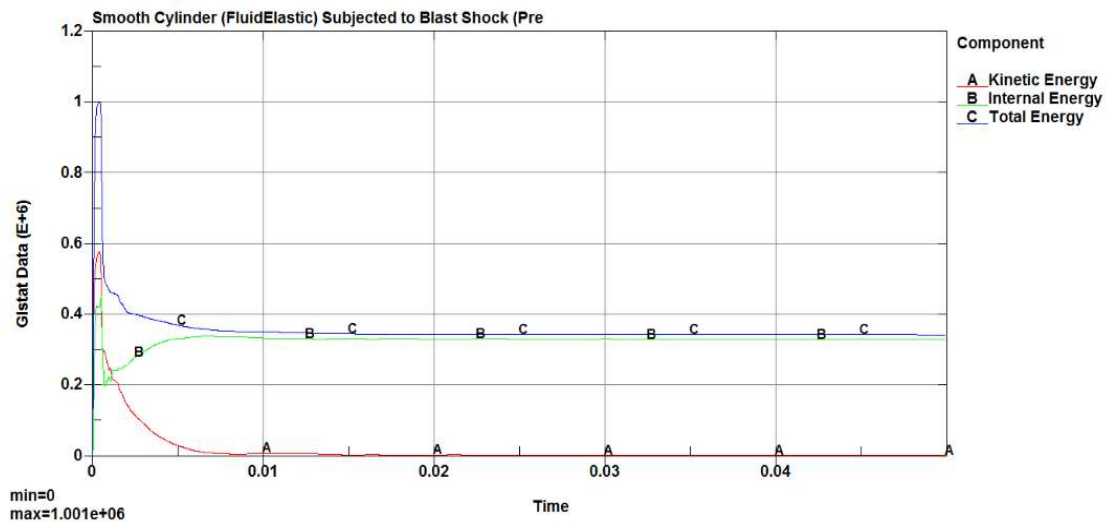


Figure 4.2-ccc Energy balance of the numerical simulation

The energy balance for the numerical calculation is presented in the Figure 4.2-ccc where in the beginning of the calculation the maximum amount of total energy was reported 1 MJ. This energy was supplied by the shock wave as a result of underwater explosion near the structure.

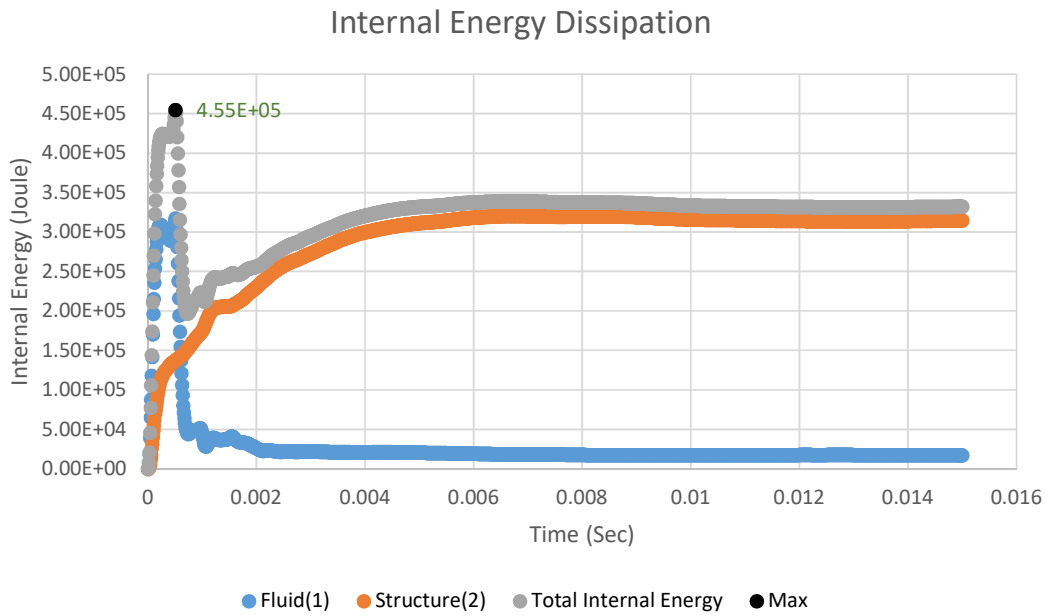


Figure 4.2-ddd Dissipation of the Internal Energy

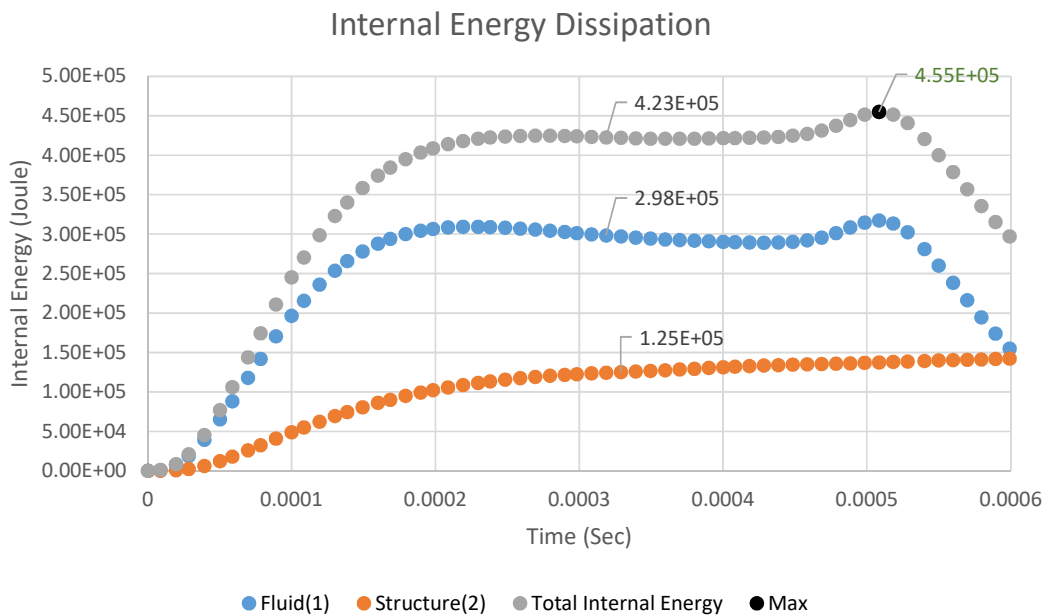


Figure 4.2-eee Internal Energy dissipation within early structural response time 0.6 milliseconds

Figure 4.2-ddd presents the level of energy dissipated separately by structure and fluid layer close to the submerged structure. It is also noted that the level of energy dissipation in the fluid layer is significant. For underwater explosion analysis, it is very important to observe early stage phenomenon within few micro-seconds. It is also remarkable to observe

that at the primary phase of the structural response, the combine total amount of internal energy supplied to fluid and structure was 455 kJ.

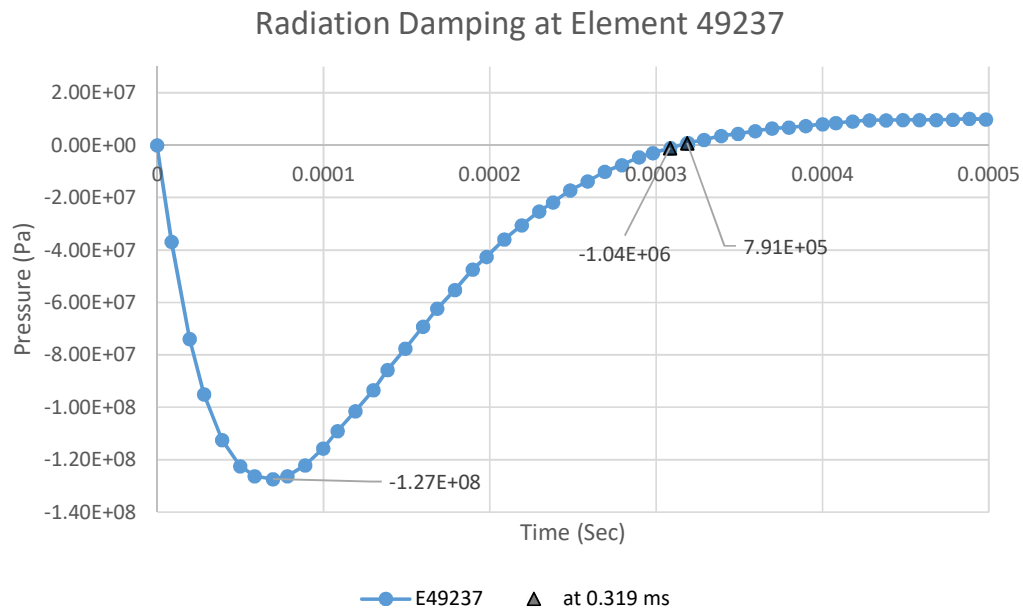


Figure 4.2-fff Radiation Damping at the fluid element 49237

Here it can be observed that at the beginning of the blast pressure applied to the structure, the structure starts to move generating a negative pressure (Figure 4.2-fff) region adjacent to the structure in the fluid layer. As a result the fluid starts to absorb more energy, here the energy is coming from the blast pressure. The fluid absorbs almost 71% (*At time 0.319 ms fluid has 298 kJ, structure has 125 kJ and the total energy 423 kJ, Figure 4.2-eee*) of the total energy supplied by the blast pressure to gain zero pressure or equilibrium from the negative pressure, which is radiation damping by the fluid in this situation. The structural deformation or the structure absorbs the rest of the energy to resist the underwater blast shock.

INTERNAL ENERGY AT 0.319MS

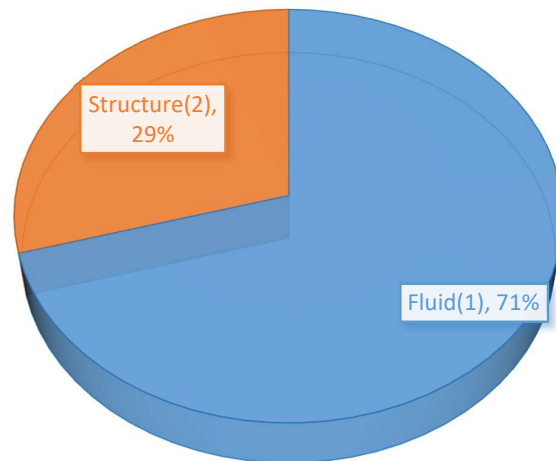


Figure 4.2-ggg Distribution of total internal energy dissipation

Figure 4.2-iii represents the evolution of the low pressure region in the fluid layer near the structure as a result of complex fluid structure interaction during the post phase of underwater explosion. Figure 4.2-hhh presents the capability of MAT Elastic Fluid element to flow the fluid mesh with the large deformation or motion of the structure. So there is no stretching or distortion of the fluid mesh like MAT Acoustic in the previous scenario.

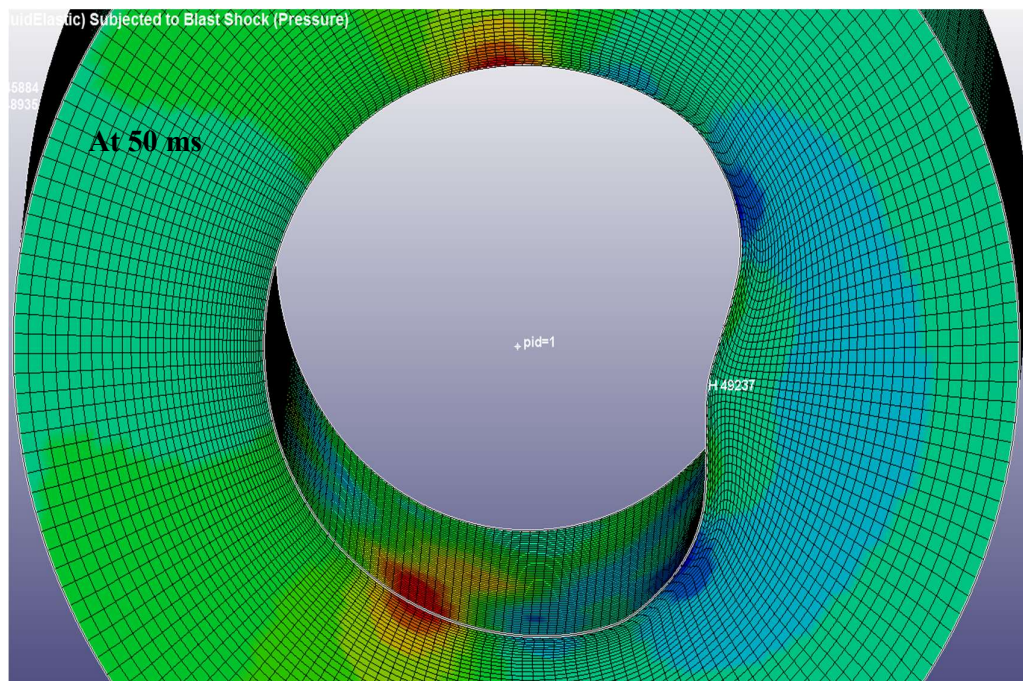


Figure 4.2-hhh Fluid mesh flow with structure Shell in MAT Elastic Fluid Model

Cavitation in the Fluid domain - Fluid modelled with MAT_Elastic_Fluid (SF 2.5)

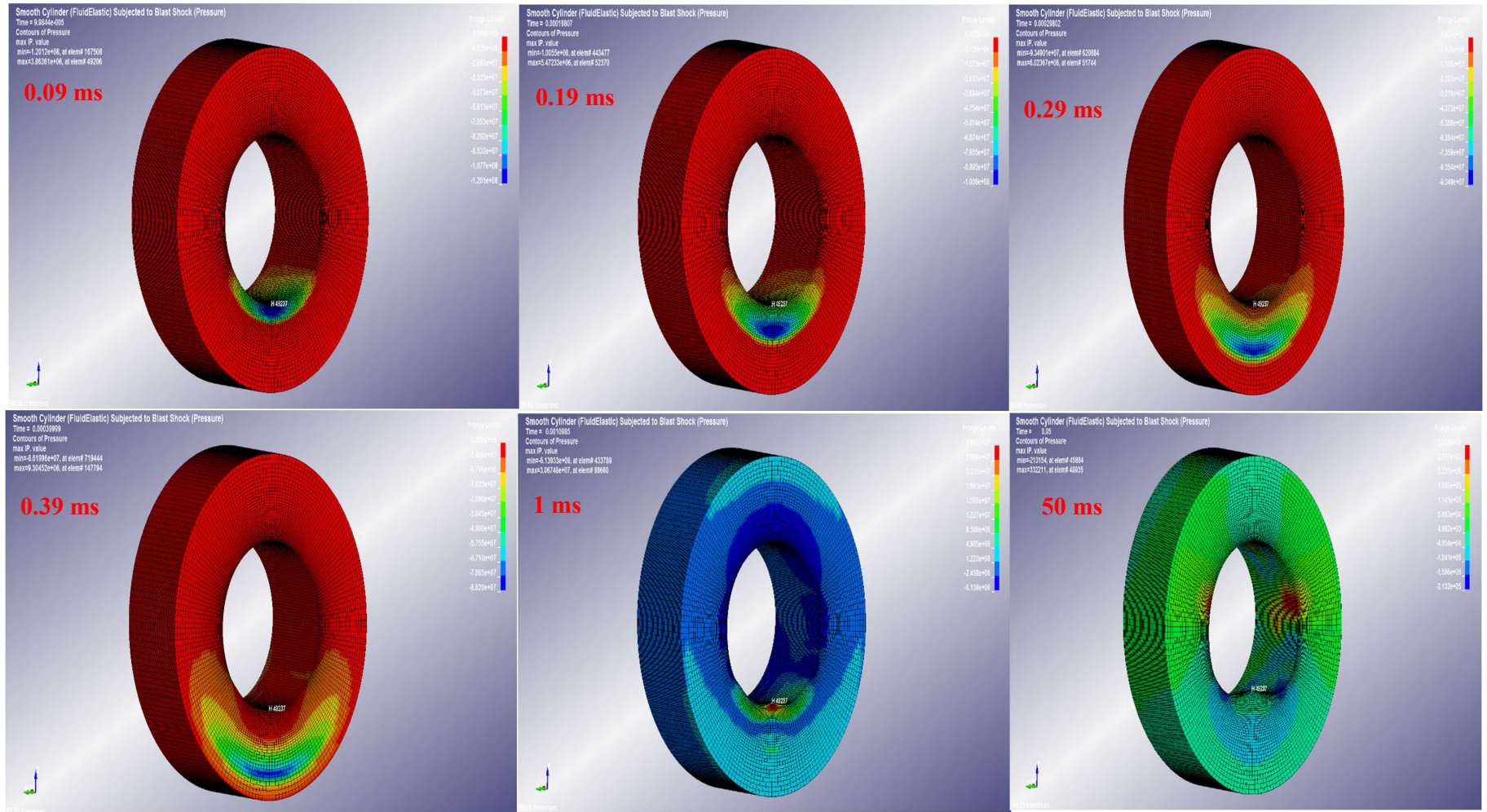


Figure 4.2-iii Cavity flow or flow of low pressure oscillation in MAT Elastic Fluid SF 2.5

4. Structure immersed in Fluid modelled with Fluid Elastic behaviour law & Cavitation Treatment

After simulating the numerical model with MAT_PLASTIC_KINEMATIC (MAT 03) for structure and MAT ELASTIC FLUID for fluid with cavitation treatment to prevent any negative pressure in the fluid domain, the maximum radial displacement was reported to be 0.503 m at the internal energy level of 1.7 MJ. The cavitation treatment was considered by LS-DYNA with the simulation parameters described in Table 4.2-b.

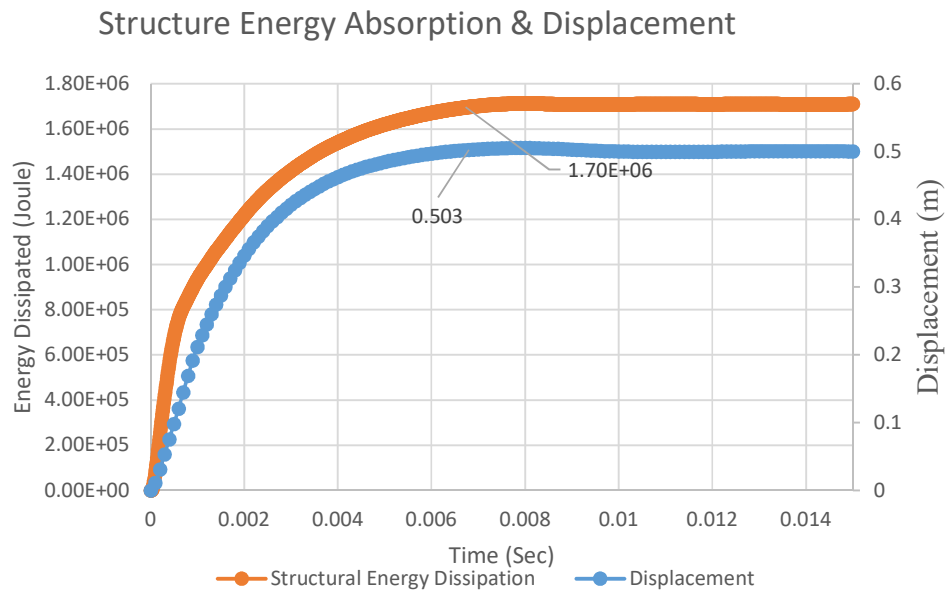


Figure 4.2-jjj Structure Internal Energy and the Radial Displacement (Fluid modelled with MAT Elastic Element & Cavitation Treatment)

The energy balance for the numerical calculation is presented in the Figure 4.2-kkk where in the beginning of the calculation, a maximum amount of total energy of 1.82 MJ was reported. Here the total energy supplied by the shock wave is larger than the numerical calculation without cavitation treatment and also quite close to the calculation where fluid is modelled with MAT Acoustic including cavitation treatment behaviour law. It is again due to the absence of negative pressure in the fluid layers near the structure.

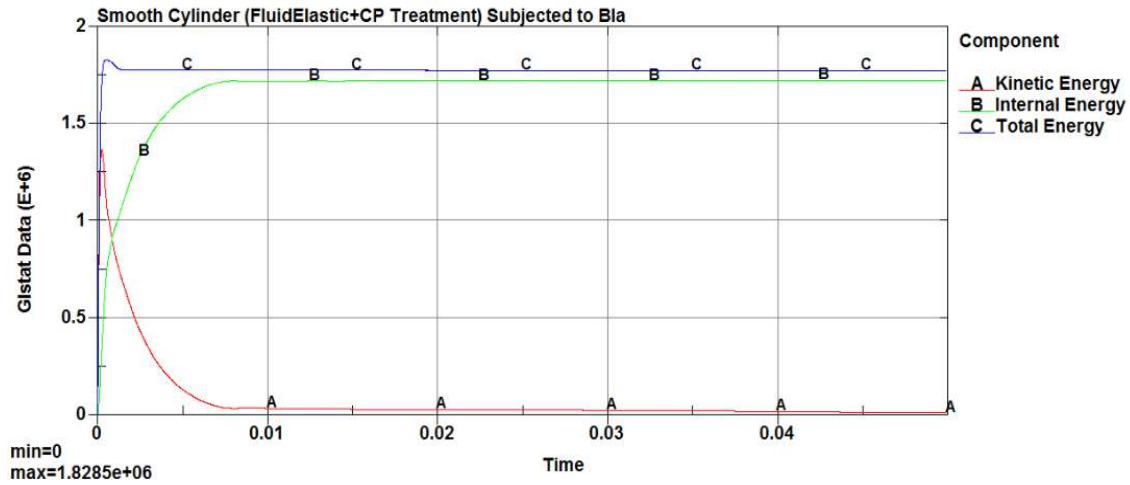


Figure 4.2-kkk Energy balance of the numerical simulation

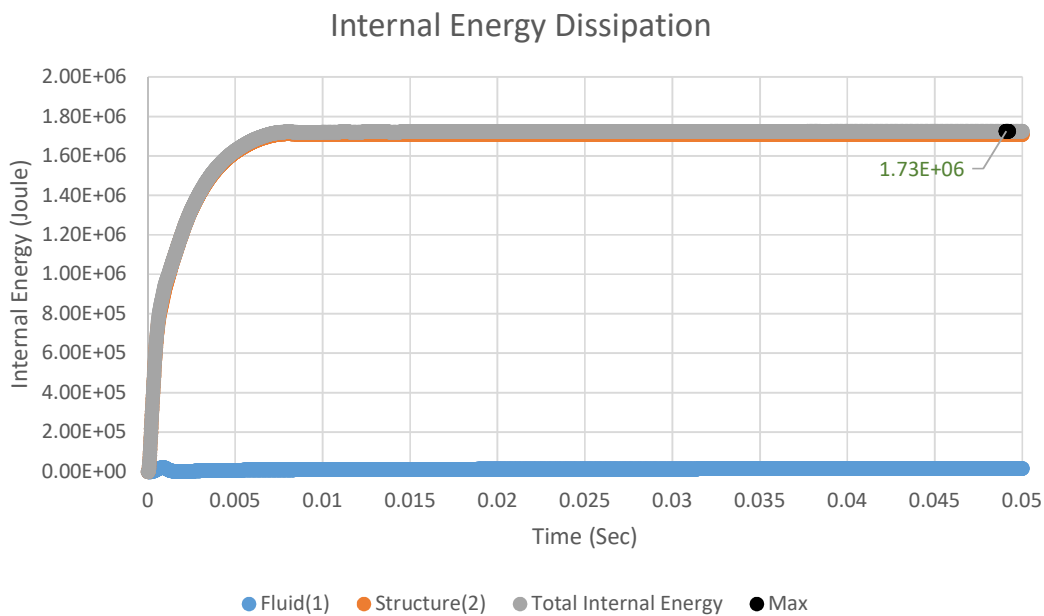


Figure 4.2-lll Dissipation of the Internal Energy

Figure 4.2-lll presents the level of energy dissipated separately by structure and fluid layer close to the submerged structure. It is also noted that the level of energy dissipation in the fluid layer is insignificant when fluid domain is treated with cavitation treatment. It is also remarkable to observe that at the primary phase of the structural response, all the supplied energy is absorbed by the structure. Consequently, the radiation damping is almost zero in this circumstance.

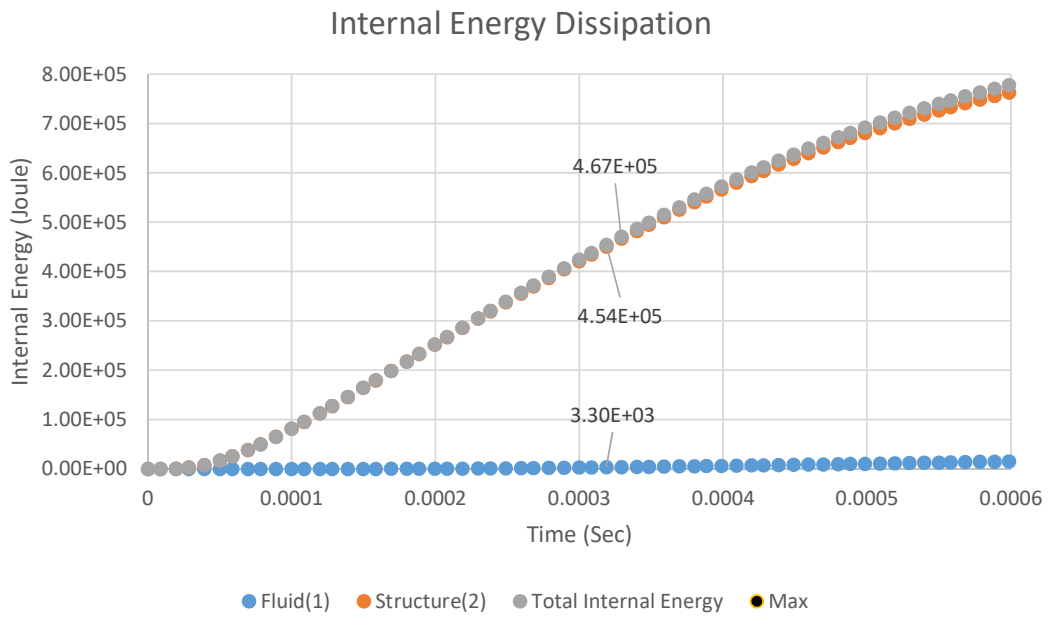


Figure 4.2-mmm Internal Energy dissipation within early structural response time 0.6 milliseconds

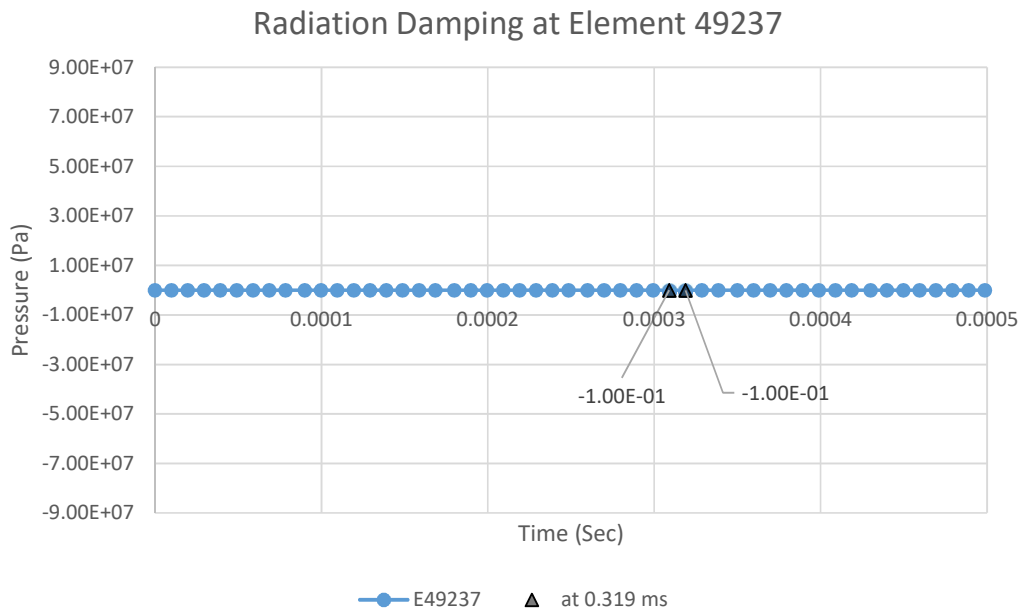


Figure 4.2-nnn Radiation Damping at the fluid element 49237

INTERNAL ENERGY AT 0.3MS

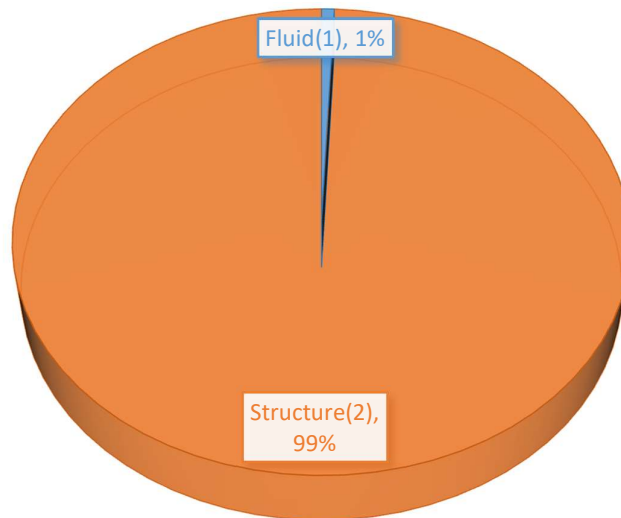


Figure 4.2-000 Distribution of total internal energy dissipation

4.2.3.4 *Double Exponential Decay of Peak*

Equation (18) calculates the pressure blast loading where the peak pressure exponentially decays with time. In this equation the peak pressure profile is decaying with single exponential fit. The single exponential fit is not capable to extend the pressure profile up to the start of oscillation phase (Geers, 2002). So double exponential fit is applied which extends up to the time when pressure is reduced approximately 5% of the peak. The equations (28) and (29) explain the condition for double decaying pressure profile, which is combined with the equation (18) and (26) to calculate the pressure field.2626 So for all the numerical calculations with double decaying pressure profile, the fluid domain material model was chosen to be as MAT ACOUSTIC and SF 1.68 and SF 2.5 was applied as the explosive characteristics.

- **Shock Factor 2.5**

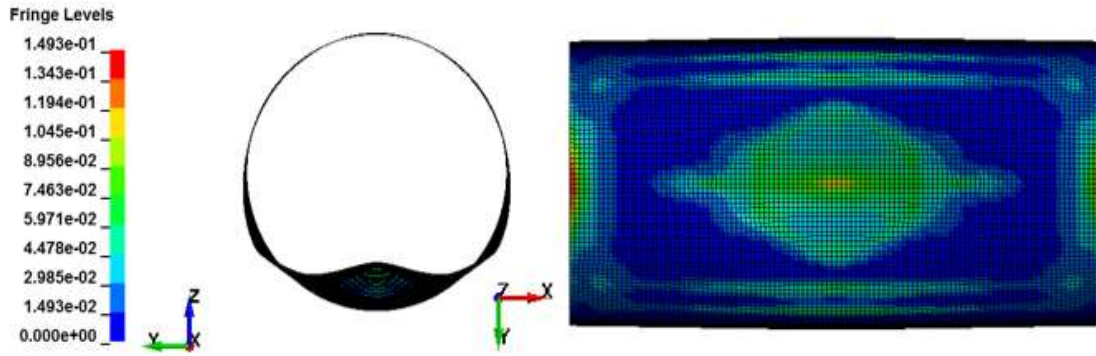


Figure 4.2-ppp Effective plastic strain distribution at 50 ms

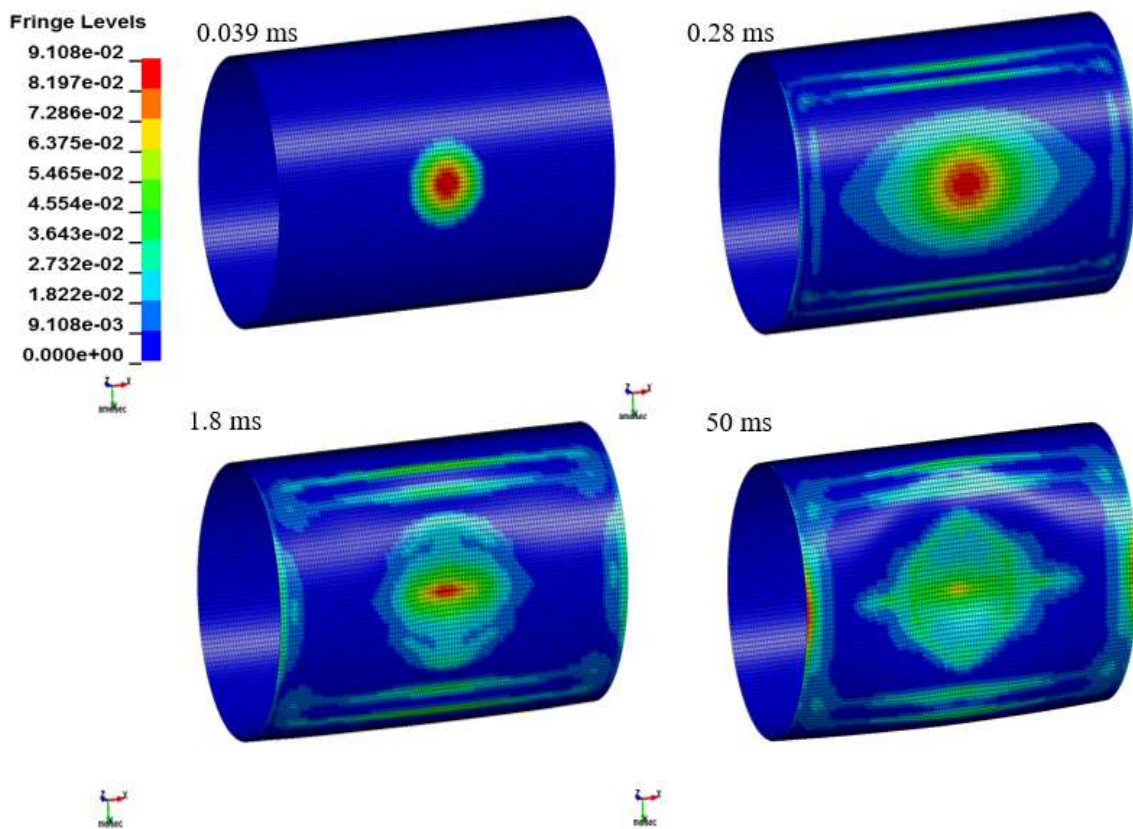


Figure 4.2-qqq Plastic strain at different time steps

After simulating the numerical model with MAT_PLASTIC_KINEMATIC (MAT 03) for structure and MAT_ACOUSTIC for the fluid, the maximum radial displacement was reported to be 0.251 m at the internal energy level of 524.8 kJ.

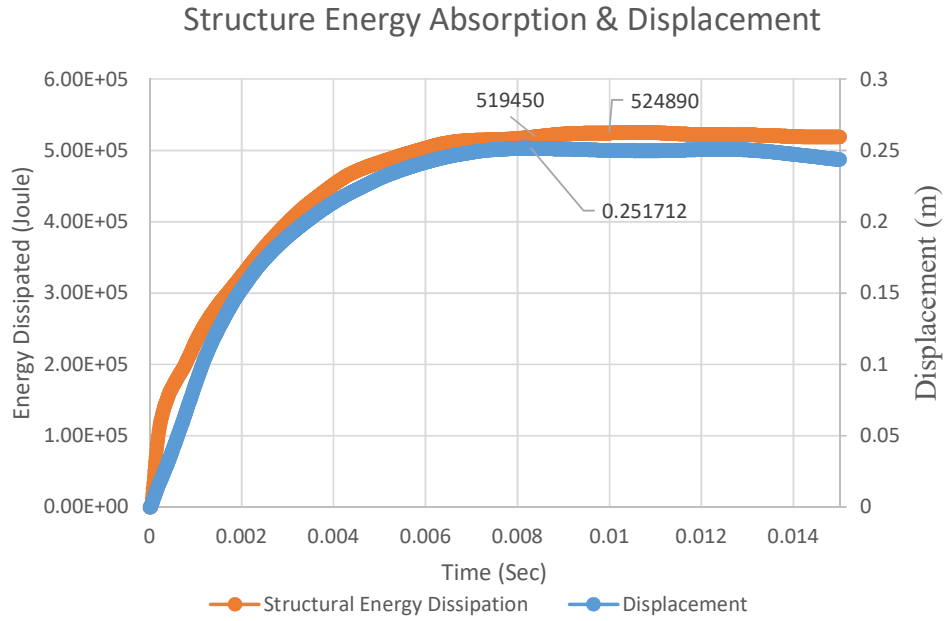


Figure 4.2-rrr Structure Internal Energy and the Displacement (Fluid modelled with MAT Acoustic)

The energy balance for the numerical calculation is presented in the Figure 4.2-sss where in the beginning of the calculation, the maximum amount of total energy was reported 593 kJ. This energy was supplied by the shock wave as a result of underwater explosion near the structure.

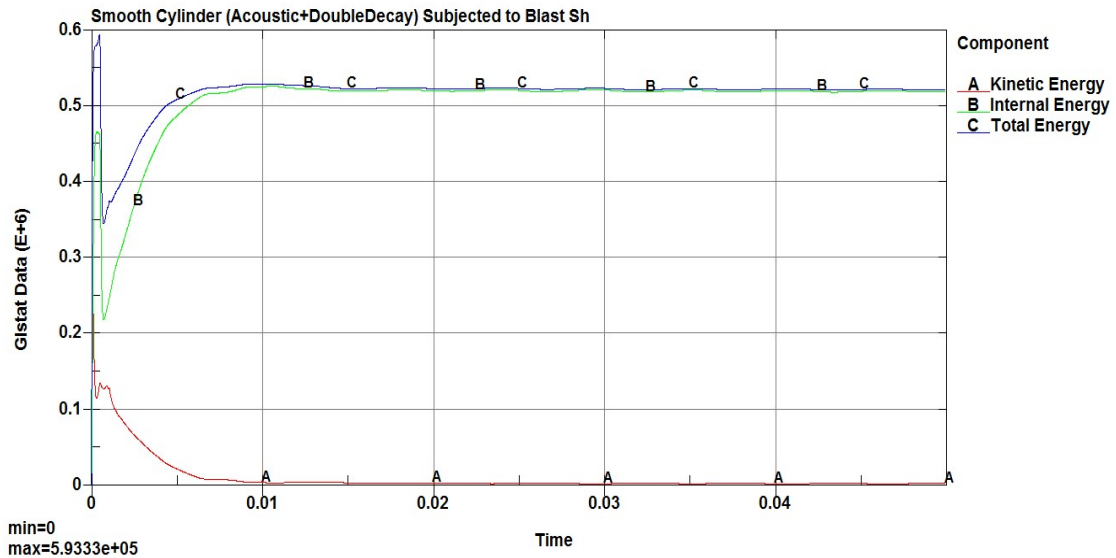


Figure 4.2-sss Energy balance of the numerical simulation

- **Shock factor 1.68**

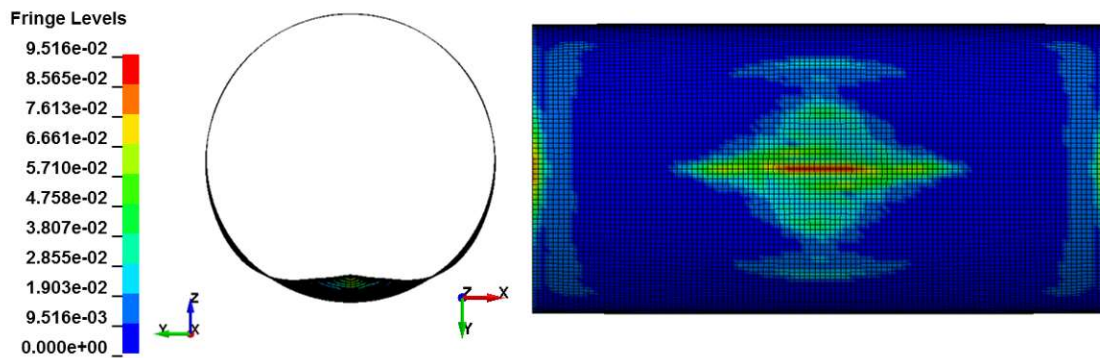


Figure 4.2-ttt Effective plastic strain distribution at 50 ms

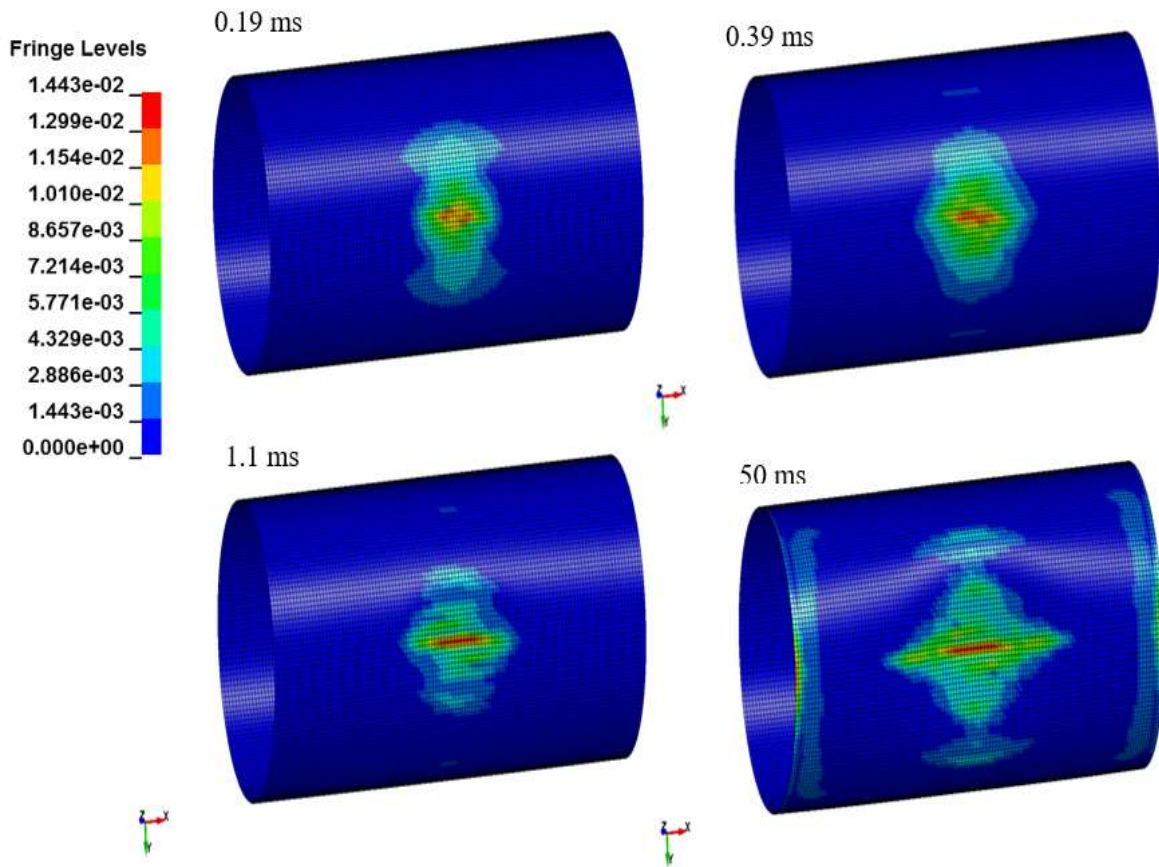


Figure 4.2-uuu Plastic strain at different time steps

After simulating the numerical model with MAT_PLASTIC_KINEMATIC (MAT 03) for structure and MAT Acoustic for fluid, the maximum radial displacement was reported to be 0.149 m at the internal energy level of 192.7 kJ.

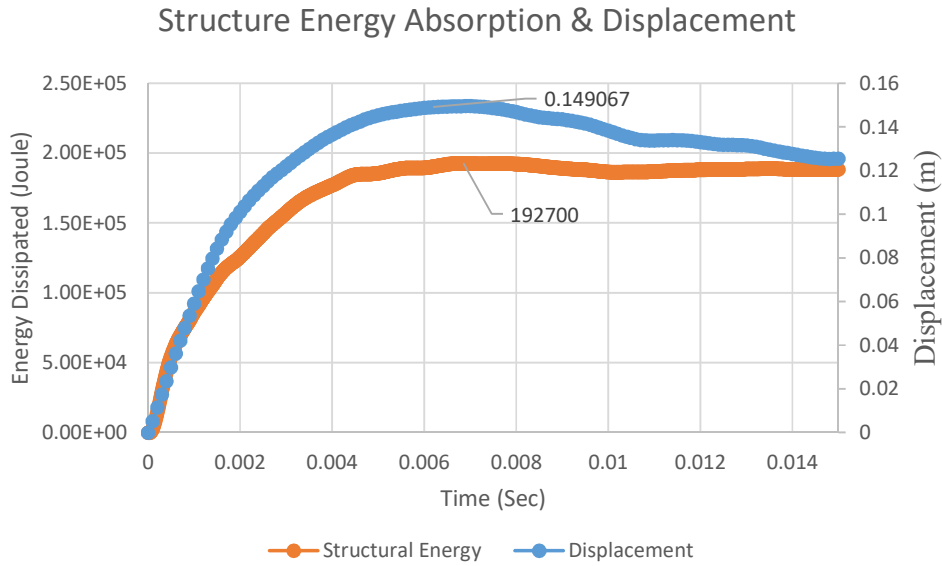


Figure 4.2-vvv Structure Internal Energy and the Displacement (Fluid modelled with MAT Acoustic)

The energy balance for the numerical calculation is presented in the Figure 4.2-www where in the beginning of the calculation, the maximum amount of total energy was reported 197.3 kJ. This energy was supplied by the shock wave as a result of underwater explosion near the structure.

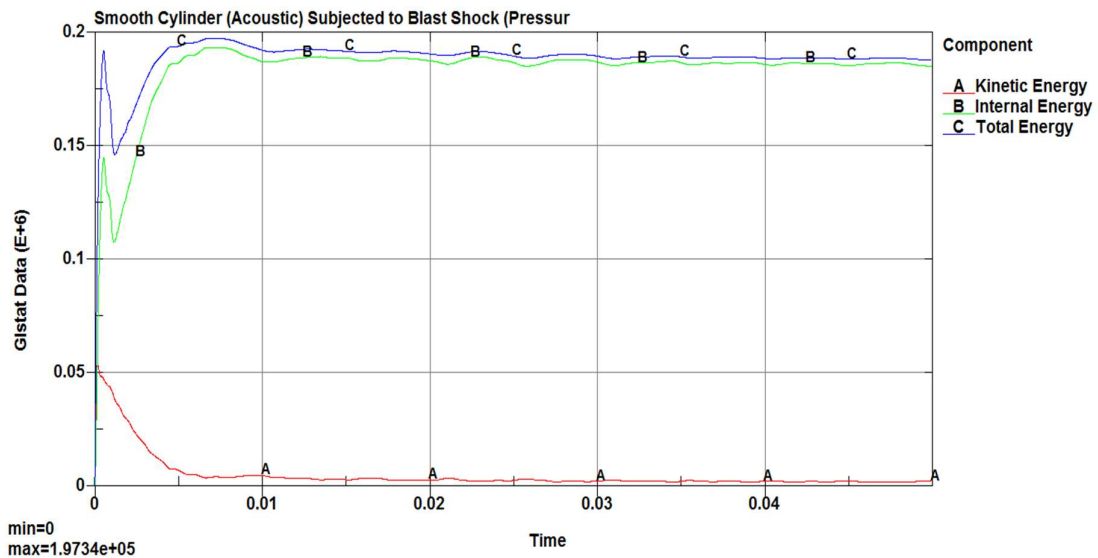


Figure 4.2-www Energy balance of the numerical simulation

4.3 Discussion & Comparison

- *Shock Factor 1.68 & Simple/Double Exponential Decay of the Peak Pressure*

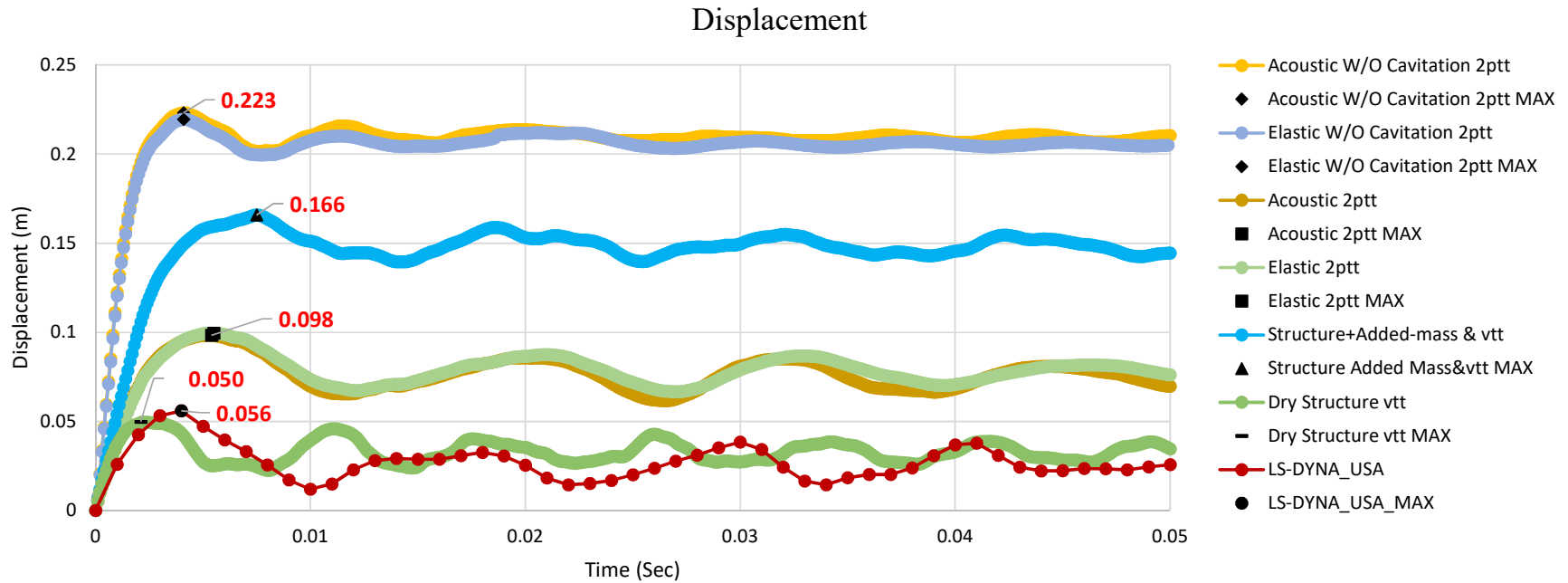


Figure 4.3-a Time evolution of Radial Displacement obtained from different methods of numerical calculation (Simple Decay). Reference for the date LS-DYNA/USA (Brochard, 2018)

Figure 4.3-a presents the structural response in terms of radial deflection for different simulation methods. Details of the different simulation conditions are discussed below,

- I. **Acoustic W/O cavitation 2ptt**, Fluid modelled with *MAT Acoustic including cavitation treatment* and the blast load on the structure is the *pressure field* coming from the shock wave. The numerical calculation was performed with LS-DYNA.
- II. **Elastic W/O cavitation 2ptt**, Fluid modelled with *MAT Elastic Fluid including cavitation treatment* and the blast load on the structure is the *pressure field* coming from the shock wave. The numerical calculation was performed with LS-DYNA.
- III. **Acoustic 2ptt**, Fluid modelled with *MAT Acoustic without cavitation treatment* and the blast load on the structure is the *pressure field* coming from the shock wave. The numerical calculation was performed with LS-DYNA.
- IV. **Acoustic 2ptt Double Decay**, Fluid modelled with *MAT Acoustic without cavitation treatment* and the blast load on the structure is the *pressure field* with Double decay coming from the shock wave. The numerical calculation was performed with LS-DYNA.
- V. **Elastic 2ptt**, Fluid modelled with *MAT Elastic Fluid without cavitation treatment* and the blast load on the structure is the *pressure field* coming from the shock wave. The numerical calculation was performed with LS-DYNA.
- VI. **Structure + Added-mass & vtt**, the blast load on the structure is the *initial velocity field* coming from the shock wave together with the *added mass effect* from the surrounding fluid layer calculated by the *analytical formulation* (considered the *Fluid-Structure interaction*). The numerical calculation was performed with LS-DYNA *without modelling the fluid* around the structure but by distributing lumped masses on the cylinder deformed area (Brochard, 2018)
- VII. **Dry Structure vtt**, the blast load on the structure is the *initial velocity field* coming from the shock wave calculated by the *analytical formulation* (considered the *Fluid-Structure interaction*). The numerical calculation was performed with LS-DYNA *without modelling the fluid* around the structure. (Brochard, 2018)
- VIII. **LS-DYNA/USA**, The blast load on the structure is the *incident pressure with single Exponential Decay* coming from the shock wave. The numerical calculation was performed with LS-DYNA and coupled with the USA (Underwater Shock Analysis) Code. (Brochard, 2018). The cavitation was not considered.
- IX. **LS-DYNA/USA Double Decay**, The blast load on the structure is the *incident pressure with Double decay Exponential Decay* coming from the shock wave. The numerical calculation was performed with LS-DYNA and coupled with the USA (Underwater Shock Analysis) Code. (Brochard, 2018). The cavitation was not considered.

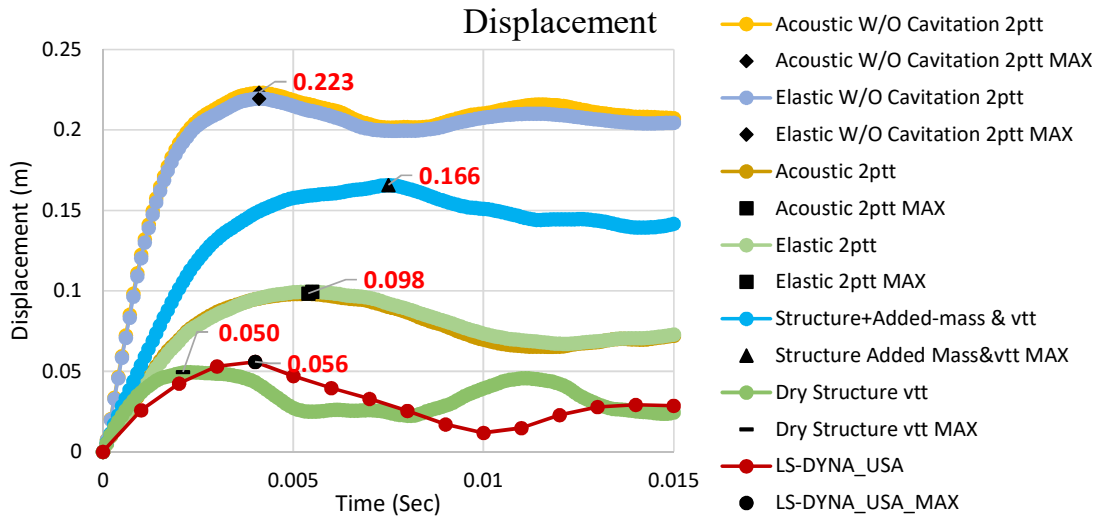


Figure 4.3-b Structural response as Radial displacement within a range of 15 ms for simple decay calculation. Reference for the date LS-DYNA/USA (Brochard, 2018)

From the Figure 4.3-b, Figure 4.3-c and Figure 4.3-e, it was observed that,

- Considering the added mass effect for the fluid adjacent to the structure leads to higher deflection.
- Lumped masses for simulating added mass effect leads to an overestimation of the deflection.
- Considering cavitation leads to an increase of the radial deflection by almost two times.
- LS-DYNA and LS-DYNA/USA give different results depending on the loading hypothesis i.e. Simple or double decay.

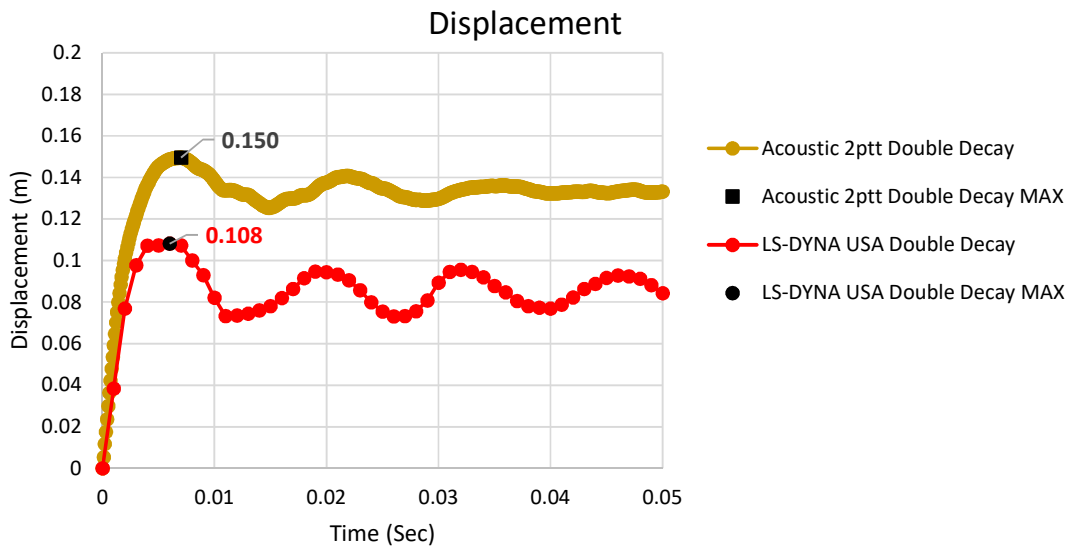


Figure 4.3-c Structural response as radial displacement for Double decay calculation. Reference for the date LS-DYNA/USA (Brochard, 2018)

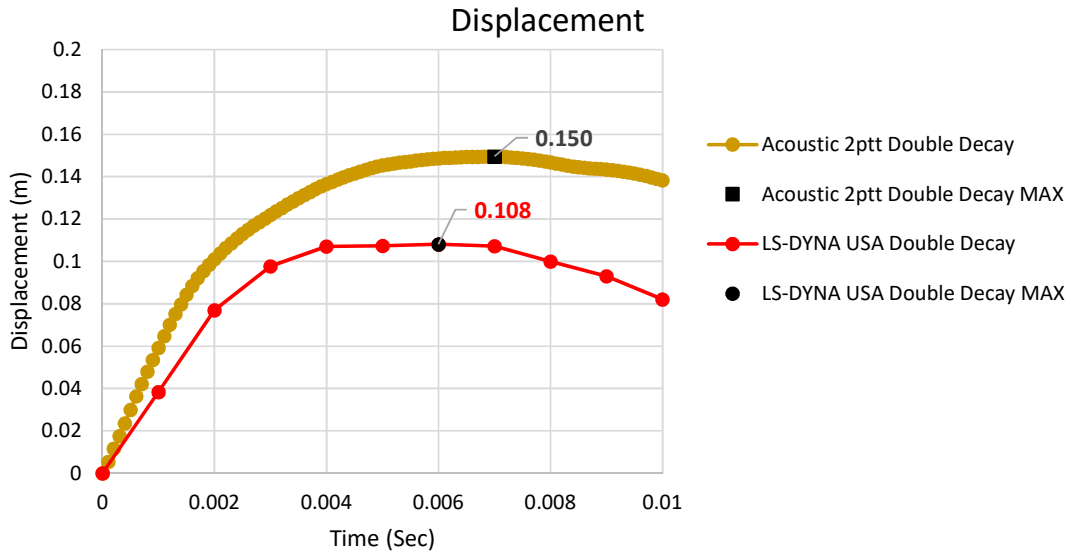


Figure 4.3-d Structural response as radial displacement within a range of 10 ms for double decay calculation. Reference for the date LS-DYNA/USA (Brochard, 2018)

Structural response as the velocity for different scenarios of numerical calculation are presented in Figure 4.3-e and Figure 4.3-f.

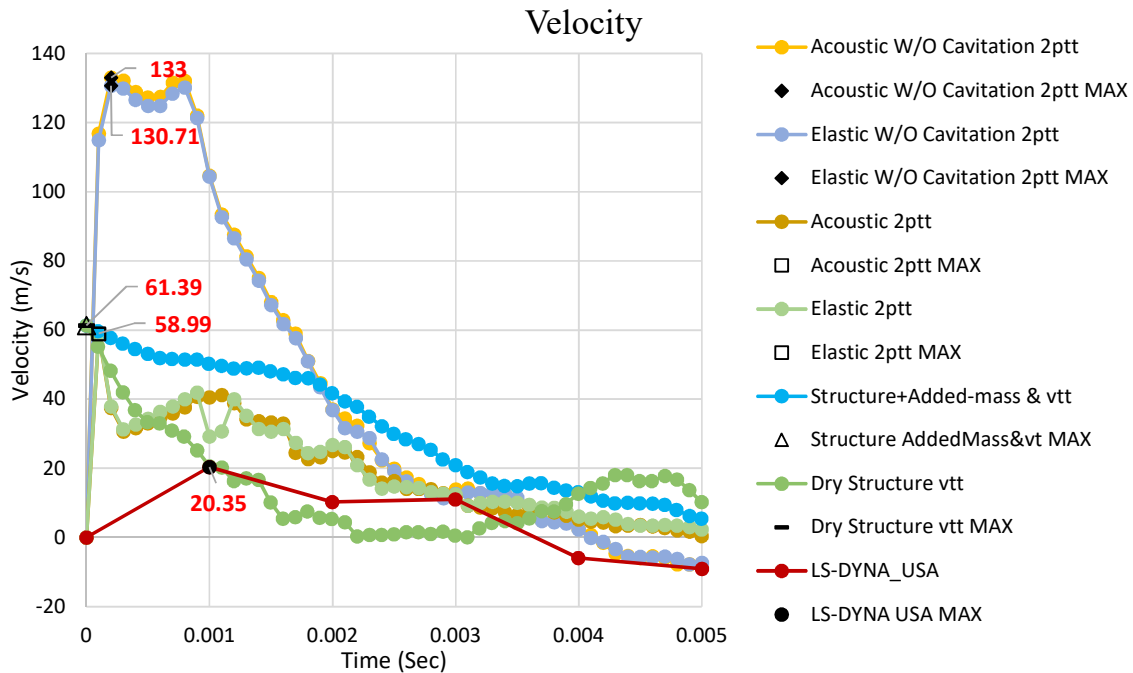


Figure 4.3-e Structural response as velocity within a range of 5 ms for simple decay calculation. Reference for the date LS-DYNA/USA (Brochard, 2018)

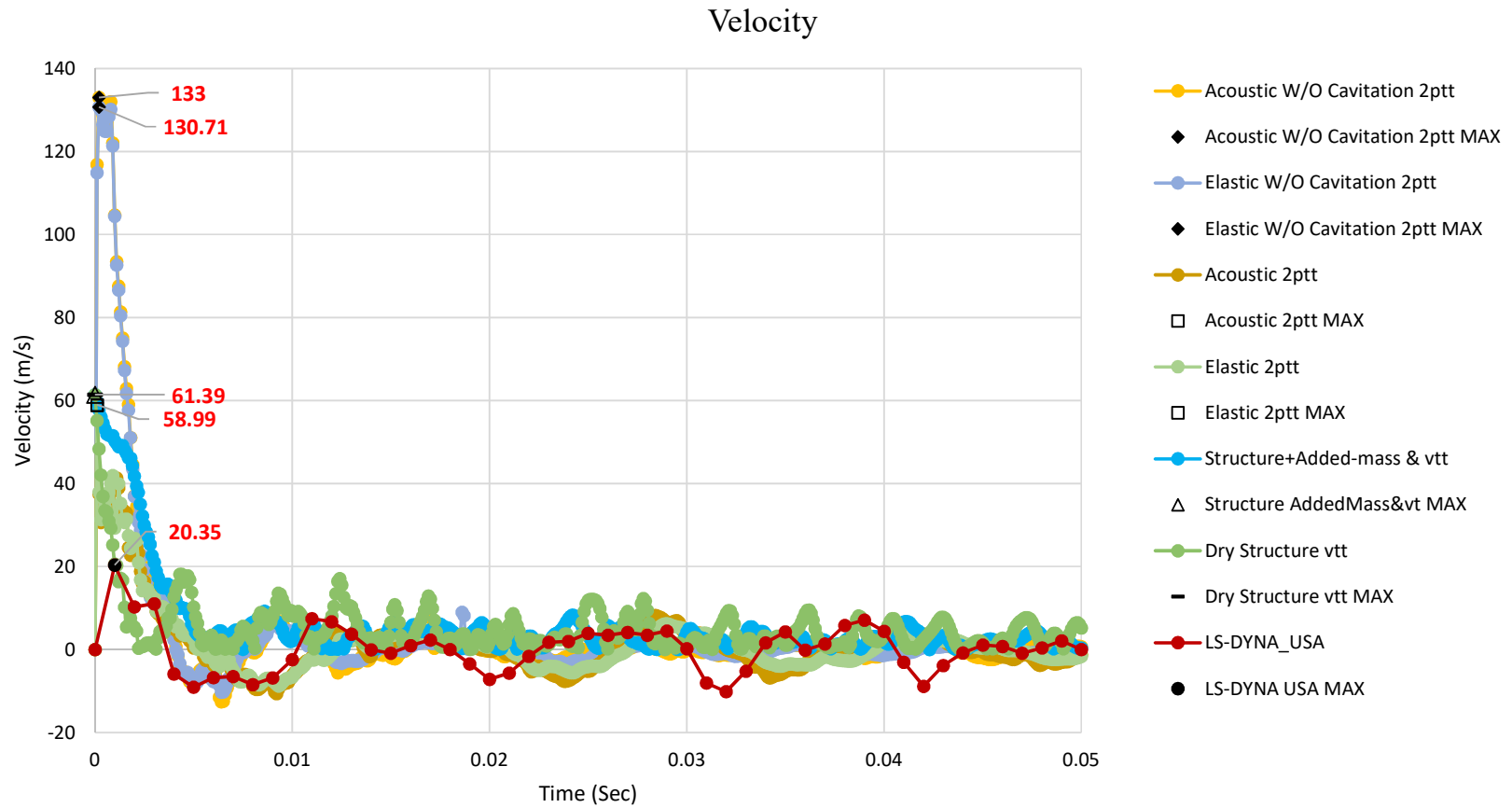


Figure 4.3-f Structural response as velocity for different scenarios of numerical calculation (for simple decay calculation). Reference for the date LS-DYNA/USA (Brochard, 2018)

- *Shock Factor 2.5 & Simple/ Double Exponential Decay of Peak Pressure*

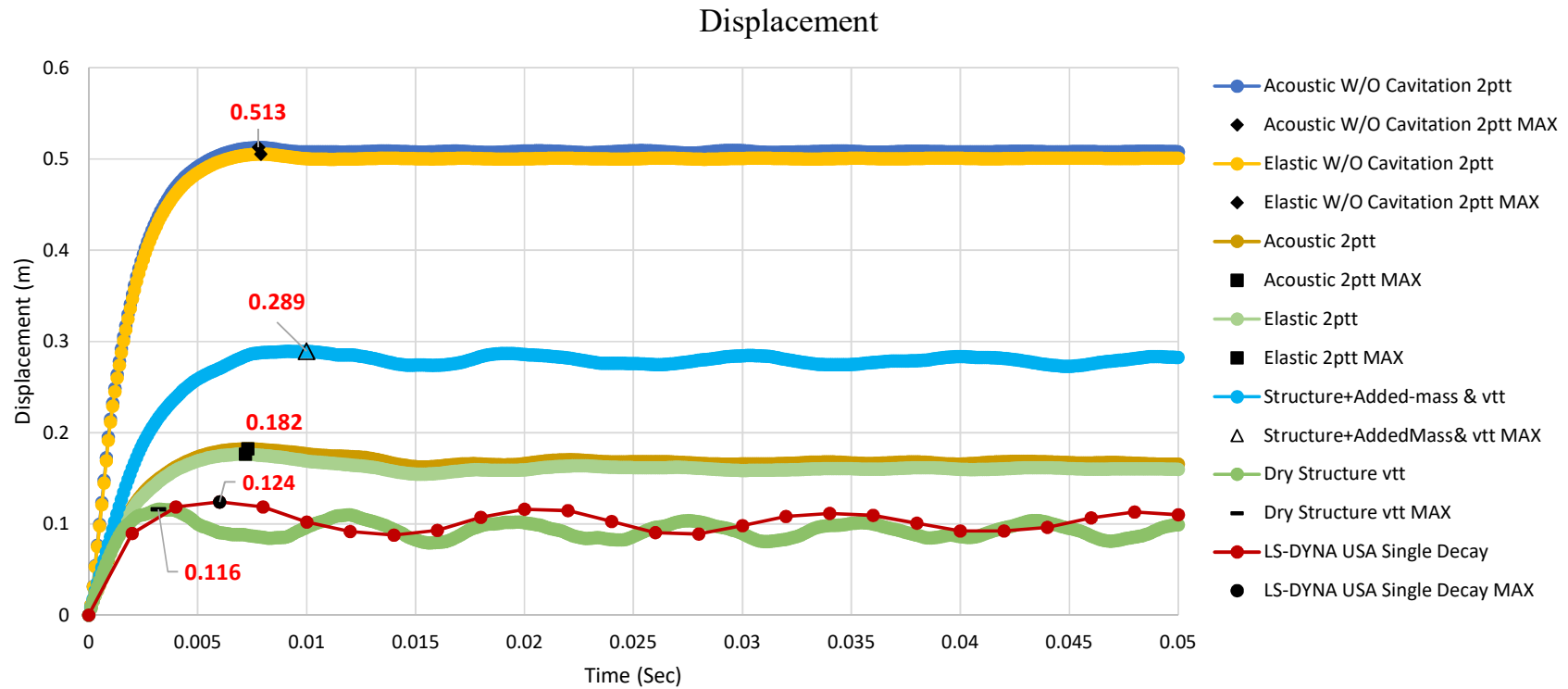


Figure 4.3-g Time evolution of Radial Displacement obtained from different methods of numerical calculation (Simple Decay). Reference for the date LS-DYNA/USA (Brochard, 2018)

Figure 4.3-g presents the structural response in terms of radial deflection for different simulation scenarios.

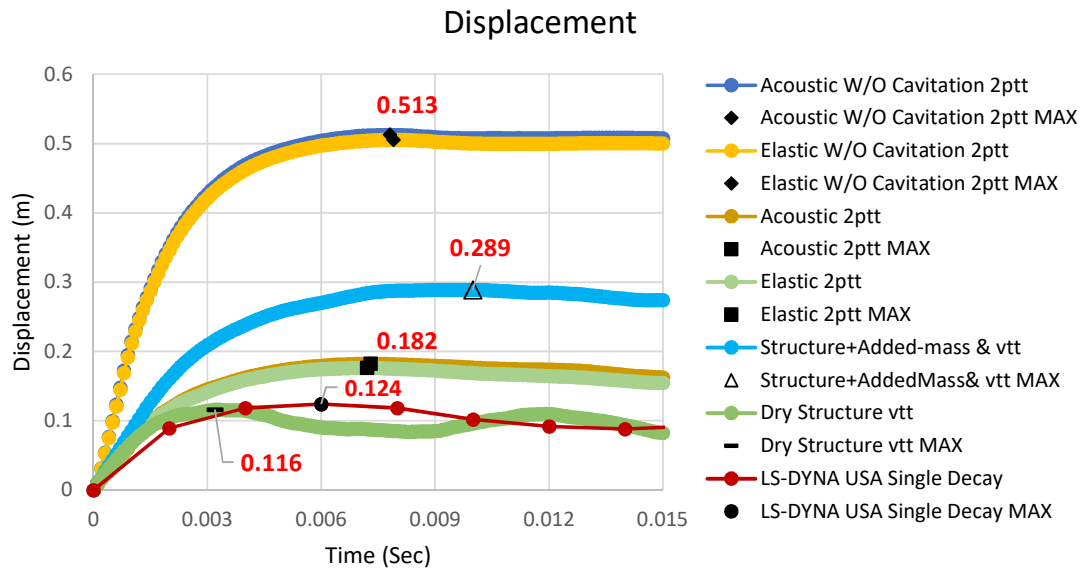


Figure 4.3-h Structural response as radial displacement within a range of 15 ms for simple decay calculation. Reference for the date LS-DYNA/USA (Brochard, 2018)

From the Figure 4.3-h, Figure 4.3-i, and, it was observed that,

- Considering the added mass effect for the fluid adjacent to the structure leads to higher deflection.
- Lumped masses for simulating added mass effect leads to an over estimation of the deflection.
- Considering cavitation leads to an increase of the radial deflection by almost two times.
- LS-DYNA and LS-DYNA/USA gives different results depending on the loading hypothesis i.e. Simple or double decay.

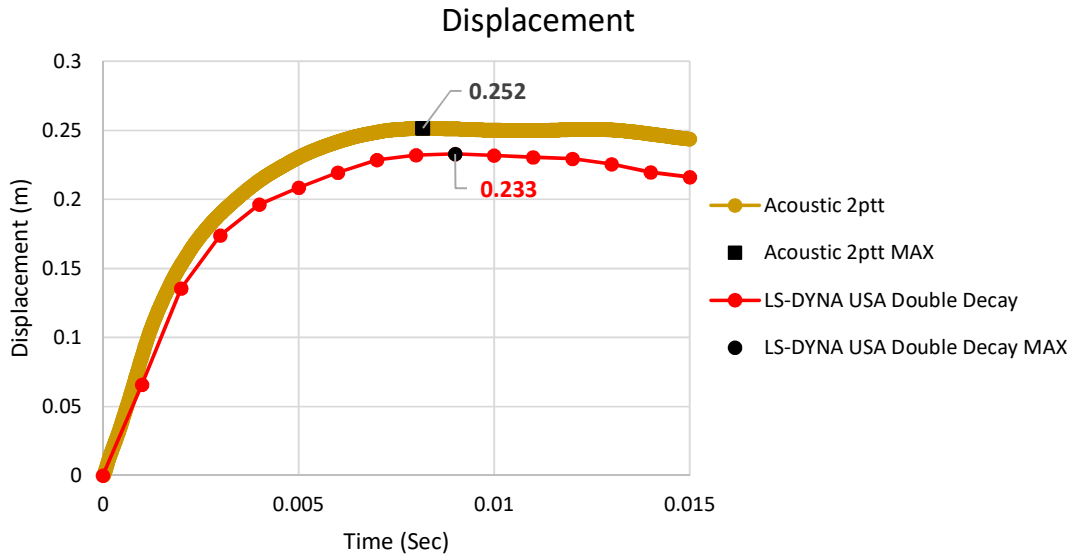


Figure 4.3-i Structural response as radial displacement within a range of 15 ms for double decay calculation. Reference for the date LS-DYNA/USA (Brochard, 2018)

Structural response as velocity for radial different scenarios of numerical calculation are presented in Figure 4.3-j and Figure 4.3-k.

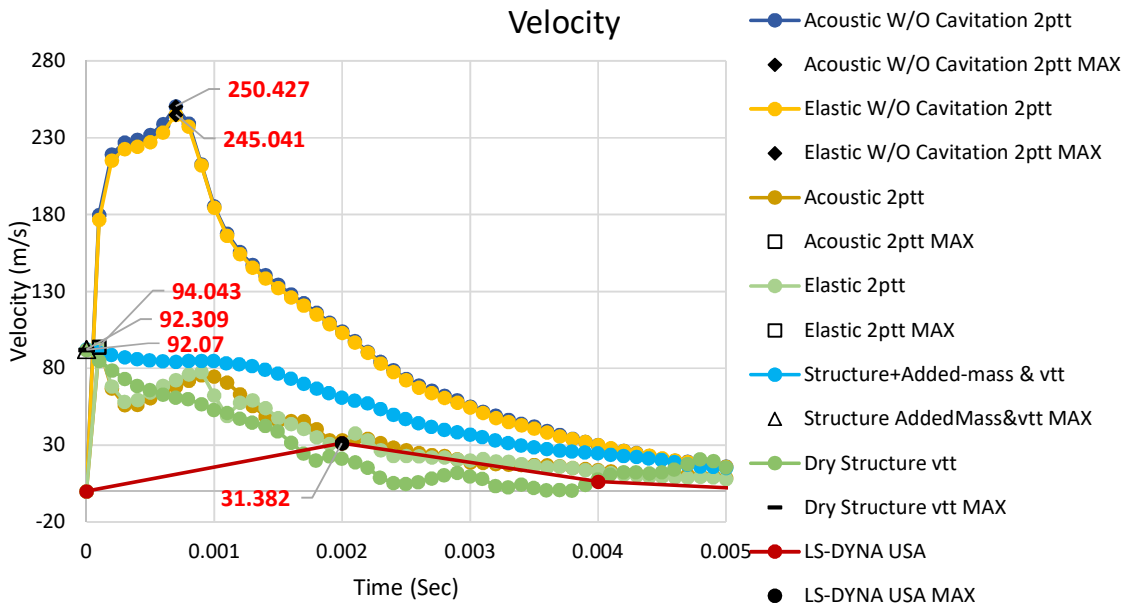


Figure 4.3-j Structural response as velocity within a range of 5 ms for simple decay calculation. Reference for the date LS-DYNA/USA (Brochard, 2018)

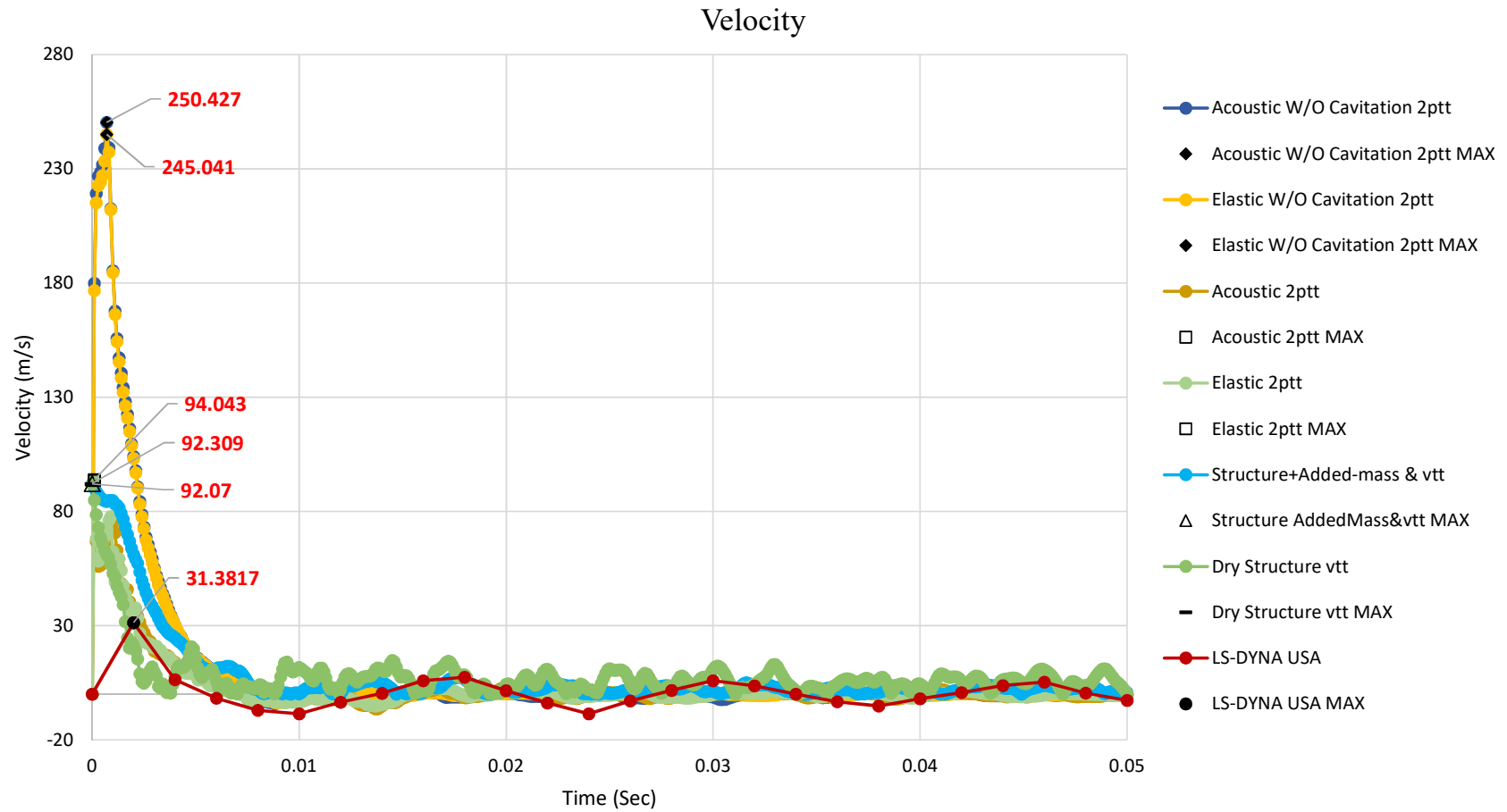


Figure 4.3-k Structural response as velocity for different scenarios of numerical calculation (for simple decay calculation). Reference for the date LS-DYNA/USA (Brochard, 2018)

After reviewing the physics of underwater explosion and the existing methods to simulate the response of a steel structure following observations can be made about the numerical analysis performed in this research work.

- I. A significant amount of energy released as a result of underwater explosion which is 57% of the total energy is carried away by the shock wave (Arons, 1948). Therefore, for a naval anti-shock design analysis, the initial shock wave is the most significant design load.
- II. Angle of incidence and spherical wave approximation was considered while calculating pressure from the initial shock wave.
- III. Loading hypothesis simple or double decay also influence the response of the submerged structure.
- IV. Surrounding fluid causing radiation damping and the dissipation of Internal energy is up to 68% - 70% in the fluid domain.
- V. So less energy was absorbed by the structure and less radial displacement of the structure was observed compared to the case with cavitation inside the fluid domain.
- VI. The dissipation of internal energy in the fluid is sensitive to the amount of charge for a fixed standoff distance.
- VII. The source of dissipation of energy in the fluid is due movement of the shell which creates a negative pressure in the fluid domain down to -128 MPa for charge weight 1.1 kg and -85.2 MPa for charge weight 0.5 kg. Cavitation may occur if the hydrostatic pressure is low.
- VIII. After enduring the shock load from the underwater explosion (such as torpedo and mine) detonated nearby fluid medium of a submerged structure can damage the vessel in the form of dished hull plating.
- IX. Fluid-Structure interaction is a major influential incident for the structural dynamic response analysis in close non-contact underwater explosion.

- X. Using MAT_ACOUSTIC material model in LS-DYNA can save computational cost compared to MAT_ELASTIC_FLUID. As the calculation results for both material model are following quite similar trend.
- XI. Non-Reflective boundary conditions are useful to simulate infinite fluid domain problem in the case of a structure operating deep in the sea or ocean.

5 NON-LINEAR FINITE ELEMENT ANALYSIS OF LAMINATED COMPOSITE STRUCTURE

The post elastic behaviour of laminated composites is a great challenge for numeric simulation due to the complex combination of failure mode within the laminate. These failure modes fibre fracture, matrix cracking, and inter-laminar damage can occur all alone or in combination. Moreover, the composite laminates can behave differently depending on the several parameters including geometry, ply layup sequence, material system and impact velocity (Carruthers, 1998) (Hull, 1991). It is also universally accepted that the existing failure criteria for composite have shortcomings which makes it more challenging to predict the damage response (Soden, 2004) (Department of Defense, 2002). Thereby, the need of a predictive material model is become an active field of research on dynamic simulations of composite structures.

The state of the art finite element (FE) codes are useful for predicting the dynamic response of composite and metallic materials are LS-DYNA, ABAQUS Explicit and RADIOSS. These FE codes are implementing internally developed material modes to define elastic, failure and post failure response of the elements. These material models consider the physical properties (strength, modulus and strain-to-failure) of the material which can be determined by experiment and also some software parameters which do not have physical meaning or cannot be measured experimentally. In order to reach the agreement with experimental results, it is essential to calibrate and tweaking of these non-physical parameter during the simulation. FE codes utilizes an explicit integration formulation which makes it computationally expensive. So it is convenient to use shell (2D) element instead of solid (3D) element. The plies of the composite laminate are grouped in an orthotropic single shell element with smeared material properties which tends to reduce the computational cost but unable to capture the inter-laminar behavior.

LS-DYNA has a small number of composite material model such as MAT 22, MAT 54 and MAT 55. These material models are capable of predicting progressive failure mode and it also utilizes a ply discount method to degrade elastic material properties. MAT 58, MAT 158 and MAT 162 are also available and they are based on continuum damage mechanics to degrade the elastic properties in the post failure phase. The material model MAT 54 is a good choice for simulating full scale large structural damage simulation because of its simplicity and minimal input parameters. Moreover, not only reduced computational requirement but also it reduces the amount of material testing and the difficulties to generate input parameters. However, oversimplification of the complex physical mechanics during composite failure can produce remarkable shortcomings.

The aim of the analysis presented in this section is to model the response of a laminated composite structure subjected to a low factor (1.68) UNDEX. The analysis will be limited to the elastic response of the structure without failure in the model. The post elastic phase, that is the damage response and the delamination of the composite structure, will be performed in a future work following this project.

5.1 Simulation Model in LS-DYNA

The setup of the model is divided into three main parts: geometry, material and the boundary conditions. The focus of this project is to analyse the material definition. However to perform an accurate simulation, it is required to have a good combination of all simulation parameters. In this study the following unit system is applied: stress in N/m^2 , force in Newton [N], distance in meter [m], energy in Newton-Meter [Nm] and time in Second [S].

A property card PART COMPOSITE has been defined to use composite material in LS-DYNA. In this property card lamina stacking sequence is defined together with the thickness of each ply and the element formulation. The material cards are coupled with the PART_COMPOSITE with the material id. The material direction of each element is defined in this card. Material direction can also be defined with an additional card called ELEMENT_SHELL_BETA which will override the material direction in the material card. It is important to remember that all material cards cannot handle all types of element formulation. Usually element definition are classified in to shell, thick shell and solid elements. For each element definition there are definite element formulation. The basic difference between them in number nodes, integration points, degree of freedom and kinematics.

MAT54 is suitable for regular shell, thick shell and also for solids. In this investigation the regular shell elements are used as this is the common approach to reduce CPU time. However the use of shell element leads to the limitations in capturing delamination and generates low accuracy of out of plane stresses.

The cylindrical shell structure is meshed with under-integrated element formulation which is type 2 (Belytschko-Tsay) with only one in-plane integration point for each layer. The under integrated elements tends to be soft and may suffer from hourglass forming but it is cost efficient.

One of the most important parameter in the CONTROL_SHELL card is the LAMSHT flag. This option allows to apply laminate theory in the calculation of shear strain through the thickness. Otherwise, shear strain will be constant through the thickness of the shell. If sandwich type of composites are used then there will be drastic differences in the elastic properties from ply to ply, so the assumption of constant shear stress through the thickness will be grossly incorrect. The response of the structure will be too stiff if this flag is not used (LS-DYNA Keyword User's Manual - Volume II, 2014). To avoid the highly distorted element before causing instabilities and lead to error termination of the simulation, the NFAIL4 parameter in the CONTROL_SHELL should be activated. In this case, when an element is highly distorted and NFAIL4 is activated, the whole element will be deleted along with the integration points of the plies.

Furthermore, one of the additional helpful parameter is History Variables which is unique for each material model and strongly recommended to activate. The History Variables contain damage parameters for each ply. In order to print out the history variables, it is necessary to activate IMATL flag in the DATABASE BINARY D3PROP section. DATABASE controls how often and what parameters will be written to the result file. NEIPS and HEIPH parameters in DATABASE EXTENT BINARY controls how many integration points that the result to the history variables are written. NEIPS is used for shells and NEIHP is used for solids.

5.2 Available material models in LS-DYNA

The behavior of material in the simulation is governed by the material model. The material model card includes parameters such as elastic anisotropic material properties, material coordinate definitions and other model parameters such as failure criterion. All the material model described in the Table 5.2-a applies different strategy for predicting failure initiation,

degradation scheme and material properties. It also has some nonphysical parameter which are useful for simulation and tune the material behavior according to the experiment results. The composite material behaves orthotropic elastic linear with the failure surface but some of the material model can introduce plastic behavior. After the failure of the material, the degradation scheme is employed to degrade the material properties. Some of the material model introduces discontinuous failure where the material properties are set to zero when a ply reaches a certain failure condition, that is either fully damage or undamaged. Degradation scheme is applied by reducing the elastic anisotropic material parameters, such as Young's moduli, shear moduli and Poisson's ratios. Material models also apply a continuum damage mechanics model where material properties are reduced after the initiation of failure. The degradation scheme manipulate the material from undamaged state to fully damage state. When the fully damage state is reached, the ply is removed. Consequently, the integration points of the ply will no longer contribute to the element stiffness.

Table 5.2-a Available Material Model for modelling composite in LS-DYNA. (LS-DYNA Keyword User's Manual - Volume II, 2014).

Material Model	Failure Criteria	Elements	Remarks
MAT22 Composite Damage	Reduced Chang-Chang	Shell, Thick shell, Solid	Simple brittle model.
MAT54/55 Enhanced Composite Damage	54: Chang-Chang 55: Modified Tsai-Wu and reduced Chang Chang	Shell, Thick shell, Solid	Improvement of MAT22. Strength reductions parameters.
MAT58 Laminated Composite Fabric	Modified Hashin	Shell, Thick shell	Similar to MAT54. Smooth stress strain relation. Continuum damage model with exponential softening. Non-Linear shear behavior.
MAT59 Composite Failure Model	Modified Hashin	Shell, Thick shell, Solid, SPH	Similar to MAT58. Super imposed linear isotropic viscoelasticity.
MAT116/117/118 Composite Layup	No failure	Shell	Elastic response only
MAT158 Rate Sensitive Composite Fabric	Modified Hashin	Shell, Thick shell	Same as MAT58. Rate sensitive.
MAT161/162 Composite MSC	Hashin	Shell, Thick shell, Solid	Extra licenses required. MAT161 offers delamination predictions with solid elements.

MAT261 Laminated Fracture Daimler Pinho	Pinho	Shell, Thick shell	Physical based failure criteria. Continuum damage model. Linear softening evolution based on fracture toughness.
MAT262 Laminated Fracture Daimler Camanho	Camanho	Shell, Thick shell	Physical based failure criteria. Continuum damage model. Similar but a simpler model than MAT261. Bi-linear/linear softening evolution based on fracture toughness.

5.3 Material Model MAT54/55

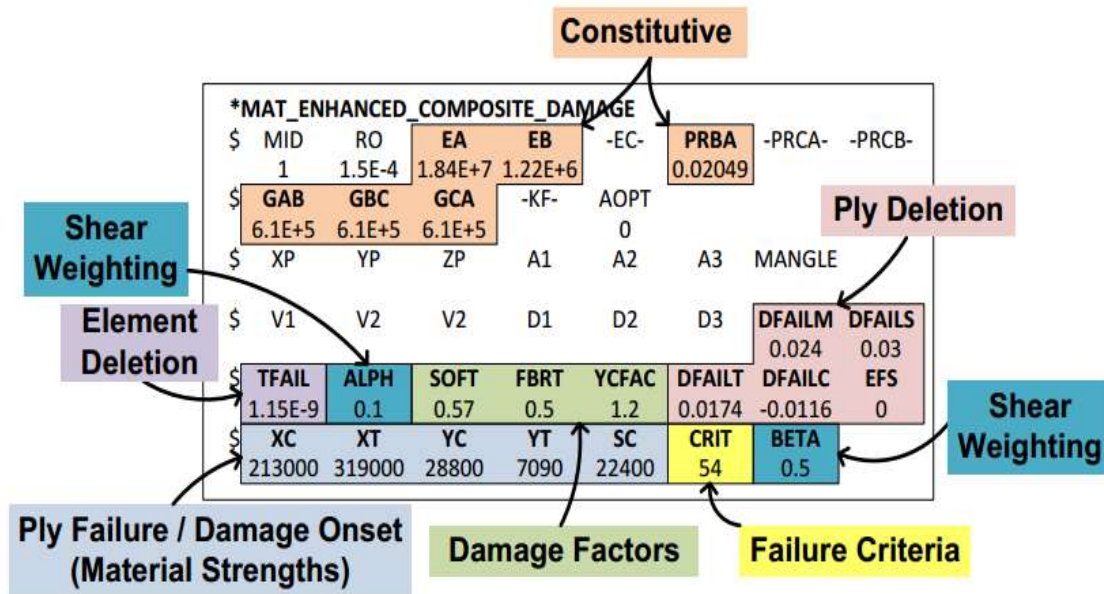


Figure 5.3-a Description of the material card MAT 54/55 (Osborne, 2012)

Material model MAT 54 is one of the most tested material model in LS-DYNA. It is the enhanced version of the material model MAT 22. MAT 54 utilizes fully Chang-Chang criteria to define four different failure modes, tensile fiber mode, compressive fiber mode, tensile matrix mode and compressive matrix mode. This material model is also capable of using Hashine failure criteria by introducing BETA (shear weighting), $\beta = 1$ and CRIT = 55; the material model becomes MAT 55 which utilizes Tsai Wu criteria. As a result the tensile and compressive fiber mode are treated with Chang-Chang criteria and the matrix modes are treated with Tsai-Wu criteria. Otherwise, if $\beta = 0$ then it will be the maximum stress criteria. Material

model MAT 54/55 simulates an elastic-plastic stress-strain behavior allowing a ductile failure process. The stresses increase linearly until the failure criteria is reached in one of the mode. The stress-strain response either plastic or the maximum stress is reduced to a residual stress dependent on certain parameters defined in material card.

5.3.1 Theory of failure model

- **Constitutive**

In the elastic region, the stress-strain response in longitudinal or fiber, transverse or matrix and shear directions are defined as,

$$\varepsilon_{11} = \frac{1}{E_1} (\sigma_{11} - \nu_{12} \sigma_{22}) \text{ Here } E_1 = EA \text{ \& } \nu_{12} = \frac{PRBA \cdot EA}{EB} \quad (39)$$

$$\varepsilon_{22} = \frac{1}{E_2} (\sigma_{22} - \nu_{21} \sigma_{11}) \text{ Here } E_2 = EB \text{ \& } \nu_{21} = PRBA \quad (40)$$

$$2\varepsilon_{12} = \frac{1}{G_{12}} \sigma_{12} + \alpha \sigma_{12}^3 \text{ Here } G_{12} = GAB \text{ \& } \alpha = ALPH \quad (41)$$

Here in the equation (41) ALPH is the weighting factor which introduces nonlinear shear stress term. This parameter cannot be measured from the experiment. It can only be determined by calibration whenever shear exists. GBC and GCA are the out of plane shear moduli (not listed in the equations).

- **Ply failure criteria (theory)**

MAT 54 follows the Chang-Chang failure criteria to define limit in each ply stresses and apply degradation scheme. Equations (42) to (45) explain the MAT54 Chang-Chang implementation. Here XT is the ply longitudinal tensile strength, XC is the ply longitudinal compressive strength, YT is the ply transverse tensile strength, YC is the ply transverse compressive strength, and SC is the ply shear strength. These orthotropic anisotropic material properties are determined from the coupon test (experimental tests) of the lamina.

$$e_f^2 = \left(\frac{\sigma_{11}}{X_t}\right)^2 + \beta \left(\frac{\sigma_{12}}{S_c}\right)^2 - 1 \begin{cases} e_f^2 \geq 0 & \text{failed} \\ e_f^2 < 0 & \text{elastic} \end{cases} \quad (42)$$

$$e_c^2 = \left(\frac{\sigma_{11}}{X_c}\right)^2 - 1 \begin{cases} e_c^2 \geq 0 & \text{failed} \\ e_c^2 < 0 & \text{elastic} \end{cases} \quad (43)$$

$$e_m^2 = \left(\frac{\sigma_{22}}{Y_t}\right)^2 + \beta \left(\frac{\sigma_{12}}{S_c}\right)^2 - 1 \begin{cases} e_m^2 \geq 0 & \text{failed} \\ e_m^2 < 0 & \text{elastic} \end{cases} \quad (44)$$

$$e_d^2 = \left(\frac{\sigma_{22}}{2S_c}\right)^2 + \left[\left(\frac{Y_c}{2S_c}\right)^2 - 1\right] \frac{\sigma_{22}}{Y_t} + \left(\frac{\sigma_{12}}{S_c}\right)^2 - 1 \begin{cases} e_d^2 \geq 0 & \text{failed} \\ e_d^2 < 0 & \text{elastic} \end{cases} \quad (45)$$

e_f , e_c , e_m and e_d in Equations (42) to (45) are the history variables that represents fiber tension e_f , fiber compression e_c , matrix tension e_m , and matrix compression e_d .

- **Damage Factors**

If compressive matrix failure takes place then the fibre strength degradation can be done by manipulating the strength reduction factors FBRT and YCFAC in the material model MAT 54. It can be applied by the following relations,

$$X_{T_{reduced}} = X_T \cdot FBRT \quad (46)$$

$$X_{C_{reduced}} = Y_C \cdot YCFAC \quad (47)$$

5.4 Materials and Specimen Manufacturing

The material in this study is a carbon fibre-reinforced epoxy (CF/EP) laminate. The material properties are collected from the reference (Heimbs, 2008). In this investigation the laminate is used with a symmetric, quasi-isotropic lay-up of 120, 192, 216 and 288 plies $[-45^\circ / 0^\circ / 45^\circ / 90^\circ]_{30S}$, $[-45^\circ / 0^\circ / 45^\circ / 90^\circ]_{48S}$, $[-45^\circ / 0^\circ / 45^\circ / 90^\circ]_{54S}$ and $[-45^\circ / 0^\circ / 45^\circ / 90^\circ]_{72S}$. The laminate were prepared with the specification of Cytec[®] 977 – 2 – 35 – 12K HTS – 134. In the unidirectional plies, the carbon fibres were impregnated with an epoxy matrix. These plies are stacked up according to the target fibre orientation angles and

cured to a plate in an autoclave. The resulting average thickness of the cured plate was 2.7 mm with a standard deviation of 0.11 mm.

Table 5.4-a CFRP elastic Properties used in this study

Material	CF/EP Laminate
ρ kg/m^3	1600
E_{11} GPa	153
E_{22} GPa	10.3
G_{12} GPa	5.2
G_{13} GPa	5.2
G_{23} GPa	3.96
ν_{12} GPa	0.3
ν_{21} GPa	0.0202
XT MPa	2540
XC MPa	1500
YT MPa	82
YC MPa	236
SC MPa	90

5.5 Response Analysis of Composite Material Structure

In order to prepare a finite element model (carbon fibre-reinforced epoxy laminated) with composite structure which can endure a shock loading of SF 1.68 (Double decay), several different models are simulated. In this analysis, four different plate thickness is applied for the structure and the fluid around the structure is modelled with MAT Acoustic.

Table 5.5-a different plate thickness is applied for the simulation.

Lay-up and Ply no	Plate thickness of the cylinder (mm)	Remarks
lay-up of 120, $[-45^\circ / 0^\circ / 45^\circ / 90^\circ]_{30S}$	13.5	Structure Failed
lay-up of 192, $[-45^\circ / 0^\circ / 45^\circ / 90^\circ]_{48S}$	21.6	Structure Failed
lay-up of 216, $[-45^\circ / 0^\circ / 45^\circ / 90^\circ]_{54S}$	24.3	Structure Failed
lay-up of 288, $[-45^\circ / 0^\circ / 45^\circ / 90^\circ]_{72S}$	32.4	-

I. lay-up of 120, $[-45^\circ / 0^\circ / 45^\circ / 90^\circ]_{30S}$

After running the simulations with material model MAT54 for structure and MAT Acoustic for the fluid, the maximum radial displacement was reported just before the structural failure 0.105 m. The structural failure was initiated at 1.29 ms.

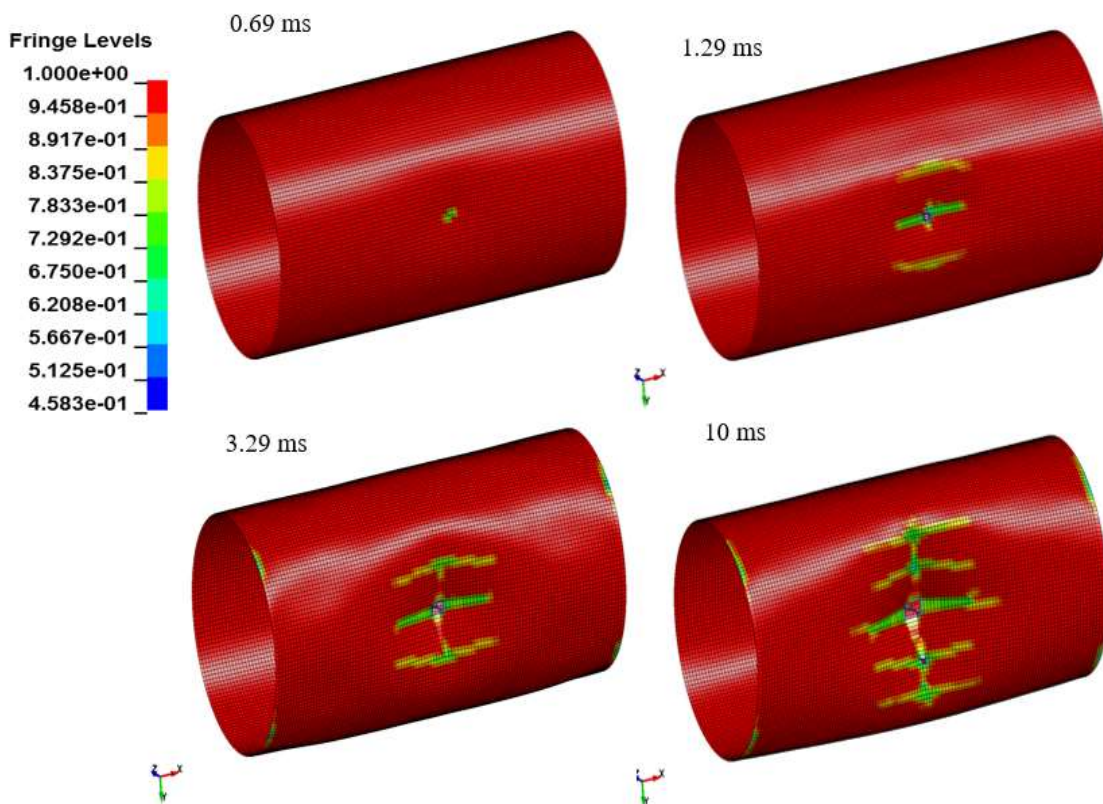


Figure 5.5-a Plastic strain and failure of the structure at different time steps

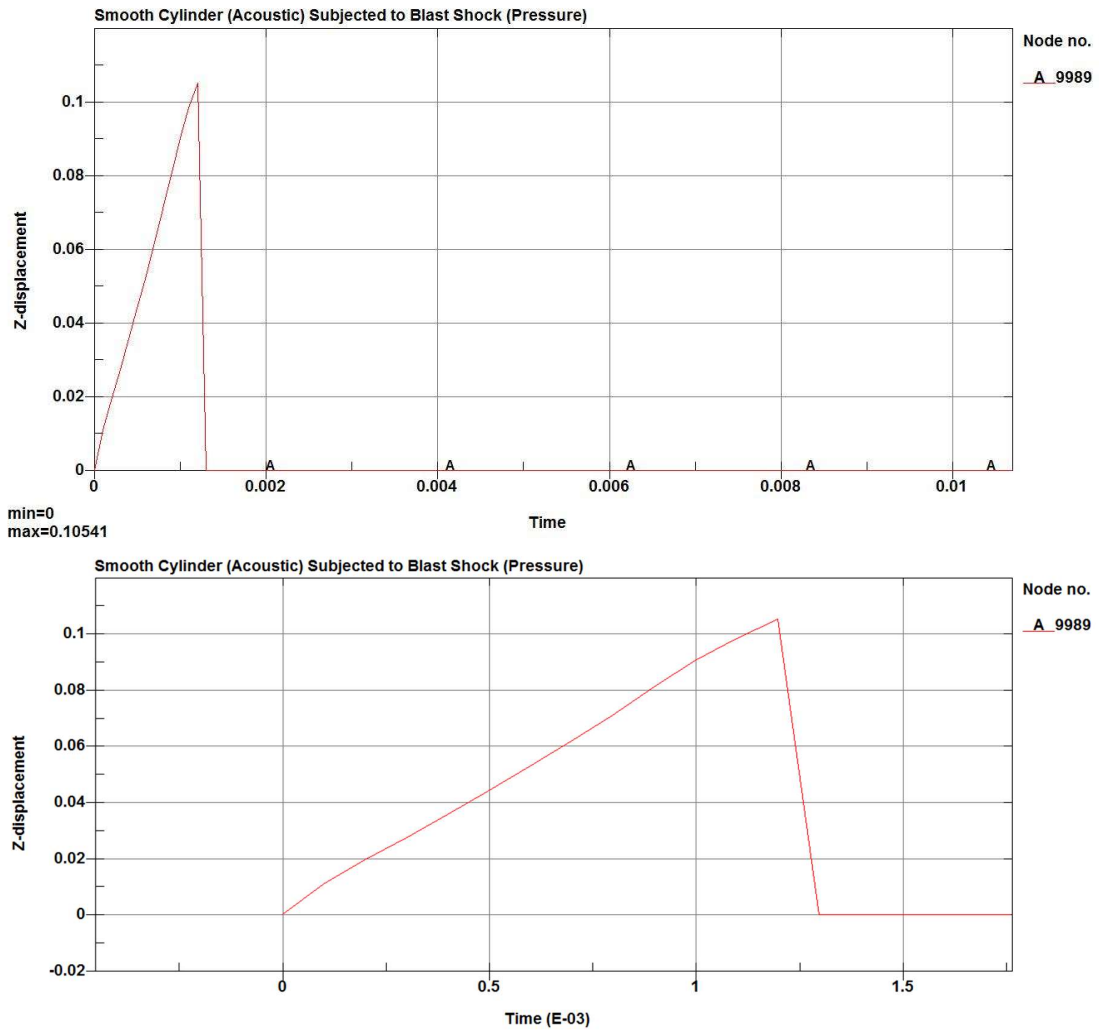


Figure 5.5-b Radial Displacement of the structure

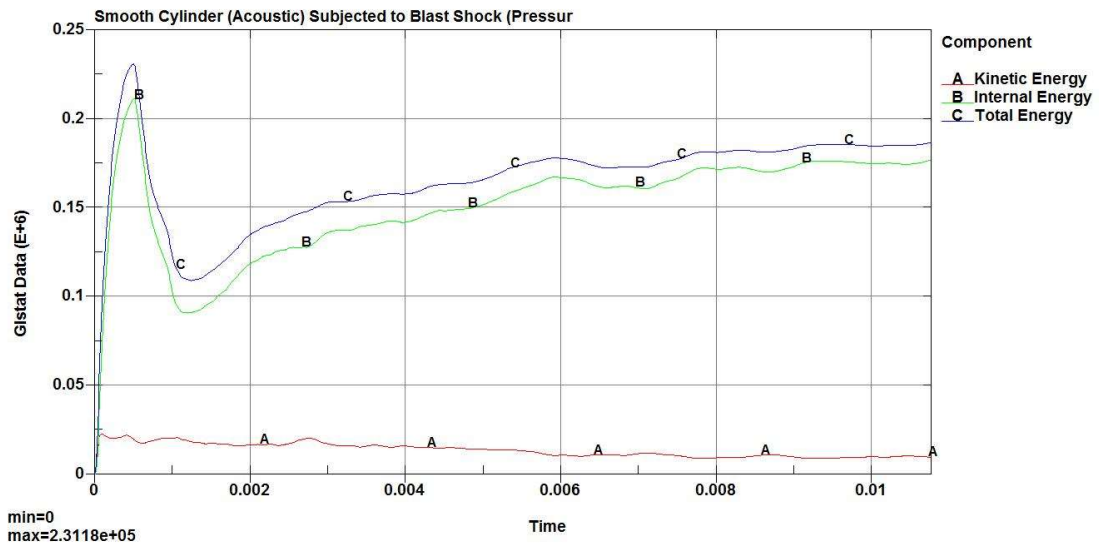


Figure 5.5-c Energy balance of the numerical simulation

II. lay-up of 192, $[-45^\circ / 0^\circ / 45^\circ / 90^\circ]_{48S}$

After running the simulations with material model MAT54 for structure and MAT Acoustic for the fluid, the maximum radial displacement was reported just before the structural failure 0.15 m. The structural failure was initiated at 3.49 ms.

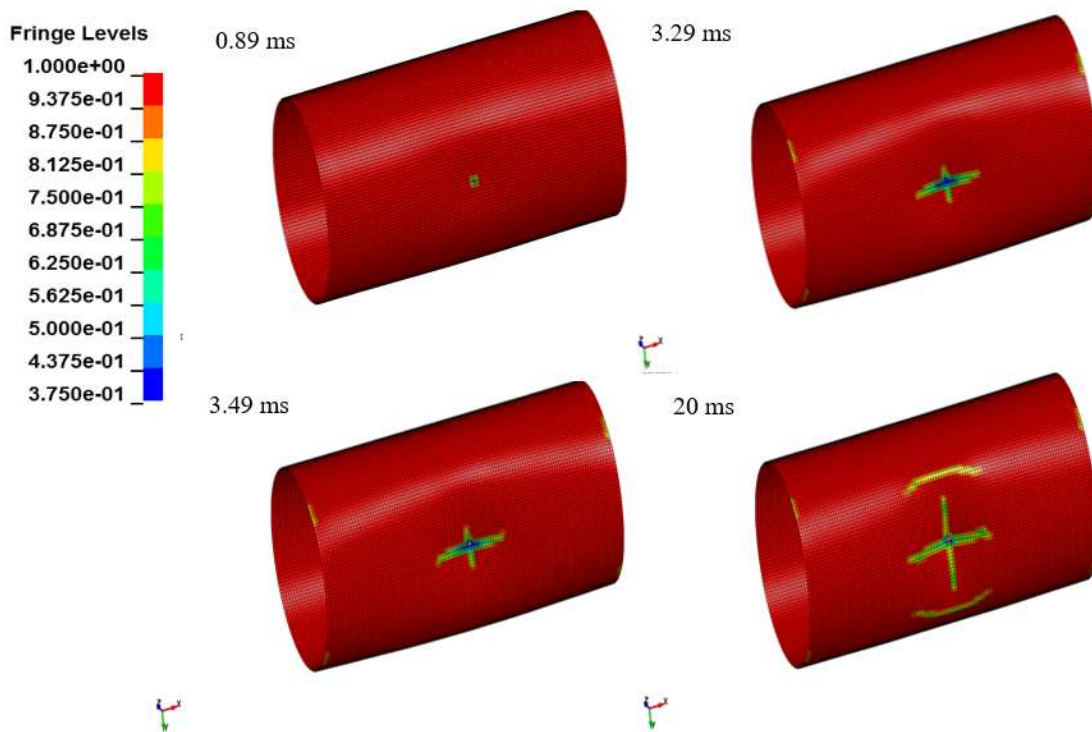


Figure 5.5-d Plastic strain and failure of the structure at different time steps

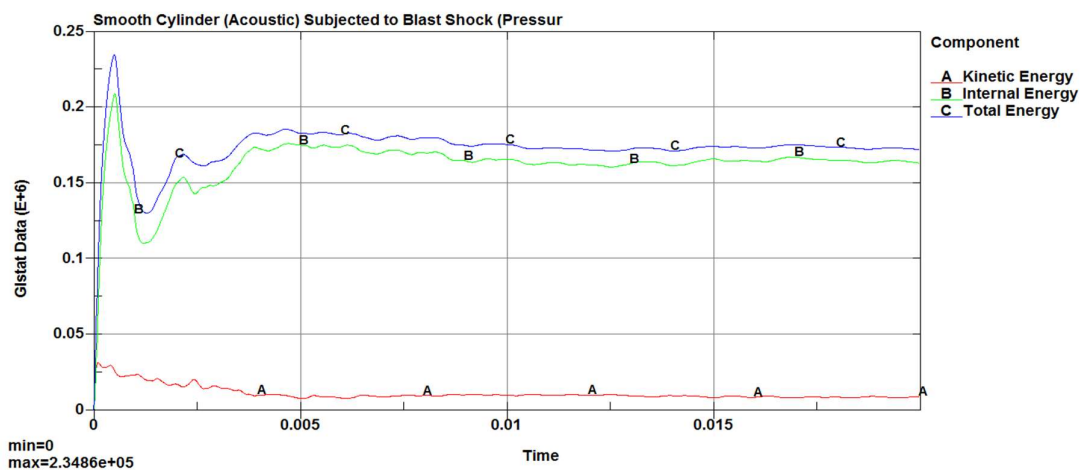


Figure 5.5-e Energy balance of the numerical simulation

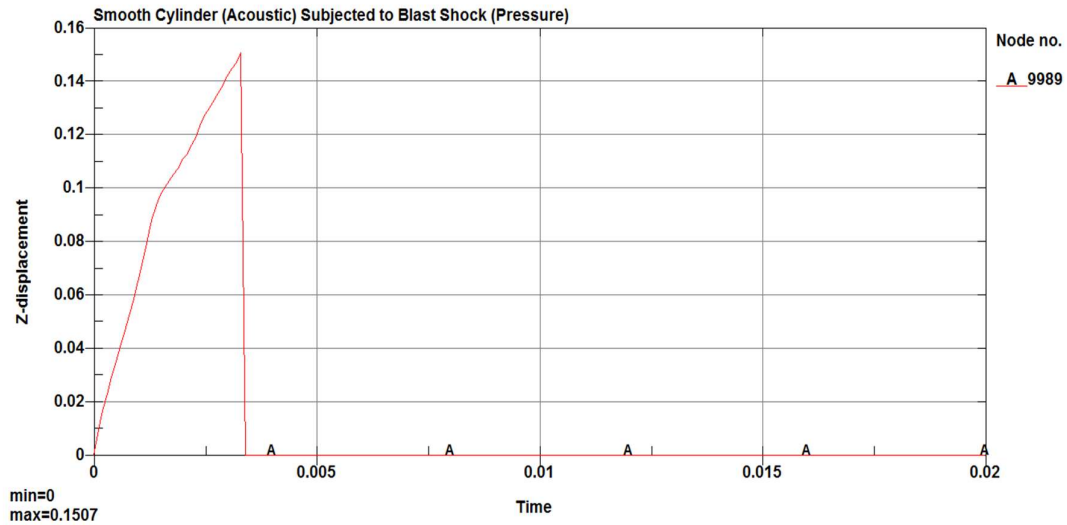


Figure 5.5-f Radial Displacement of the structure

III. lay-up of 216, $[-45^\circ / 0^\circ / 45^\circ / 90^\circ]_{54S}$

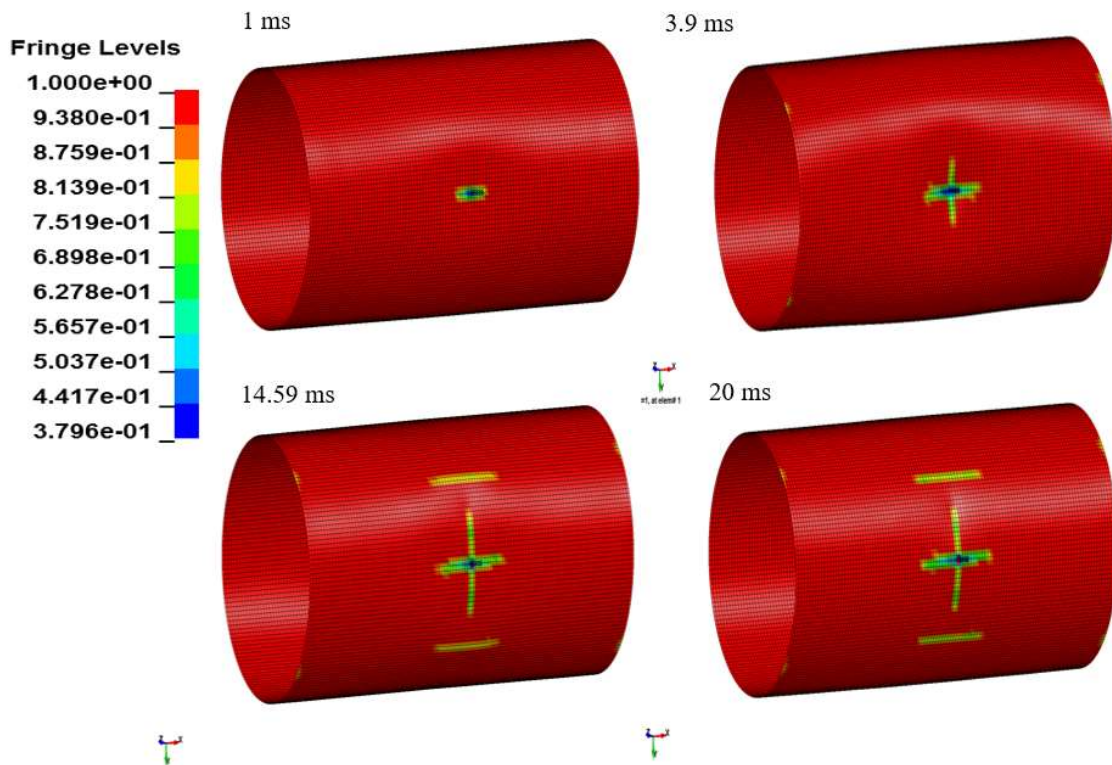


Figure 5.5-g Plastic strain and failure of the structure at different time steps

After running the simulations with material model MAT54 for structure and MAT Acoustic for the fluid, the maximum radial displacement was reported just before the structural failure 0.165 m. The structural failure was initiated at 14.59 ms.

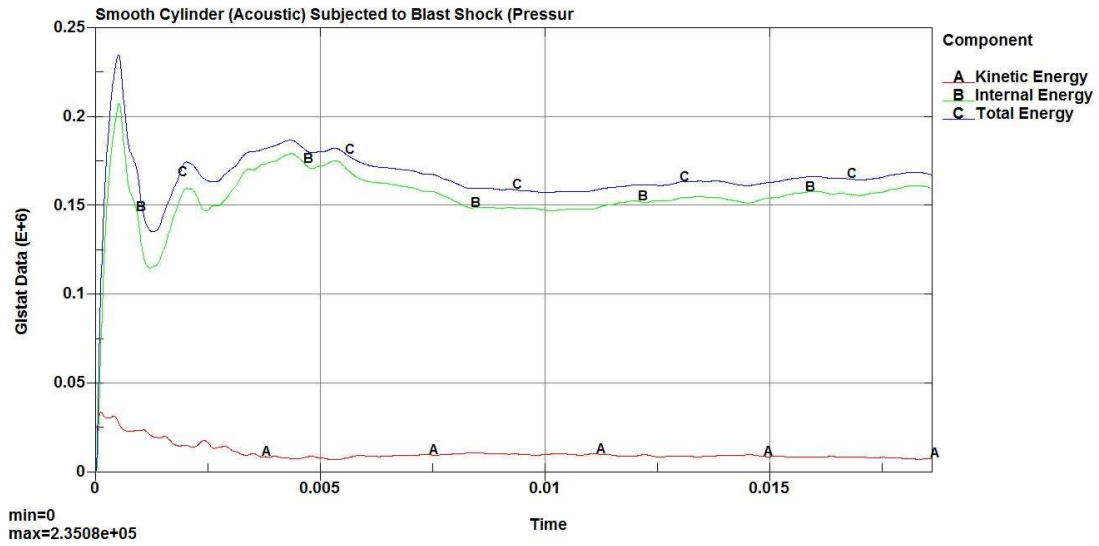


Figure 5.5-h Energy balance of the numerical simulation

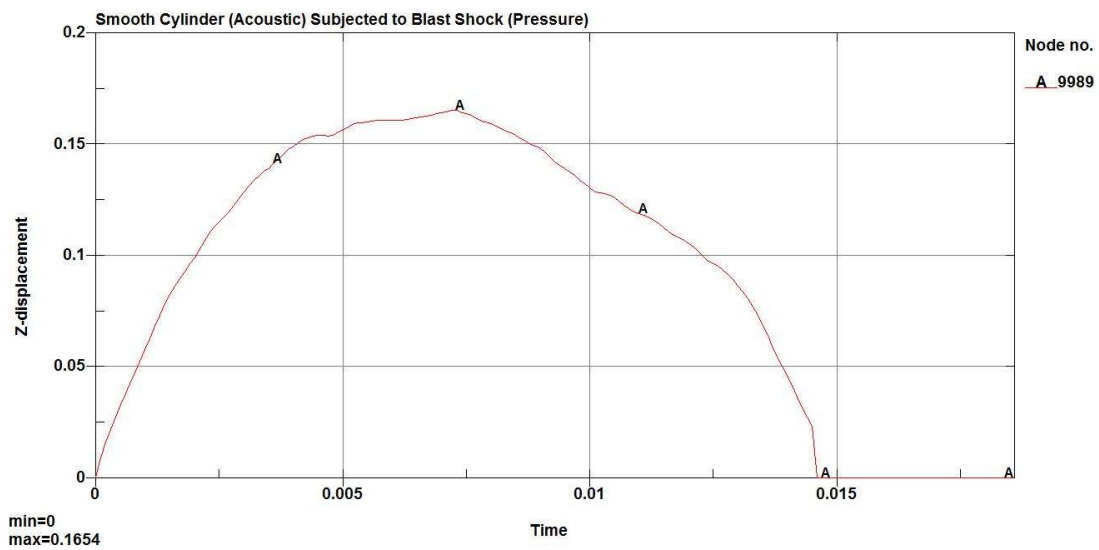


Figure 5.5-i Radial Displacement of the structure

IV. Lay-up of 288, $[-45^\circ / 0^\circ / 45^\circ / 90^\circ]_{72s}$

There is no structural failure was observed for configuration of $[-45^\circ / 0^\circ / 45^\circ / 90^\circ]_{72s}$ where the number plies are 288 with the plate thickness of 32.4 mm.

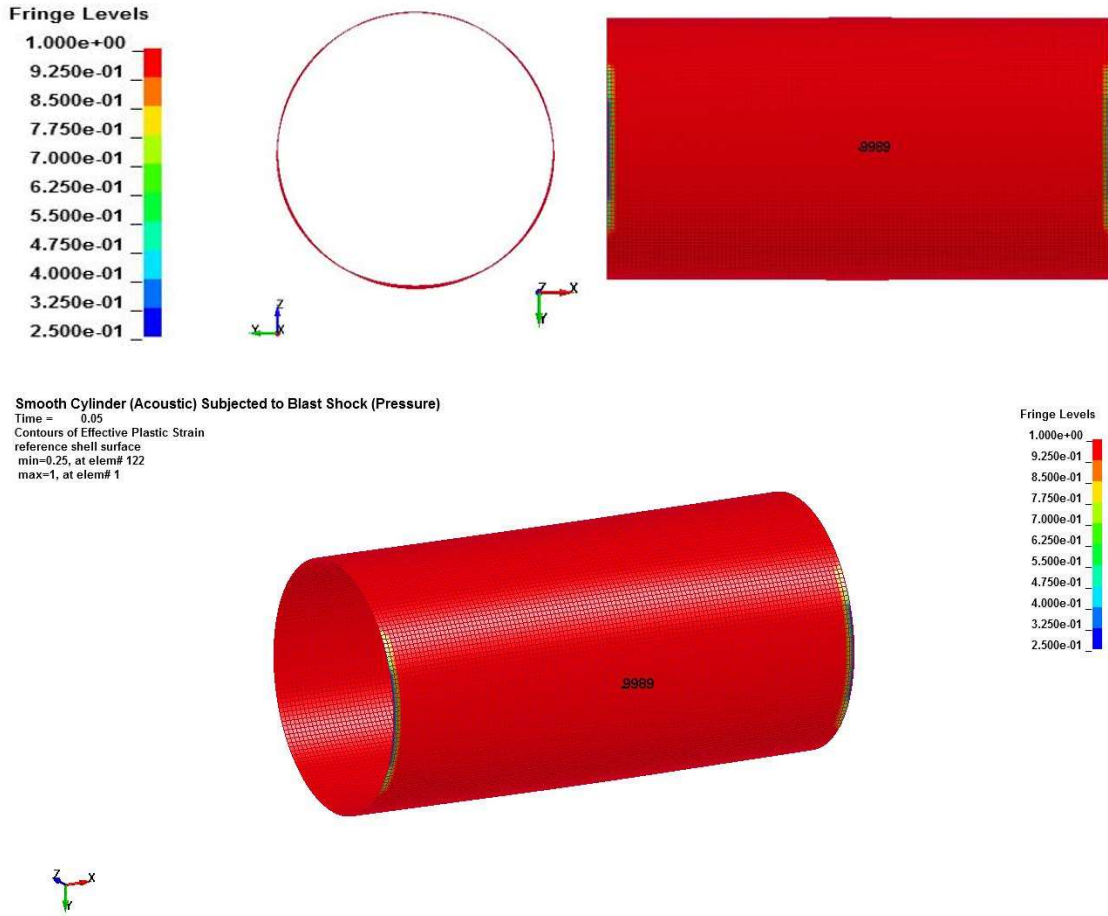


Figure 5.5-j Plastic strain distribution at 50 ms

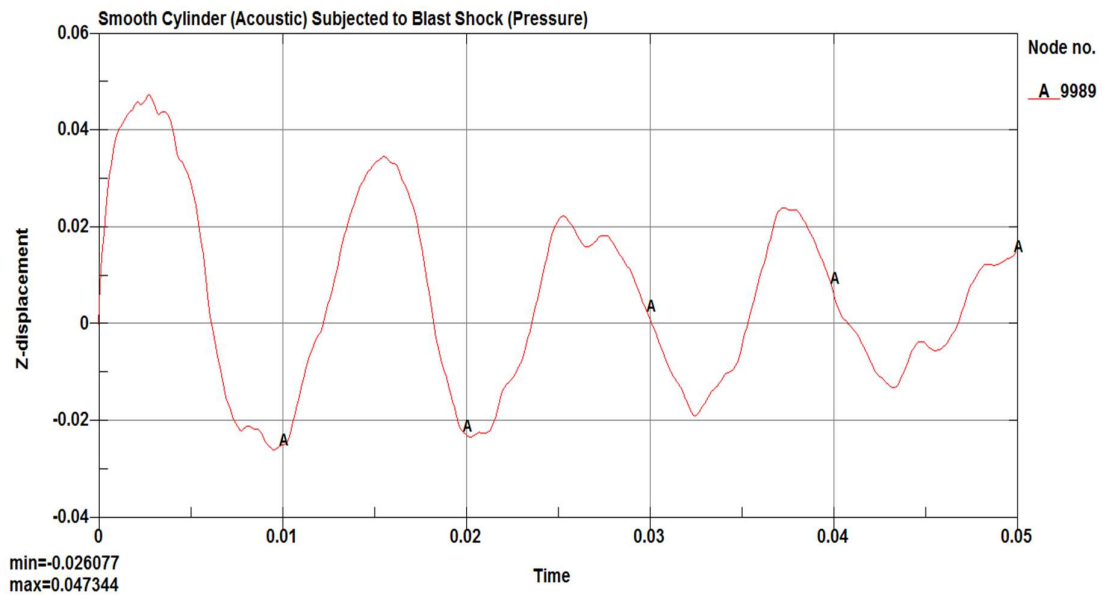


Figure 5.5-k Radial Displacement of the structure

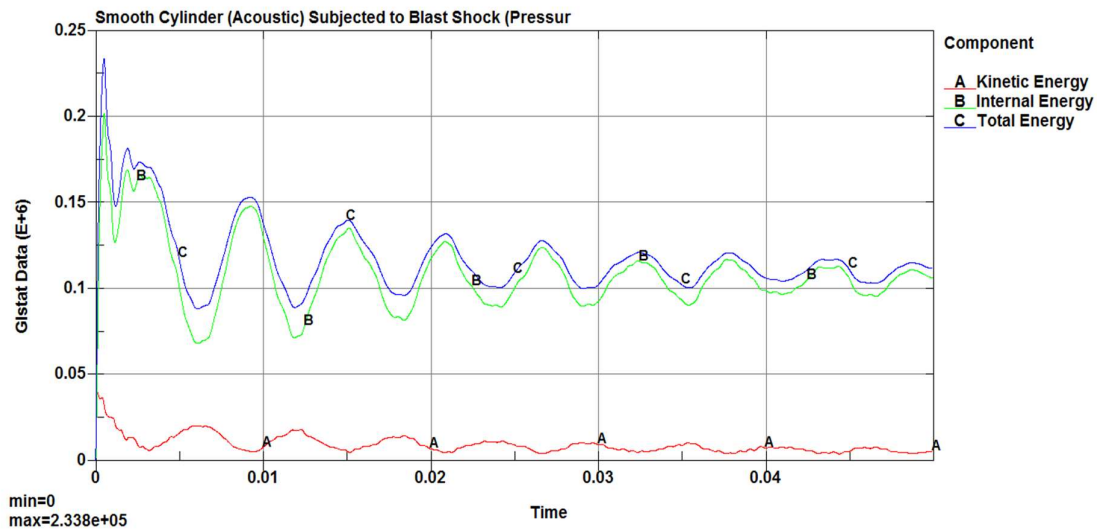


Figure 5.5-l Energy balance of the numerical simulation

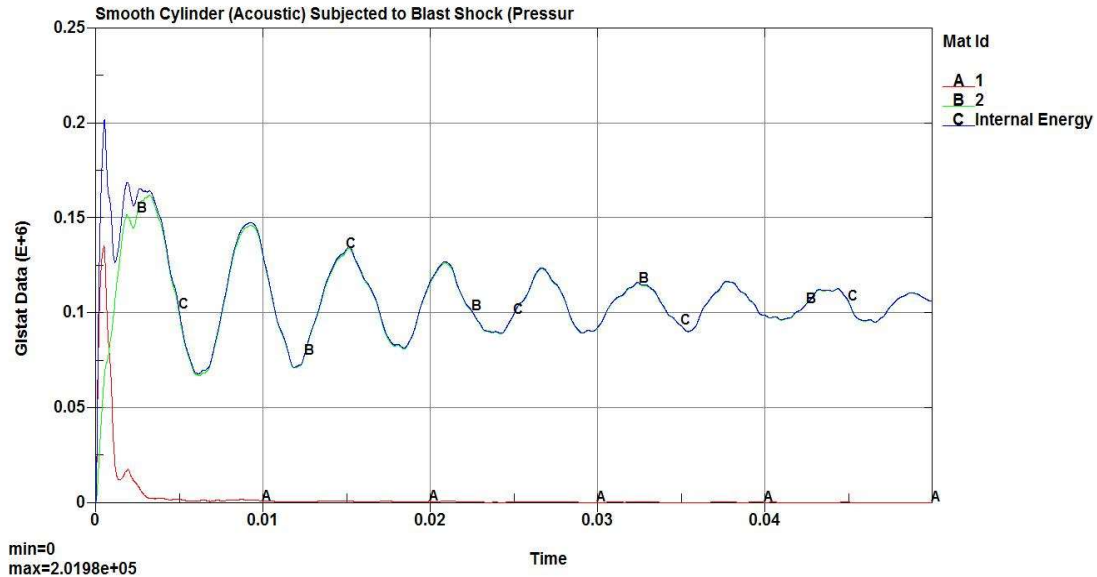


Figure 5.5-m Dissipation of the internal energy in the simulation (1 indicates Fluid & 2 indicates Structure)

5.6 Discussions

The purpose of the numerical analysis presented in this section was to initiate some modelling of an immersed composite structure subjected to an underwater explosion. This work will be continued by a future research work for predicting the progressive failure of the structure. So in this scope of the investigation, the basic requirement of the numerical model for composite structure was analysed. As a progress here it clearly observed that the prepared numerical model is capable of simulating within the elastic region of the material. For modelling the post

elastic behaviour, significant nonphysical and experimental parameters are highlighted in the discussions of material model section and the theory of failure. With this information, it will be easier to model the damage degradation in the post failure phase.

6 FURTHER WORK

- I. For the dynamic response analysis of the steel structure (monolithic material) submitted to UNDEX, a number of different scenarios are simulated in this research work. In the future, it would be interesting to observe the influence of hydrostatic pressure on the fluid domain and the complex fluid structure interaction. It is also useful to analyze the influence of mesh size on the various results of the structural behavior under the blast loading.
- II. In order to validate the results from the dynamic response analysis of the composite structure, experimental testing should be performed and for the progressive failure analysis, it will be necessary to calibrate the model parameters and simulations thereafter be repeated with these parameters to have a better assess for the predictability of shock resistant model.
- III. In order to model delamination of composites, multiple shells tied together with either cohesive elements or tie contacts should be used. This will increase the complexity and size of the model compared to single-shell modelling, but by only using cohesive elements between some of the plies, the size increase of the model does not have to be too great. This type of modelling should definitely be considered and investigated in future work.
- IV. Adding solid elements, or more advanced shell elements, could also be tested in order to capture out-of-plane stresses and may improve quality of the results. This should also be investigated further.
- V. In order to fully understand the material models that are available, simulations of specimens with other geometries and different load cases need to be performed.

7 ACKNOWLEDGEMENT

I would like to express my sincere gratitude to Prof. Hervé Le Sourne for the continuous support for my master study and for providing me with the unique opportunity to perform my Master Thesis in ICAM. I would also like to thank him for the trust that he placed in me while working under his tutelage.

I am also indebted to the encouraging and guiding eye of Kévin Brochard. Throughout his incredibly busy day he always could take the time to answer questions of my research. His professionalism and patience are to be admired. To him I am sincerely grateful.

Besides, I am also grateful for the wonderful computer Lab in ICAM and the valuable support during my research.

To Yeye, I wish you best of luck for your PhD studies at ICAM. I am thankful you for your cooperation and knowledge as I learned from you. It was a learning experience that I really enjoyed and I am glad that you were there as an extra set of eyes.

Moreover, I would like to thank Prof. Rigo Philippe and all members who provided me the access to this meaningful and advanced EMSHIP program. Without their precious support, it would not be possible to conduct this research.

Lastly, but certainly not least, I would like to extend by sincere appreciation and thanks to my wife, Sohela and my family. Thank you for your patience and understanding as I completed my studies.

This thesis was developed in the frame of the European Master Course in “Integrated Advanced Ship Design” named “EMSHIP” for “European Education in Advanced Ship Design”, Ref.:159652-1-2009-1-BE-ERA MUNDUS-EMMC.

Mousum, Md Mahabub Hasan

This page is intentionally left blank.

8 REFERENCE

1. Arons, AB., Yennie, DR. (1948). Energy partition in underwater explosion phenomena. *Rev Mod Phys*; 20:519-536
2. Barras, G. (2007). Réponse dynamique des structures aux explosions sous-marines. These de Máster SMA, École Centrale de Nantes.
3. Brett JM, Yiannakopoulos G. A, (2008). Study of explosive effects in close proximity to a submerged cylinder. *Int J Impact Eng* 2008; 35:206-25.
4. Brett JM, Yiannakopoulos G, Van der Schaaf PJ. (2000). Time-resolved measurement of the deformation of submerged cylinders subjected to loading from a nearby explosion. *Int J Impact Eng* 2000; 24: 875-90.
5. Batra RC, Hassan NM, (2007). Response of fibre reinforced composites to underwater explosive loads. *Compos B: Eng* 38: 448–468.
6. Brochard, K., Sourne, H.L. and Barras, G. (2018). Extension of the string-on-foundation method to study the shock wave response of an immersed cylinder. *Journal of Impact Energy* (Under review).
7. Cole, RH. (1946). *Underwater explosions*. Princeton: Princeton University Press.
8. Cole RH (1965) *Underwater Explosions*, Dover, New York
9. Carruthers, J., Kettle, A. and Robinson, A. (1998). "Energy Absorption Capability and Crashworthiness of Composite Material Structures: A Review," vol. 51, pp. 635-649, 1998.
10. Chirica, I., Boazu, D., and Beznea, E. (2012). "Response of ship hull laminated plates to close proximity blast loads," *Computational Materials Science*, vol. 52, no. 1, pp. 197–203
11. Cimpoeru, S.J., Ritzel, D.V., and Brett, J.M. (2017). *Physics of Explosive Loading of Structures, Explosion Blast Response of Composites* (2017) 1-22.
12. DeRuntz, J. A. (1989). *The Underwater Shock Analysis Code and Its Applications*. In 60th Shock and Vibration Symposium, pages 89–107.
13. Department of Defense, (2002). *Composite Materials Handbook (CMH-17)*, vol. 2. *Polymer Matrix Composites Materials Properties*, 2002.
14. Farley, T. E., and Snay, H. G. (1978). "Unclassified data from classified source," in *Explosion Effects and Properties: Part II—Explosion Effects in Water*, edited by M. M. Swisdak, NSWC/WOL TR 76-116, NSWC
15. Felippa, CA. (1980). Top-down derivation of doubly asymptotic approximations for structure–fluid interaction analysis. In: Shaw RP, editor. *Proceedings of the international symposium on numerical analysis in applied engineering sciences*, Montreal, Canada; p. 79–88.

16. Forghani, A., McGregor, C., McClelland, S. et al., (2007). "Modelling of damage development in blast loaded composite panels," in Proceedings of the 16th International Conference on Composite Materials, pp. 1–8, Kyoto-Japan, July 2007
17. Geers, T.L. (1978). Doubly asymptotic approximations for transient motions of submerged structures. *Journal of Acoustical Society of America* 1978;64(5):1500–8
18. Geers, T. L. (1978). Doubly Asymptotic Approximations for Transient Motions of Submerged Structures. *Journal of Acoustical Society of America*, 64(5)
19. Gupta AD, Gregory FH, Bitting RL, Bhattacharya S (1987) Dynamic analysis of an explosively loaded hinged rectangular plate. *Comput Struct* 26(1–2): 339–344.
20. Gong SW, Lam KY. (1998). Transient response of stiffened composite submersible hull subjected to underwater explosive shock. *Compos Struct* 41: 27–37.
21. Geers, T.L. and Hunter, K.S. (2002). An integrated wave-effects model for an underwater explosion bubble. *Journal of the Acoustical Society of America* 111, 1584 (2002).
22. Gupta NK, Nagesh S, (2007). Deformation and tearing of circular plates with varying support conditions under uniform impulsive loads. *Int J Impact Eng* 34: 42–59.
23. Gupta, N. K., Kumar, P. and Hegde, S. (2010). "On deformation and tearing of stiffened and un stiffened square plates subjected to underwater explosion-a numerical study," *International Journal of Mechanical Sciences*, vol. 52, no. 5, pp. 733–744, 2010.
24. Hollyer, R. S. (1959). *Direct Shock-Wave Damage to Merchant Ships From Non-Contact Underwater Explosions*. Norfolk Naval Shipyard.
25. Holt, M. (1977). Underwater explosions, *Ann. Rev. Fluid Mech.* 9 (1977) 187-214.
26. Harres JF, Cheneau H. (1963). Les experiences de choc sur navres methodes de mesure et de depouillement. *Bull Assoc Tech Marit Aeronaut* 1963;63:783-812.
27. Houlston R., Slater JE, Pegg N, Desrochers CG, (1985). On analysis of structural response of ship panels subjected to air blast loading. *Comput Struct* 21(1–2): 273–289.
28. Houlston, R., Slater JE. (1991). Global and local modelling of naval panels subjected to shock loads. *Comput Struct* 40(2): 353–364.
29. Hull, D. (1991). "A Unified Approach to Progressive Crushing of Fibre-Reinforced Composite Tubes," vol. 40, pp. 377-421, 1991.
30. Houlston, R., Slater JE. (1993). Damage analysis with ADINA of naval panels subjected to a confined air-blast wave. *Comput Struct* 47(4–5): 629–639.
31. Hayman, B. (1995). Underwater explosion loading on foam-cored sandwich panels. Proceedings from the third inter-national conference on sandwich construction, Southampton, England.

32. Hammond, L. and Grzebieta, R. (1999). The requirement for hydrostatic initialisation in LS-DYNA/USA finite element models. *Shock and Vibration* 7 (2000) 57–65
33. Hassan NM, Batra RC, (2008). Modelling damage in polymeric composites. *Compos B: Eng* 39: 66–82.
34. Heimbs, S., Heller, S. and Middendorf, P. (2008). Simulation of Low velocity Impact on Composite Plates with Compressive Preload. LS-DYNA Anwenderforum, Bamberg 2008, Material II - Composites
35. Hung C, Lin B, Hwang-Fuu J, Hsu P. (2009). Dynamic response of cylindrical shell structures subjected to underwater explosion. *Ocean Eng* 2009; 36:564-77.
36. Jiang J, Olson MD (1991). Nonlinear dynamic analysis of blast loaded cylindrical shell structures. *Comput Struct* 40: 1139–1149.
37. Jacinto, A. C., Ambrosini, R. D. and Danesi, R. F. (2001). “Experimental and computational analysis of plates under air blast loading,” *International Journal of Impact Engineering*, vol. 25, no. 10, pp. 927–947, 2001.
38. ISSC. (2006). 16th INTERNATIONAL SHIP AND OFFSHORE STRUCTURES CONGRESS. 1, pp. 35-38. Southampton, UK.
39. Jen, C. Y. (2009). “Coupled acoustic-structural response of optimized ring-stiffened hull for scaled down submerged vehicle subject to underwater explosion,” *Theoretical and Applied Fracture Mechanics*, vol. 52, no. 2, pp. 96–110, 2009.
40. Keil, A.H. (1956). Introduction to underwater explosion research, UERD report 19–56, Norfolk naval ship yard, Portsmouth, Virginia, 1956
41. Keil, A.H. (1961). The response of ships to underwater explosions, *Proceedings of Annual Meeting of the Society of Naval Architects and Marine Engineers*, New York, NY, 1961, pp. 16-16.
42. Klaus, M.H. (1985). Response of a Panel Wall Subjected to Blast Loading, *Computers and Structures* 21 (1985), 129–135
43. Kwon, YW. Cunningham, RE. (1998). Comparison of USA-DYNA finite element models for a stiffened shell subject to underwater shock. *Comput Struct* 66(1): 127–144.
44. Krueger, S.R. (2006). Simulation of cylinder implosion initiated by an underwater explosion. Master’s Thesis Naval Postgraduate School, Monterey, California, USA.
45. Kwon, YW. Jo, JC. (2008). 3D modelling of fluid–structure interaction with external flow using coupled LBM and FEM. *J Press Vessel Technol-Trans ASME* 130: 8.
46. Louca LA, Pan YG, Harding JE (1998) Response of stiffened and unstiffened plates subjected to blast loading. *Eng Struct* 20(12): 1079–1086.

47. Li QM, Jones N, (1999). Shear and adiabatic shear failures in an impulsively loaded fully clamped beam. *Int J Impact Eng* 22: 589–607.
48. Liang, C.-C., & Tai, Y.-S. (2006). Shock responses of a surface ship subjected to noncontact underwater explosions. *Ocean Engineering*, 748-772.
49. Librescu L, Oh S-Y, Hohe J. (2006). Dynamic response of anisotropic sandwich flat panels to underwater and in-air explosions. *Int J Solids Struct* 43: 3794–3816.
50. LS-DYNA Keyword User's Manual - Volume I. Version R7.1. Livermore Software Technology Corporation, February 2014.
51. LS-DYNA Keyword User's Manual - Volume II. Material Models. Version R7.1. Livermore Software Technology Corporation, February 2014.
52. Mouritz, A. (1995). The effect of underwater explosion shock loading on the fatigue behaviour of GRP laminates. *Composites*; 26(1):3–9.
53. Mouritz, A. (1995). The damage to stitched GRP laminates by underwater explosion shock loading. *Compos Sci Technol*;55(4): 365–374
54. Mouritz, A. (1996). The effect of underwater explosion shock loading on the flexural properties of GRP laminates. *Int J Impact Eng*; 18(2):129–139.
55. Menkes, S.B. and Opat, H.J. (1973). Tearing and shear failures in explosively loaded clamped beams, *Explosion Mechanics* 13 (1973), 480–486.
56. Mehaute, B. L., & Wang, G. (1996). *Water Waves Generated By Underwater Explosions*. Miami.
57. McCoy, R.W, Sun, CT. (1997). Fluid–structure interaction analysis of a thick-section composite cylinder subjected to underwater blast loading. *Compos Struct* 37: 45–55.
58. Mair, H.U. (1999). Review: Hydrocodes for structural response to underwater explosions, *Shock Vib*. 6 (1999) 81-96.
59. Makinen, K. (1999). The transverse response of sandwich panels to an underwater shock wave. *J Fluids Struct* 13: 631–646.
60. Nurick, G.N., Olson, M.D., Fagnan, J.R., and Levin, A. (1995). Deformation and tearing of blast loaded stiffened square plates, *International Journal of Impact Engineering* 15 (1995), 273–291
61. Nu, Z., Zhi, Z., & Wepeng, Z. (2014). Dynamic response of a surface ship structure subjected to an underwater explosion bubble. *Marine Structures*, 26-44
62. Oleson M, Belsheim R. (1976). Shipboard shock environment and its measurement. *J Acoust Soc Am* 1976; 60:S61.

63. Osborne, M. (2012). Single-Element Characterization of the LS-DYNA MAT54 Material Model. Master thesis University of Washington, USA.
64. Price, R. S. (1979). "Similitude equations for explosives fired underwater," Technical Report NSWC TR 80-299, NSWC.
65. Qin, Z., Batra, RC. (2009). Local slamming impact of sandwich composite hulls. *Int J Solids Struct* 46: 2011–2035.
66. Qiankun, J. and Gangyi, D. (2011). "A finite element analysis of ship sections subjected to underwater explosion," *International Journal of Impact Engineering*, vol. 38, no. 7, pp. 558–566, 2011.
67. Reid, WD. (1996). The response of ships to underwater explosions. DSTO-GD-0109. Melbourne Victoria 3001: Aeronautical and Maritime Research Laboratory.
68. Rajendran R, Narashimhan K. (2001). Performance evaluation of HSLA steel subjected to underwater explosion. *J Mater Eng. Perform* 2001; 10: 66-74.
69. Rajendran R, Narashimhan K. (2001). "Damage prediction of clamped circular plates subjected to contact underwater explosion," *International Journal of Impact Engineering*, vol. 25, no. 4, pp. 373–386, 2001.
70. Rajendran R, Narasimhan K. (2006). Deformation and fracture behaviour of plate specimens subjected to underwater explosion a review. *Int J Impact Eng* 2006; 32: 1945-63.
71. Rajendran R, Paik JK, Kim BJ. (2006). Design of warship plates against underwater explosions. *Ships Offshore Struct* 2006; 1: 347-56.
72. Rajendran R, Paik JK, Lee JM. (2007). Of underwater explosion experiments on plane plates. *Exp Tech* 2007; 31: 18-24.
73. Rajendran R, Lee J. (2008). A comparative damage study of air-and water-backed plates subjected to non-contact underwater explosion. *Int J Mod Phys B* 2008; 22: 1311-8.
74. Rajendran R. (2009). Effective shock factors for the inelastic damage prediction of clamped plane plates subjected to non-contact underwater explosion. *J Strain Anal Eng* 2009; 44:211-20
75. Rajendran, R. (2009). "Numerical simulation of response of plane plates subjected to uniform primary shock loading of non-contact underwater explosion," *Materials & Design*, vol. 30, no. 4, pp. 1000–1007, 2009
76. Shin, YS. (2004). Ship shock modelling and simulation for far-field underwater explosion. *Computers and Structures*; 82: 2211-9.

77. Snay, H.G. (1957). Hydrodynamics of underwater explosions, Proceedings of the Symposium on Naval Hydrodynamics, Publication 515, National Academy of Science, National Research Council, Washington, DC, 1957, pp. 325-352.
78. Soden, P., Kaddour, A. and Hinton, M. (2004). "Recommendations For Designers and Researchers Resulting from The World-Wide Failure Exercise," vol. 64, pp. 589-604, 2004.
79. Shin, Y.S. (2004), "Naval Ship Shock and Design Analysis," Course Notes for Underwater Shock Analysis, Naval Postgraduate School, Monterey, CA, 2004.
80. Taylor, G.I. (1963). The pressure and impulse of submarine explosion waves on plates, 1941. The Scientific Papers of G I Taylor, Vol. III, Cambridge University Press, Cambridge, pp. 287–303.
81. Tsai, S.C. (2017). Numerical simulation of surface ship hull beam whipping response due to submitted to underwater explosion. Master's Thesis developed at ICAM (Nantes, France) in the framework of the "EMSHIP" Erasmus Mundus Master Course in "Integrated Advanced Ship Design
82. Wang, H., Zhu, Xi., Cheng, Y.S., Liu, J. (2014). Experimental and numerical investigation of ship structure subjected to close-in underwater shock wave and following gas bubble pulse. *Marine Structures* 39, 90-117.
83. Wardlaw AB, (2000). Luton JA. Fluid-structure interaction mechanisms for close-in explosions. *Shock Vib* 2000; 7: 265-75.
84. Zong, Z., Lam, KY., Liu, GR. (1999). Probabilistic risk prediction of submarine pipelines subjected to underwater explosion shock. *J Offshore Mech Arctic Eng-Trans ASME* 121(4): 251–254.
85. Zong, Z., Zhao, Y., and Li, H. (2013). "A numerical study of whole ship structural damage resulting from close-in underwater explosion shock," *Marine Structures*, vol. 31, pp. 24–43
86. Zhang, N., Zong, Z. and Zhang, W. (2014). "Dynamic response of a surface ship structure subjected to an underwater explosion bubble," *Marine Structures*, vol. 35, pp. 26–44, 2014.